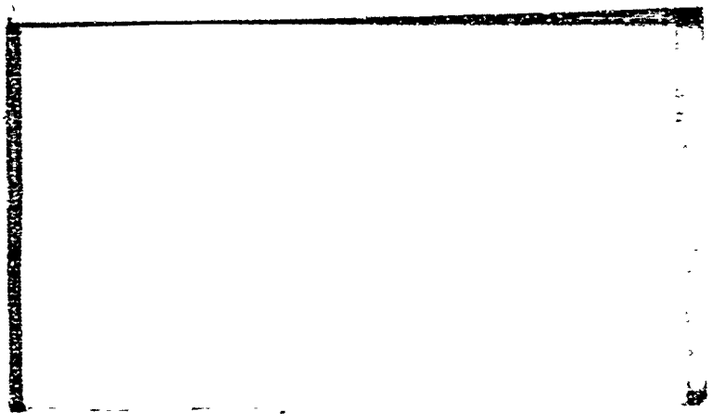

NEDERLANDSCH SCHEEPSBOUWKUNDIG PROEFSTATION

NETHERLANDS SHIP MODEL BASIN

WAGENINGEN
NEDERLAND

CLEARINGHOUSE FOR FEDERAL SCIENTIFIC AND TECHNICAL INFORMATION CFSTI
DOCUMENT MANAGEMENT BRANCH 410.11

LIMITATIONS IN REPRODUCTION QUALITY

ACCESSION # AD 608194

☒ 1. WE REGRET THAT LEGIBILITY OF THIS DOCUMENT IS IN PART UNSATISFACTORY. REPRODUCTION HAS BEEN MADE FROM BEST AVAILABLE COPY.

☐ 2. A PORTION OF THE ORIGINAL DOCUMENT CONTAINS FINE DETAIL WHICH MAY MAKE READING OF PHOTOCOPY DIFFICULT.

☐ 3. THE ORIGINAL DOCUMENT CONTAINS COLOR, BUT DISTRIBUTION COPIES ARE AVAILABLE IN BLACK-AND-WHITE REPRODUCTION ONLY.

☐ 4. THE INITIAL DISTRIBUTION COPIES CONTAIN COLOR WHICH WILL BE SHOWN IN BLACK-AND-WHITE WHEN IT IS NECESSARY TO REPRINT.

☐ 5. LIMITED SUPPLY ON HAND: WHEN EXHAUSTED, DOCUMENT WILL BE AVAILABLE IN MICROFICHE ONLY.

☐ 6. LIMITED SUPPLY ON HAND: WHEN EXHAUSTED DOCUMENT WILL NOT BE AVAILABLE.

☐ 7. DOCUMENT IS AVAILABLE IN MICROFICHE ONLY.

☐ 8. DOCUMENT AVAILABLE ON LOAN FROM CFSTI (TT DOCUMENTS ONLY).

☐ 9.

PROCESSOR: Berman

TSL-107-10 64

NETHERLANDS SHIP MODEL BASIN

HAAGSTEEG 2 - WAGENINGEN - NETHERLANDS

Final Report

Experimental and theoretical research on the hydrodynamic characteristics of large hub to diameter ratio propellers.

CONTRACT NO. N 62558-3463

Modification no. 1

PERIOD COVERED BY THE REPORT:

From 1 october 1962 through 30 april 1964

"The research reported in this document has been made possible through the support and sponsorship of the U.S. Department of the Navy, Office of Naval Research, through its U.S. Navy European Research Contracts Program".

Contents:

1. Summary.

Experimental results are presented of the side force generating characteristics of propellers with a large hub to diameter ratio, due to cyclic pitch variations. The effect of the cyclic pitch on the propeller torque and thrust are examined as well.

In addition a theory has been formulated for calculation of the properties of large hub to diameter ratio propellers.
This theory enables to optimize the design of the propeller with respect to efficiency.
The first numerical results of the theoretical analysis are given.

2. Introduction.

Recently a new propulsion and control system suitable for underwater vehicles has been proposed by Cdr. F.R. Haselton of the U.S.N.

The system utilizes a pair of large hub to diameter ratio propellers, one located near the bow, and the other near the stern of the vehicle. Of particular significance in addition to the position of the propellers and the way in which these are mounted is the fact that the pitch of the blades can be varied collectively as well as cyclically and that the propellers rotate in opposite directions in order to produce any desired combination of forces and moments. It is intended that these forces will be used for both the propulsion and the maneuvering of the buoyant vehicle.
To establish the feasibility of this concept for a full scale submarine, it is necessary to obtain quantitative knowledge of the propulsion and maneuvering capabilities of the device and to determine the mutual effects between the device and the vehicle body.

In October 1961 a feasibility study was started by the N.S.M.B. under an O.N.R. research contract (No. N.62558-3102) on propellers with large hub to diameter ratio and cyclic pitch control. The purpose of this research was to investigate the efficiency of such a device, the excitation of transverse forces by the propeller due to cyclic pitch changes and finally the power required for generating a certain transverse force.
From the experimental results the following conclusions could be drawn:

a. the maximum propulsion efficiency is of the same order as obtained with more conventional propeller types with small hubs.
b. the transverse forces do not decrease with increasing velocity.
c. the direction of the transverse forces changes by an appreciable amount when the velocity is increased.

The much promising results of this study have given the justification for a continuation of the experiments under the O.N.R.-research contract No. N.62558-3463.

In October 1962 the N.S.M.B. started with the design and the manufacture of a submarine model with two (forward and aft) large hub to diameter ratio propellers with programmed blade control. A description of the structural design of the tandem propeller submarine model is given in section 3,1. The forces and moments on the submarine and the torque on the propellers were increased in the way as described in section 3,2.

In order to yield test data with respect to the hydrodynamic characteristics of the tandem propeller submarine the following experiments were planned in the deep water towing tank of the N.S.M.B.:

a. Experiments to test the maneuvrability of the tandem propeller submarine (T.P.S.) under low speed-, cruising- and high speed conditions.
   At low speed the forward- and aft propeller should produce opposite and almost equal thrusts. Under cruising condition only the aft propeller produces the thrust, the forward propeller is stopped. At high speed both propellers should produce a positive thrust.
   Thus with this test program a more detailed determination of the generated transverse forces could be obtained, due to the cyclic pitch changes of the propeller blades.
b. Experiments to determine the efficiency of the entire propulsion device.
c. Experiments to determine the maximum generated thrust of the propellers under high speed condition.
d. Some experiments to test the static stability of the tandem propeller submarine under cruising- and high speed condition.

The available testing time for the execution of the test program was very short. Hardly any testing time was available for an extension or repeating of experiments which appeared to be necessary after the first measurements. This is the reason why several parts of the test program were cancelled.

A description of the reduction of the test data is given in section 3,2. The analysed test data are given in section 3,3 and the supplements 1 through 5. Section 3,4 contains a critical consideration of the analysed data.

The N.S.M.B. started simultaneously with the design of the one propeller model (October 1961) for experiments the development of a quasi stationary theory for this special propeller type.
The first results of the theoretical analysis were given in a paper presented at the fourth symposium on Naval Hydrodynamics (Office of Naval Research, Washington D.C. August 1962) [1].[4].
In designing the model, no attempt was made to optimize the design of the propeller systems of the tested submarine models because design data for this kind of propulsion system were not available. The design of the shrouds was based on the experience with more conventional shrouded propellers with small hubs.[3].
Numerical results of the theoretical analysis are now available and will be given in section 4.4. Sections 4,2, 4,3, 4,4, contain the general outline of the theoretical analysis.
As starting point for an extension of the research of the hydrodynamic characteristics of large hub to diameter ratio propellers, the results of the theoretical analysis can be used. From the view point of optimum efficiency for example, the best shape of the camberline of the shroud of a propeller can be calculated as function of the remaining design variables.

The most important conclusions and the suggestions for further research are given in section 5.

3. Experimental Research.

3.1. Structural design of the tandem propeller submarine model.

3.2. Measuring technique.

3.2.1. Definitions of the various parameters
3.2.2. Measurements of forces and moments
3.2.3. Measurements of torques
3.2.4. Reduction of the test data to force and moment parameters

3.3. Reduction and presentation of test data.

3.3.1. Originally planned experiments
3.3.2. Discussion of the measuring technique with respect to the experimental results
3.3.3. Presentation of the test data

3.4. Discussion of the results

3.4.1. Resistance tests
3.4.2. Propulsion tests. Results for zero cyclic pitch.
3.4.3. Propulsion tests. Results for the transverse forces due to cyclic pitch.

3.1. Structural design of the tandem propeller submarine model.

The original specification for the design of the two rotor model is given in Q.T.S.R. no. 1.
The submarine configuration chosen for the tandem propeller submarine test program is shown in profile in Figure 3.1.
The hull of the model is a body of revolution representing the shape of a submarine of the "ALBACORE" class.
The most important characteristics of the model hull are summarized below (see also Figure 3.1.):

L = 4.10 m
D_m = 0.60 m
L_0 = 1.78 m
$L_1 = L_2$ = 1.32 m

The metacentric height of the model is adjustable including zero height by means of a vertical displacement of the ballast weights.
The propellers of the model are shrouded large hub to diameter ratio propellers. The design of the removable shrouds is based on investigations described in [2] [3] . The forward- and aft propeller are contrarotating. The submarine model with unshrouded forward- and shrouded aft propeller is shown in Figure 3.2.

The proportions of the propeller blades, the shroud, the blade profiles and the location of the shroud in regard to the propeller blades would originally be similar to the previous single rotor model [1] . Some modifications were considered to be necessary however in order to be able to adapt the propeller characteristics to the thrust-speed relation ship of the full scale tandem propeller submarine. (see Q.T.S.R. nr.2)
The most important characteristics of the propellers are summarized below:

propeller:

b (blade span)	=	0.045 m
c (blade chord)	=	0.0225 m
N (number of blades)	=	12
D (blade tip diameter)	=	0.49 m
d (hub diameter)	=	0.40 m

shroud:

ℓ (shroud length)	= 0.090 m
a (percentage of shroud length in front of propeller disk)	= 60 %
angle of inclination with respect to streamline curvature	= 4^{o}
profile for the thickness	= NASA 0007
profile for the camberline	= NASA 250

In order to accomplish pitch control each blade is mounted on a spindle. The mechanical system consists of a wobble plate with the propeller blades rotated through a bevel gear by a crank which follows the wobble plate. This wobble plate can be moved parallel to the axial direction of the body thus effecting a change in the collective propeller pitch. In addition this wobble plate can rotate around two mutually perpendicular axes situated in the plane normal to the propeller axis.
This results in a cyclic pitch change. The position of the wobble plate is controlled by servo motors.

The following variations in propeller pitch could be realized:

a. the collective pitch angle is adjustable between + 10^{o} and - 10^{o}, with respect to zero blade setting. The zero blade setting is adjustable by turning the blades in their seats.

b. the cyclic pitch angle amplitude is adjustable in two mutually perpendicular planes through the longitudinal axis of the submarine from - 25^{o} to + 25^{o}. The cyclic pitch in these planes can be varied independently.

In order to provide sufficient power two D.C. engines per propeller were installed. The engines were coupled by means of gears and drive the propeller via a torque measuring unit and a flexible coupling. The r.p.m. of the propellers were automatically kept constant and were adjustable between zero and 250. A view of the forward propeller arrangement is given in Figure 3.3.

For the experiments which would be carried out in the deep water towing tank of the N.S.M.B. the model was equipped with a six component balance. The forces and moments on the submarine were measured by means of strain gauge elements.

The torque on the propellers was also measured by means of strain gauge elements.

The center section of the model was equipped with the holes required for the D.T.M.B. planar motion mechanism because also experiments would be carried out at the D.T.M.B.

The N.S.M.B. constructed a second center section resulting in a total model length of 5.49 m. Front and aft part are the same for both models. With this enlarged model, experiments will be carried out in the U.S.A. with an operator aboard of the submarine model.

A detailed description of the structure of the model is given in Q.T.S.R. 3 and Q.T.S.R. 4.

3.2. Measuring technique.

3.2.1. Definitions of the various parameters.

The submarine geometry is defined in Figure 3.4. The forces and moments on the tandem propeller submarine in the balance plane are written in the x-y-z body axis system.

The x-y-z body axis system is a right handed orthogonal triad with its origin in the center of the balance plane. x is positive in the astern direction ; y is positive in the starboard direction and z is positive in the upward direction.

Generalized forces and moments are F_x, F_y, F_z and M_x, M_y, M_z along and around x, y, z.

The total pitch angle α for each blade of the forward propeller could be varied according to the following program:

$$\alpha = \alpha_0 + \alpha_1 \sin\varphi + \alpha_2 \cos\varphi$$

The pitch angle for positive α_1 and α_2 equal to zero is thus maximum in the top position of the blade and minimum in the bottom position. The pitch angle for α_1 equal to zero and positive α_2 is maximum for the blade to starboard and minimum for the blade to port.

The pitch angle β for each blade of the aft propeller could be varied according to the program:

$$\beta = \beta_0 + \beta_1 \sin\varphi + \beta_2 \cos\varphi$$

The torques on the forward- and the aft propeller were defined by respectively M_1 and M_2.

The measured forces and moments were made non-dimensional with respectively $\rho n^2 D^4$ and $\rho n^2 D^5$. The non-dimensional force- and moment parameters obtained from the resistance tests are denoted by:

$$K(K_x),\ K(K_y),\ K(K_z);\ M(M_x),\ M(M_y),\ M(M_z)$$

The force- and moment parameters obtained from the propulsion tests are denoted by:

$$K_x,\ K_y,\ K_z,\ M_x,\ M_y,\ M_z,\ M_1,\ M_2$$

The parameters ρ, n and D were defined by:

n = number of revolution per second (1/sec.)
D = diameter of the propeller blade tips (m)
ρ = specific density of water ($kg.m^{-3}$)

The forces and moments have been measured as a function of the advance ratio Λ.

$$\Lambda = \frac{U}{nD}$$

U = speed of the submarine (m/sec.)

The efficiency of the propulsion device is defined by:

$$\eta_{1\text{ or }2} = \frac{\Lambda_{1\text{ or }2}}{2\pi} \frac{K_x}{Q_{1\text{ or }2}}$$

K_x is corrected for the resistance of the body without propeller blades and shroud.

The angle of attack of the T.P.S. is defined by ψ.

3.2.2. Measurements of the forces and moments.

The model was equipped with a six component balance placed in the center section of the model (see Figure 3.5). The forces and moments on the submarine were measured with respect to the balance shaft by means of strain gauge elements. For the deflections of the strain gauge meters corresponding to the six elements, the parameters U_1; U_2, U_3, U_4; U_5 and U_6 were introduced.

The following equations give the linear relations between $U_1, U_2 \ldots U_6$ and the forces and moments F_x; F_y, F_z and M_x, M_y, M_z respectively:

$$U_1 = a_{11}F_x + a_{12}F_y + a_{13}F_z + a_{14}M_x + a_{15}M_y + a_{16}M_z$$
$$U_2 = a_{21}F_x + a_{22}F_y + a_{23}F_z + a_{24}M_x + a_{25}M_y + a_{26}M_z$$
$$U_3 = a_{31}F_x + a_{32}F_y + a_{33}F_z + a_{34}M_x + a_{35}M_y + a_{36}M_z$$
$$U_4 = a_{41}F_x + a_{42}F_y + a_{43}F_z + a_{44}M_x + a_{45}M_y + a_{46}M_z$$
$$U_5 = a_{51}F_x + a_{52}F_y + a_{53}F_z + a_{54}M_x + a_{55}M_y + a_{56}M_z$$
$$U_6 = a_{61}F_x + a_{62}F_y + a_{63}F_z + a_{64}M_x + a_{65}M_y + a_{66}M_z.$$

The model has been placed under water in a cage to calibrate the balance. The calibration equipment enabled loading of the model by a pure F_x force, or a pure F_y force and so on. The results of the calibrations have been given in Q.T.S.R. no. 4. The coefficients $a_{11}, a_{12}, \ldots a_{66}$ have been calculated according to the calibration results.

3.2.3. Measurements of the torques.

The engines of the submarine drove the propellers via torque measuring units. The propeller torque has been measured by means of strain gauge elements.

For the deflection of the strain gauge meters corresponding to the torque of the forward-; respectively the aft propeller the parameters U_7 and U_8 were introduced.

The following equations give the relations between U_7 and M_1 ; U_8 and M_2

$$M_1 = b_1 + b_2 U_7 + b_3 U_7^2 + b_4 U_7^3$$

$$M_2 = c_1 + c_2 U_8 + c_3 U_8^2 + c_4 U_8^3$$

The configuration of the calibration equipment is given in detail in Q.T.S.R. no. 4. That report contains also the results of the calibrations of the torque measuring elements. The coefficients $b_1 \ldots b_4$, $c_1 \ldots c_4$ have been calculated with the aid of the calibration results.

The calibrations pointed out that the friction torque generated by O-seals, gearings and bearings is not sufficient constant. Consequently the accuracy of the measurements of the propeller torque is rather poor.

3.2.4. Reduction of the test data to force and moment parameters.

The control panel of the tandem propeller submarine made it possible to adjust four combinations of collective- and cyclic pitch angles and numbers of revolutions of the propellers. With a selection switch one of the four combinations could be given to the propellers of the submarine. Thus during one run of the submarine through the towing tank, four several submarine configurations could be tested.

The recording of the measurements has been performed by taking photographs of a panel with 16 voltmeters and with the aid of observation blades (see Q.T.S.R. no. 4).

The meter deflections on the panel are indications for:

a. the forces and moments on the submarine
$(U_1, U_2 \text{ ----- } U_6 \rightarrow X, K_y, K_z; M_x, M_y, M_z)$

b. the torque on forward- and aft propeller
$(U_7, U_8 \rightarrow M_1, M_2)$

c. the collective- and cyclic pitch angles of the propellers $(\alpha_0; \alpha_1, \alpha_2, \beta_0, \beta_1, \beta_2)$

d. the numbers of revolutions per second of the forward- and aft propeller $(n_1; n_2)$

At the same time, the meter panel shows the test number.

The amplification factors of the eight strain gauge meters, the speed (U) and the angle of attack ψ of the submarine during the experiments have been recorded with the aid of observation blades.

The data have been read off from the photographs and further be worked out by the computer of the N.S.M.B. Use could be made of two numerical programs. Program 1 served to reduce the data of the resistance tests ; program 2 those of the propulsion tests, corrected for the forces and moments on the submarine body without propellers and shrouds.

The detailed numerical programs for the reduction of the test data from the deflections of the strain gauge meters $U_1, \text{ - - - - }, U_8$ and the given numbers of revolutions of the propellers n_1 and n_2 and the speed of the submarine U have been given in supplement 1 of Q.T.S.R. no. 3.

3.3. Presentation of the test data.

3.3.1. Originally planned experiments.

As already remarked in the introduction, the experiments were carried out in order to yield data with respect to the hydrodynamic characteristics of the tandem propeller submarine. Experiments were originally planned under the following speed conditions:

A. Low speed condition.

At low speed the forward- and aft propeller should produce opposite and almost equal thrust. Most time it is desired to compensate the aft propeller torque by the torque of the forward propeller.
Experiments would be carried out to test the maneuvrability of the submarine. Also the hydrodynamic forces generated by the propellers should be determined under cross-flow condition or with running astern. Special attention should be paid to the value of the collective pitch at which a maximum volume of flow is generated through the propeller disk. Consequently, maximum transverse forces are to be expected in that case due to cyclic propeller pitch.

B. Cruising condition.

Under cruising condition only the aft propeller generates thrust, the forward propeller is stopped. Experiments were planned in order to yield data with respect to:

1. the efficiency of the propulsion device
2. the generated transverse forces due to cyclic pitch of the aft propeller.
3. the power required for generating the transverse force.
4. the forces generated by the stopped forward propeller.

It is desired to compensate the aft propeller torque by the forward propeller torque. Under cruising condition the forward propeller should have just sufficient collective pitch with respect to the feathered position in order to compensate for the torque of the aft propeller. Therefore item 4 was added to the test program.

C. High speed condition.

At high speed both propellers should produce a positive thrust. It is desired to compensate the aft propeller torque by the forward propeller torque. Special attention would be paid to the collective pitch of the propellers at which the thrust is maximum. Also the generated forces due to cyclic pitch would be determined.

Further experiments would be carried out to test the static stability of the tandem propeller submarine. Thus the forces and moments on the submarine would be measured with the submarine inclined under a small angle of attack. These experiments were planned for cruising condition as well as for high speed condition.

The design of the propeller of the tandem propeller submarine was based on the previous at the N.S.M.B. tested one propeller model [1].
Consequently the range of collective pitch angles for the several speed conditions of the T.P.S. were chosen according to the experimental results obtained with the one rotor model.

With a view to application in practice most experiments were planned with unshrouded forward and shrouded aft propeller. Also experiments were planned to examine the effect of the shrouds. Some tests have been carried out with forward- and aft propeller unshrouded and with forward- and aft propeller shrouded.

The experiments were performed in the deep water towing tank of the N.S.M.B. The tests have been carried out at speeds of the T.P.S. between zero and 3.5 m/sec., a centerline submergence of 1.0 m and numbers of revolutions per minute of the propellers between zero and 250.

3.3.2. Discussion of the measuring technique with respect to the obtained results.

From the obtained experimental results, taking into account the measuring technique, the following conclusions can be drawn:

1. the original intention was to perform the experiments at infinite depth. The experiments pointed out that the submergence depth of the tandem propeller submarine was not large enough to avoid the effect of the free surface.
2. the accuracy of the torque measurements was rather poor.
3. the period available for the execution of the test program was very short. The accuracy of the measurements has been influenced by this fact.

At low speed and especially under cross-flow condition it appeared from visual observations of the water surface that the flow around the tandem propeller submarine was very irregular. The irregularity of the flow was also demonstrated by large and slow variations of the forces and moments acting on the T.P.S. observed by the deflections of the strain gauge meters.
With the method of recording used the observation period of each measurement was too short to obtain accurate average values of the deflections of the strain meters.
The available testing time made it impossible to increase the submergence depth of the submarine or to change the recording method. Thus sufficient accurate measurements of the hydrodynamic characteristics of the submarine at low speed condition could not be obtained. This part of the test program was dropped.

Under cruising condition or at high speed, a wave pattern was generated at the water surface by the streamlined fairing around the balance shaft and probably also by the submarine body. The disturbance of the water surface resulted in an undesired force (F_z) and moment (M_y) on the submarine. The undesired force and moment increased with increasing speed of the submarine.

The results of the propulsion tests were corrected by the forces and moments acting on the submarine body without propeller blades and shrouds. However, the flow had an incidence angle with respect to the propeller axis, resulting in an effective cyclic pitch of the propeller due to the free surface effect. The results of the propulsion tests were corrected for the undesired force and moment generated by the effective cyclic propeller pitch.

In consequence with the above mentioned free surface effects and the very short period in which the experiments were to be carried out, we judged the accuracy of the measurements too low to examine small effects such as the effect of the forward acting propeller on the transverse force generated by the aft propeller and so on.

We decided to present the experimental results in the following way:

1. Resistance tests
2. Propulsion tests
    a. hydrodynamic characteristics of the shrouded aft propeller
    b. idem of the unshrouded aft propeller
    c. idem of the shrouded forward propeller
    d. idem of the unshrouded forward propeller.

With the aid of the above mentioned experimental results, the several speed conditions of the submarine can be composed by means of superposition. The detailed test data are presented in the following section.

3.3.3. Presentation of the test data.

1. Resistance tests.

The forces and moments acting on the submarine body without propeller blades have been measured during the resistance tests. The force- and moment coefficients [$k(K_x)$; $K(K_y)$; $K(K_z)$; $M(M_x)$; $M(M_y)$; and $M(M_z)$] (see also Figure 3.4) have been plotted as a function of the advance ratio Λ_o , [$\Lambda_o = \frac{u}{n_o D}$] with the angle of attack of the tandem propeller submarine ψ as parameter. The force- and moment coefficients and the advance ratio have been calculated with a fictive number of revolutions per minute (n_o) equal to 200.
The results are given in the following diagrams:

Resistance of the submarine body without forward- and with aft shroud:

Fig. 1.1	$K(K_x)$	as a function of Λ_o for $\psi = 0^o, 2^o$ and 4^o
Fig. 1.2	$K(K_y)$	idem
Fig. 1.3	$K(K_z)$	idem
Fig. 1.4	$M(M_y)$	idem
Fig. 1.5	$M(M_z)$	idem

Resistance of the submarine body with forward and aft shroud.

Fig. 2.1	$K(K_x)$	as a function of Λ_o for $\psi = 0^o, 2^o$ and 4^o
Fig. 2.2	$K(K_y)$	idem
Fig. 2.3	$K(K_z)$	idem
Fig. 2.4	$M(M_y)$	idem
Fig. 2.5	$M(M_z)$	idem

Resistance of the submarine body without both forward- and aft shroud.

Fig. 3.1	$K(K_x)$	as a function of Λ_o for $\psi = 0^o, 2^o$ and 4^o
Fig. 3.2	$K(K_y)$	idem
Fig. 3.3	$K(K_z)$	idem
Fig. 3.4	$M(M_y)$	idem
Fig. 3.5	$M(M_z)$	idem

The forces and moments on the submarine with the body inclined under a large angle were only measured at low speed. The effects of the shrouds on the resistance forces appeared to be small. The results are given in the following diagrams:

Fig. 4.1 $K/(K_x)$ as a function of Λ_o for $\psi = 0^o$; 45^o; 90^o 135^o; 180^o

Fig. 4.2 $K/(K_y)$ idem

Fig. 4.3 $M/(H_z)$ idem

The results of the resistance tests are given in supplement 1.

2. Propulsion tests.

A. Shrouded aft propeller.

The hydrodynamic characteristics of the shrouded aft propeller are given in supplement 2. The force- and moment coefficients are corrected for the forces and moments on the submarine body without shroud.
The experimental results are given in the following diagrams:

Thrust and torque coefficients K_x and Q_l as a function of the advance ratio Λ, for collective pitch angles $\beta_o = 24^o$; 28^o ; 32^o ; 36^o ; 40^o. Fig. 1.1.1.

Moment coefficient Q_x and efficiency η as a function of the advance ratio Λ for collective pitch angles $\beta_o = 24^o$; 28^o ; 32^o ; 36^o and 40^o. Fig. 1.2.1.

Thrust and torque coefficients K_x and Q_l as a function of the advance ratio Λ for some values of the collective pitch β_o and the values $\beta_{1,2} = |\beta_1| = |\beta_2| = 0^o$; 4^o ; 8^o ; 16^o and 24^o of the cyclic pitch

$\beta_o = 24^o$ Fig. 1.3.1.

$\beta_o = 28^o$ Fig. 1.3.2.

$\beta_o = 32^o$ Fig. 1.3.3.

$\beta_o = 36^o$ Fig. 1.3.4.

$\beta_o = 40^o$ Fig. 1.3.5.

Moment coefficient M_x as a function of the advance ratio Λ for a collective pitch of $\beta_o = 24^o$, 28^o, 32^o, 36^o, 40^o and a cyclic pitch of $\beta_{1,1} = |\beta_1| = |\beta_2| = 0^o$, 4^o, 8^o, 16^o, 24^o. Figure 1.4.1.

Thrust and torque coefficients K_x and Q_x as a function of the advance ratio Λ for some values of the collective pitch β_o and for an angle of attack of the submarine $\psi = 0^o$, 2^o and 4^o.

$\beta_o = 32^o$	Figure 1.5.1.
$\beta_o = 36^o$	Figure 1.5.2.
$\beta_o = 40^o$	Figure 1.5.3.

Transverse force coefficients K_y and K_z as a function of the advance ratio Λ for some values of the collective pitch β_o and for the cyclic pitch angles β_1 and β_2 equal to 0^o ; $\pm 4^o$; $\pm 8^o$; $\pm 16^o$ and $\pm 24^o$.

$\beta_o = 24^o$	Figure 1.6.1.
$\beta_o = 28^o$	Figure 1.6.2.
$\beta_o = 32^o$	Figure 1.6.3.
$\beta_o = 36^o$	Figure 1.6.4.
$\beta_o = 40^o$	Figure 1.6.5.

Moment coefficients M_y and M_z as a function of the advance ratio Λ for some values of the collective pitch β_o and for the cyclic pitch angles β_1 and β_2 equal to 0^o ; $\pm 4^o$; $\pm 8^o$; $\pm 16^o$; $\pm 24^o$.

$\beta_o = 24^o$	Figure 1.7.1.
$\beta_o = 28^o$	Figure 1.7.2.
$\beta_o = 32^o$	Figure 1.7.3.
$\beta_o = 36^o$	Figure 1.7.4.
$\beta_o = 40^o$	Figure 1.7.5.

The force coefficients K_y ; K_z and the moment coefficients M_y ; M_z respectively are also plotted in vectorial form for some values of the collective pitch β_o , for a cyclic pitch $\beta_1 = 0^o$; $\pm 4^o$; $\pm 8^o$ $\pm 16^o$; $\pm 24^o$ and for the advance ratio Λ equal to 0 ; 0.25 ; 0.50 ; 0.75 ; 1.00 ; 1.25 ; 1.50 ; 1.75.

$\beta_o = 24^o$	Figure 1.8.1.
$\beta_o = 28^o$	Figure 1.8.2.
$\beta_o = 32^o$	Figure 1.8.3.
$\beta_o = 36^o$	Figure 1.8.4.
$\beta_o = 40^o$	Figure 1.8.5.

B. Unshrouded aft propeller.

The hydrodynamic characteristics of the unshrouded aft propeller are given in supplement 3. The force- and moment coefficients are corrected for the forces and moments on the submarine body without shrouds. The experimental results are given in the following diagrams:

K_x and Q_2 as a function of Λ for β_o equal to 24^o ; 28^o ; 32^o ; 36^o and 40^o.

Figure 2.1.1.

Q_x and η as a function of Λ for β_o equal to 24^o ; 28^o ; 32^o ; 36^o and 40^o.

Figure 2.2.1.

K_x and Q_2 as a function of Λ for some values of β_o , and for some values of $\beta_{12} = |\beta_1| = |\beta_2|$

$\beta_o = 28^o ; 40^o$	$\beta_{12} = 0^o$; 8^o	Fig. 2.3.1.
$\beta_o = 32^o$	$\beta_{12} = 0^o$; 4^o ; 8^o ; 16^o ; 24^o	Fig. 2.3.2.
$\beta_o = 36^o$	$\beta_{12} = 0^o$; 4^o ; 8^o ; 16^o ; 24^o	Fig. 2.3.3.

Q_x as a function of Λ for some values of β_o and for some values of $\beta_{12} = |\beta_1| = |\beta_2|$

$\beta_o = 28^o ; 40^o$	$\beta_{12} = 0^o$; 8^o	
$\beta_o = 32^o$	$\beta_{12} = 0^o$; 4^o ; 8^o ; 16^o ; 24^o	Fig. 2.4.1.
$\beta_o = 36^o$	$\beta_{12} = 0^o$; 4^o ; 8^o ; 16^o ; 24^o	

K_x and Q_z as a function of Λ for β_o equal to 24^o ; 28^o ; 32^o ; 36^o ; 40^o and for $\beta_{1,2}$ equal to 0^o ; 2^o and 4^o.

Figure 2.5.1.

K_y and K_z as a function of Λ for some values of β_o and for some values of β_1 and β_2

$\beta_o = 28^o$ $\beta_1 = 0^o$; $\pm 8^o$ $\beta_2 = 0^o$; $\pm 8^o$ Fig. 2.6.1.

$\beta_o = 32^o$ $\beta_1 = 0^o$; $\pm 4^o$; $\pm 8^o$; $\pm 16^o$; $\pm 24^o$
$\beta_2 = 0^o$; $\pm 4^o$; $\pm 8^o$; $\pm 16^o$; $\pm 24^o$
Fig. 2.6.2.

$\beta_o = 36^o$ $\beta_1 = 0^o$; $\pm 4^o$; $\pm 8^o$; $\pm 16^o$; $\pm 24^o$
$\beta_2 = 0^o$; $\pm 4^o$; $\pm 8^o$; $\pm 16^o$; $\pm 24^o$
Fig. 2.6.3.

$\beta_o = 40^o$ $\beta_1 = 0^o$; $\pm 8^o$ $\beta_2 = 0^o$ $\pm 8^o$
Fig. 2.6.4.

Q_y and Q_z as a function of Λ for some values of β_o and for some values of β_1 and β_2

$\beta_o = 28^o$ $\beta_1 = 0^o$; $\pm 8^o$ $\beta_2 = 0^o$; $\pm 8^o$ Fig. 2.7.1.

$\beta_o = 32^o$ $\beta_1 = 0^o$; $\pm 4^o$; $\pm 8^o$; $\pm 16^o$; $\pm 24^o$
$\beta_2 =$ id Fig. 2.7.2.

$\beta_o = 36^o$ $\beta_1 =$ id
$\beta_2 =$ id Fig. 2.7.3.

$\beta_o = 40^o$ $\beta_1 = 0^o$; $\pm 8^o$ $\beta_2 = 0^o$; $\pm 8^o$ Fig. 2.7.4.

K_y; K_z and Q_y ; Q_z respectively in vectorial form for some values of β_o ; for some values of β_1 and for Λ equal to 0 ; 0.25 ; 0.50 ; 0.75 ; 1.00 ; 1.25 ; 1.50 ; 1.75.

$\beta_o = 28^o$ $\beta_1 = 0^o$; $\pm 8^o$ Fig.2.8.1.

$\beta_o = 32^o$ $\beta_1 = 0^o$; $\pm 4^o$; $\pm 8^o$; $\pm 16^o$; $\pm 24^o$ Fig.2.8.2.

$\beta_o = 36^o$ $\beta_1 = 0^o$; $\pm 4^o$; $\pm 8^o$; $\pm 16^o$; $\pm 24^o$ Fig.2.8.3.

$\beta_o = 40^o$ $\beta_1 = 0^o$; $\pm 8^o$ Fig.2.8.4.

C. Shrouded forward propeller.

The hydrodynamic characteristics of the shrouded forward propeller are given in supplement 4. The force- and moment coefficients are corrected for the forces and moments on the submarine body without shrouds. The experimental results are given in the following diagrams:

K_x and Q_1 as a function of Λ for α_o equal to 24^o, 28^o, 32^o, 36^o and 40^o.

Figure 3.1.1.

Q_x and η as a function of Λ for α_o equal to 24^o, 28^o, 32^o, 36^o and 40^o.

Figure 3.2.1.

K_x and Q_1 as a function of Λ for some values of α_o, and for $\alpha_{1,2} = |\alpha_1| = |\alpha_2| = 0^o ; \pm 4^o ; \pm 8^o ; \pm 16^o ; \pm 24^o$.

$\alpha_o = 24^o$	Figure 3.3.1.
$\alpha_o = 28^o$	Figure 3.3.2.
$\alpha_o = 32^o$	Figure 3.3.3.
$\alpha_o = 36^o$	Figure 3.3.4.
$\alpha_o = 40^o$	Figure 3.3.5.

Q_x as a function of Λ for α_o equal to 24^o ; 28^o ; 32^o ; 36^o and 40^o and for $\alpha_{1,2} = |\alpha_1| = |\alpha_2| = 0^o ; \pm 4^o ; \pm 8^o ; \pm 16^o ; \pm 24^o$. Figure 3.4.1.

K_y and K_z as a function of Λ for some values of α_o and for $\alpha_{1,2} = |\alpha_1| = |\alpha_2| = 0^o ; \pm 4^o ; \pm 8^o ; \pm 16^o ; \pm 24^o$.

$\alpha_o = 24^o$	Figure 3.6.1.
$\alpha_o = 28^o$	Figure 3.6.2.
$\alpha_o = 32^o$	Figure 3.6.3.
$\alpha_o = 36^o$	Figure 3.6.4.
$\alpha_o = 40^o$	Figure 3.6.5.

Q_y and Q_z as a function of Λ for some values of α_o and for $\alpha_{1,2} = 0^\circ ; \pm 4^\circ ; \pm 8^\circ ; \pm 16^\circ ; \pm 24^\circ$.

$\alpha_o = 24^\circ$	Figure 3.7.1.
$\alpha_o = 28^\circ$	Figure 3.7.2.
$\alpha_o = 32^\circ$	Figure 3.7.3.
$\alpha_o = 36^\circ$	Figure 3.7.4.
$\alpha_o = 40^\circ$	Figure 3.7.5.

$K_y ; K_z$ and Q_y , Q_z respectively in vectorial form for some values of α_o , for $\alpha_1 = 0^\circ ; \pm 4^\circ ; \pm 8^\circ ; \pm 16^\circ ; \pm 24^\circ$ and for Λ equal to 0°; 0.25 ; 0.50 ; 0.75 ; 1.0 ; 1.25 ; 1.50 ; 1.75.

$\alpha_o = 24^\circ$	Figure 3.8.1.
$\alpha_o = 28^\circ$	Figure 3.8.2.
$\alpha_o = 32^\circ$	Figure 3.8.3.
$\alpha_o = 36^\circ$	Figure 3.8.4.
$\alpha_o = 40^\circ$	Figure 3.8.5.

D. Unshrouded forward propeller.

The hydrodynamic characteristics of the unshrouded forward propeller are given in supplement 5. The force- and moment coefficients have been corrected for the forces and moments on the submarine body without shrouds. The experimental results are given in the following diagrams:

K_x and Q_1 as a function of Λ for $\alpha_o = 24^\circ ; 28^\circ ; 32^\circ ; 36^\circ ; 40^\circ$ Figure 4.1.1.

Q_x and η as a function of Λ for $\alpha_o = 24^\circ ; 28^\circ ; 32^\circ ; 36^\circ ; 40^\circ$ Figure 4.2.1.

K_x and Q_1 as a function of Λ for some values of α_o and for $\alpha_{1,2} = /\alpha_1/ = \alpha_2 = 0^\circ ; \pm 4^\circ ; \pm 8^\circ ; \pm 16^\circ ; \pm 24^\circ$

$\alpha_o = 24^\circ$	Figure 4.3.1.
$\alpha_o = 28^\circ$	Figure 4.3.2.
$\alpha_o = 32^\circ$	Figure 4.3.3.
$\alpha_o = 36^\circ$	Figure 4.3.4.

Q_x as a function of Λ for some values of α_o and for $\alpha_{f2} = 0^o$; $\pm 4^o$; $\pm 8^o$; $\pm 16^o$; $\pm 24^o$.

$\alpha_o = 24^o$	Figure 4.4.1.
$\alpha_o = 28^o$	Figure 4.4.2.
$\alpha_o = 32^o$	Figure 4.4.3.
$\alpha_o = 36^o$	Figure 4.4.4.
$\alpha_o = 40^o$	Figure 4.4.5.

K_y and K_z as a function of Λ for some values of α_o and for $\alpha_{f2} = 0^o$; $\pm 4^o$; $\pm 8^o$; $\pm 16^o$; $\pm 24^o$

$\alpha_o = 24^o$	Figure 4.6.1.
$\alpha_o = 28^o$	Figure 4.6.2.
$\alpha_o = 32^o$	Figure 4.6.3.
$\alpha_o = 36^o$	Figure 4.6.4.
$\alpha_o = 40^o$	Figure 4.6.5.

Q_y and Q_z as a function of Λ for some values of α_o and for $\alpha_{f2} = 0^o$; $\pm 4^o$; $\pm 8^o$; $\pm 16^o$; $\pm 24^o$.

$\alpha_o = 24^o$	Figure 4.7.1.
$\alpha_o = 28^o$	Figure 4.7.2.
$\alpha_o = 32^o$	Figure 4.7.3.
$\alpha_o = 36^o$	Figure 4.7.4.
$\alpha_o = 40^o$	Figure 4.7.5.

K_y, K_z and Q_y, Q_z respectively in vectorial form for some values of α_o , for $\alpha_f = 0^o$, $\pm 4^o$; $\pm 8^o$; $\pm 16^o$; $\pm 24^o$ and for Λ equal to 0^o ; 0.25 ; 0.50 ; 0.75 ; 1.00 ; 1.25 ; 1.50 ; 1.75.

$\alpha_o = 24^o$	Figure 4.8.1.
$\alpha_o = 28^o$	Figure 4.8.2.
$\alpha_o = 32^o$	Figure 4.8.3.
$\alpha_o = 36^o$	Figure 4.8.4.
$\alpha_o = 40^o$	Figure 4.8.5.

3.4. Discussion of the results.

3.4.1. Resistance tests.

The value of the drag coefficient as a function of the Reynolds number and the thickness ratio can be obtained from the experimental results on streamlined bodies as collected by Hoerner [2] (see section 6c). The flow around the submarine body is fully turbulent because the value of the Reynolds number based on the model length is beyond 10^6 and the surface imperfections of the forward rotor serves as a turbulence promotor. The drag in axi-symmetric condition is a function of the thickness ratio. The total drag coefficient based on the wetted area of the submarine body is:

$$C_{d,WET} = C_{f,WET}\left[1 + 1.5\left(\frac{D_o}{L_o}\right)^{3/2} + 7.0\left(\frac{D_o}{L_o}\right)^3\right]$$

where $C_{f,WET}$ is the turbulent mean skin friction coefficient of a smooth wall. $C_{f,WET}$ is plotted as a function of the Reynolds number in figure 3.6. according to the experimental results collected by Hoerner [2].

The drag of the submarine model can be calculated with the aid of the following relation:

$$D = \tfrac{1}{2}\rho U^2 A_{WET}\, C_{d,WET}$$

The calculated drag coefficient and the measured drag coefficient of the submarine body without shrouds, with shrouds fitted and without forward shroud and aft shroud fitted are plotted as a function of the Froude number in Figure 3.7.

The measured drag coefficient based on the wetted area of the submarine and the Froude number are defined by:

$$C_{Kx} = \frac{K_x}{\frac{1}{2}\rho U^2 A_{MET}}$$

$$F_R = \frac{U}{\sqrt{g L}}$$

The shape of the drag curves agree with each other up to a value of the Froude number of 0.2. As could be expected from the surface imperfections of the submarine model, the measured drag is somewhat higher than the calculated drag.

The drag of the submarine increases with a considerable amount if compared with the calculated drag for values of the Froude number beyond 0.2. Visual observations pointed out that a wave pattern has been generated at the water surface by the streamlined fairing around the balance shaft and probably also by the submarine body. The disturbance of the water surface resulted in a modification of the pressure along the model giving a larger drag. The disturbance of the water surface resulted also in an additional side force (F_z) and moment (M_y) on the submarine.
The force (F_z) and the moment (M_y) are made non-dimensional in the following way:

$$C_{Fz} = \frac{F_z}{\frac{1}{2}\rho U^2 A_{MET}}$$

$$C_{My} = \frac{M_y}{\frac{1}{2}\rho U^2 A_{MET} L}$$

C_{Fz} and C_{My} are plotted as a function of the Froude number in Figure 3.8. The force F_z increases with increasing speed of the submarine.

Experiments have also been carried out with the submarine at a drift angle (ψ = 2 or 4 degrees). These experiments revealed that the drag of the model in longitudinal direction has not been changed with a perceptible amount over the range of drift angles tested. The effect of the drift angle on the side force F_y and the moment M_z is given in the Figures 3.9 and 3.10. F_y and M_z are made non-dimensional in the following way:

$$C_{F_y} = \frac{F_y}{\frac{1}{2}\rho U^2 A_{MFT}}$$

$$C_{Mz} = \frac{M_z}{\frac{1}{2}\rho U^2 A_{MFT} L}$$

C_{F_y} and C_{Mz} appeared to be proportional with the drift angle ψ for values of ψ between 0 and 4 degrees.

At low speed experiments have been carried out to determine the effect of large angles of attack on the forces and moments on the model. The measured force- and moment coefficients are plotted as a function of the drift angle ψ and with the Froude number as parameter in Figure 3.11. The presence of the shrouds did not have an appreciable effect on the forces and moments at low speeds of the submarine.

3.4.2. Propulsion tests. Results for zero cyclic pitch.

The maximum propulsion efficiency of the forward- or aft propeller attained with a shroud respectively without a shroud, are around 50 - 55 % at a value of Λ of around 1.3. These maximum efficiences are lower as found for the large hub to diameter ratio propeller of the previous tested single rotor model. The difference can be explained by the following reasons:

a. the thrust of a propeller is obtained from the measured total axial force on the model corrected for the resistance of the submarine body without propeller blades and shrouds. In consequence, the obtained thrust includes interaction effects between propeller and submarine body. (thrust deduction and wake fraction).
The interaction effects will be different for the forward- and the aft propeller of the tandem propeller submarine and the single rotor model.
In addition the thrust of the propeller of the single rotor model has been obtained from measurements of the axial force on the forward part of the model only.

b. in order to be able to adapt the propeller characteristics of the tandem propeller submarine to the thrust-speed relationship of the full scale T.P.S., some modifications of the geometrical configuration of the propellers appeared to be necessary with respect to the propeller geometry of the single rotor model. An important design parameter for large hub to diameter ratio propellers will be the ratio between propeller and hub diameter. These ratios are for the propellers of the T.P.S. and the single rotor model around 11/9 and 4/3 respectively. It may be expected that the efficiency at lower values of this ratio will decrease.

c. the optimum shape of the shroud is a function of the design variables (hub to diameter ratio, propeller loading etc.) and also depends on the shape of the body in combination with which the propeller will be tested. The shroud shapes of the T.P.S. propellers and the propeller of the single rotor model were corrected by an approximate procedure for the expected streamline-curvature and inclination as induced by the bodies.

From the results and from the fact that the wall inclinations at the propeller location are larger for the T.P.S. propeller it may be speculated that the shroud shape determined in this way is less favourable for the T.P.S. than for the single rotor model. A more refined method for the determination of the optimum shroud shape would therefore probably result in efficiencies for the T.P.S. propeller that are more close to those obtained for the single rotor model.

The thrust- and torque coefficients of the forward- and aft propeller of the T.P.S., with respectively without shroud are given as a function of the advance ratio Λ in the Figures 3.12 and 3.13. With the aid of these diagrams the following conclusions can be drawn:

1. the aft propeller produces in comparison with the forward propeller a larger thrust for high values of Λ . This phenomenon can be explained by the wake effect.
2. shrouded propellers produce in comparison with unshrouded propellers a larger thrust for low values of Λ,
3. the efficiency of the unshrouded forward propeller in comparison with the shrouded forward propeller appeared to be larger.
4. already for low values of the collective pitch probably flow separation occurs in the case of the unshrouded aft propeller, resulting in a decrease of the thrust. This fact makes a comparison between the efficiencies of the aft propeller with- and without shroud rather difficult.
   The large change in characteristics obtained by fitting a shroud at low Λ for the aft propeller shows that the influence of the shape of the shroud may be very important.

After the first test series with the single rotor model and the T.P.S., it has been concluded that it might be very difficult to determine ad hoc the shroud shapes for large hub to diameter ratio propellers. It must be possible to increase the efficiency of the large hub to diameter ratio propellers of the T.P.S. as shown by the previous tests on the single rotor model. As starting point for further research, it seems advisible to optimize the shape of the shroud with respect to efficiency as a function of the design variables (hub to diameter ratio, propeller loading etc.) and the kind of body in combination with which the propeller will be used. The procedure to be followed has been discussed in section 4.

For a given power (thus torque coefficients) the thrust coefficients of the propellers (forward- and aft propeller, with respectively without shroud) have been plotted as a function of the advance ratio (λ) in the Figures 3.14 through 3.17. In addition the collective pitch angles have been given for which the optimum values of the thrust are obtained.

The maximum thrust (in tons) has been plotted as a function of the speed (in knots) for a given power (h.p.) for full scale propellers in the Figures 3.18 and 3.19. The scale ratio has been assumed to be 20. The numbers of revolutions per minute of the propellers are assumed to be equal to 50.
The total thrust produced with both forward- and aft propeller operating at the installed power is given in Figure 3.20.

The maximum speed of a submarine equiped with this kind of large hub to diameter ratio propellers can be roughly derived from these diagrams. The submarine size used for these diagrams is given on the next page.

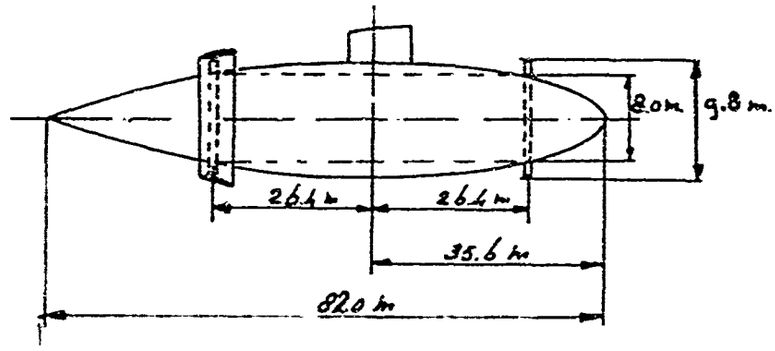

3.4.3. Propulsion tests. Results for the transverse forces due to cyclic pitch.

The following phenomena are of interest with respect to the generated side forces, namely:

a. the magnitude and the direction of the generated side force. It has appeared that the torques Q_{Y_1}, Q_{Y_2}, Q_{Z_1} and Q_{Z_2} generated in the propeller planes are rather unimportant. The contribution of the side forces to the moment around the ship's c.q. is much larger.
b. the change in thrust due to cyclic pitch.
c. the change in torque due to cyclic pitch.

With respect to the magnitude and the direction of the generated side force the following conclusions can be drawn:

1. the magnitude of the total transverse force increases by an appreciable amount if the velocity is increased. The total transverse force coefficients of the forward- and aft propeller with respectively without shroud are plotted as a function of Λ with the cyclic pitch angles α_1 or β_1 as parameters and for a collective pitch angle of 36°, in Figure 3.21.
2. it is evident that an appreciable rotation of the transverse force takes place when the speed of the submarine increases. The angle $[\chi]$ between the total transverse force and the positive y -axis (see Figure 3.4.) of the forward- and aft propeller

pitch angle as parameter for a collective pitch of 36° in Figure 3.22. The direction of the force vector is in accordance with the results of a qualitative theoretical analysis as described in Appendix A. The results of the experiments and the theoretical analysis are given in Figure 3.23. A reasonable agreement has been found for $\Lambda = 1.50$.

3. the magnitude of the total transverse force generated by the forward propeller of the submarine is if compared with the aft propeller, much smaller. The transverse forces have been determined by measuring the transverse force on the body correcting for the forces of the body without propeller blades and shrouds. In consequence the measured transverse forces include the interaction effects between the propeller and th' submarine body. It is clear that opposing side forces are generated on the body as a consequence of the sideways deflection of the propeller jet. Especially in the case of the forward propeller therefore a drastic reduction in the generated side forces nas been found if compared with the aft propeller (see Figure 3.21).

4. A shroud can in principal also have an unfavourable effect in the same way as explained above. In order to minimize this effect the shrouds were located rather forward with respect to the propeller disk. It appeared however that the presence of a shroud did not have a large effect on the magnitude of the side forces. (see par example Figure 3.21). The direction of the side force is however somewhat effected by the presence of a shroud.

ts

With respect to the change in thrust and torque due to cyclic pitch the following conclusions can be drawn. The generation of the side forces is accompanied by a decrease in thrust and an increase in propeller torque. The additional thrust- and torque coefficients ΔK_x and ΔQ_2 have for instance been plotted as a function of Λ for a collective pitch of 32^o in Figure 3.24.

A fortunate coincidence is that the major influence is on the thrust K_x and a relatively smaller one on the propeller torque Q_1 or Q_2. Moreover for low values of the propeller torque the increase in the torque due to cyclic pitch appeared to be large and for large values of the propeller torque the increase in torque due to cyclic pitch appeared to be small.

The decrease in thrust due to cyclic pitch appeared to be small for low values of the propeller torque. For large values of the propeller torque, the decrease in thrust due to cyclic pitch appeared to be large.

The most important conclusion which can be drawn from the foregoing is that the required power for the propellers of the submarine will not be primarily defined by requirements concerning the maneuvrability.

4. Theoretical Research.

4.1. Introduction.

4.2. Calculation of the flow field.

4.2.1. Mathematical model
4.2.2. Calculation of the induced velocities
4.2.3. Calculation of the ring vortex distribution along the hub.

4.3. Calculation of the frictionless torque, thrust and efficiency.

4.3.1. Torque and thrust of the propeller
4.3.2. Thrust on the shroud
4.3.3. Thrust on the hub
4.3.4. Calculation of the torque- and thrust coefficients and the efficiency
4.3.5. Calculation of the shroud camberline
4.3.6. Pressure distributions along the shroud

4.4. Effect of drag on thrust, torque and efficiency.

4.4.1. Drag of the propeller
4.4.2. Drag of the shroud
4.4.3. Drag of the hub
4.4.4. Calculation of the drag coefficients
4.4.5. Calculation of total torque, total thrust and efficiency.

4.5. Presentation and discussion of the computed results.

4. Theoretical research.

4.1. Introduction.

Recently interest has been shown in the application of shrouded large hub to diameter ratio propellers. Design data for this kind of propulsion systems are not available. Due to this fact no attempt was made to optimize the design of the propeller systems of the tested submarine models.

The design of the shrouded large hub to diameter ratio propeller depends on a large number of variables. Therefore it is a complicated problem to optimize the design of this propulsion device.

The N.S.M.B. started simultaneously with the design of the submarine models for experiments the development of a stationary theory for this special propeller type. The first numerical results of this theoretical analysis are now available.

Investigations to optimize the design of the shrouded large hub to diameter ratio propeller can be based on this theory. The general outline of the theoretical analysis and the first numerical results are given in the following sections.

4.2. Calculation of the flow field.

4.2.1. Mathematical model.

Important design parameters of shrouded large hub to diameter ratio propellers are: (see figure 4,1)

1. the ratio between shroud length and propeller diameter. ($\frac{L}{D}$)
2. the ratio between hub- and propeller diameter ($\frac{d}{D}$)
3. percentage of shroud length in front of propeller disk (a)
4. the advance ratio (Λ)
5. the loading of the screw (K_T)
6. the thickness form and the maximum thickness

The calculations of the flow field of the shrouded propeller were based on the following assumptions. The shrouded propeller moves steadily forward. The forward velocity was assumed to be sufficiently large, the shroud camber loading and the blade loading of the screw sufficiently low to permit the application of linearized theory. The effect of the friction on the flow field was neglected.

The shrouded propeller consists of an annular airfoil of finite length with an internally operating propeller having an infinite number of blades. The hub of the propeller is of constant diameter and has an infinite length.

The mathematical model of the geometrical configuration of the shroud-propeller-hub system can be composed by means of vortex- and source distributions. (see Figure 4,2).

The propeller flow field is represented by a disk with a continuous bound vortex distribution of constant strength in circumferential direction. Assume the vortex strengths per unit area to be equal to:

$$\gamma(r)$$

The vortex strength is also constant along lifting lines in which we can split up the bound vortex distribution representing the propeller disk. The vortex strength per length unit along a lifting line is

$$\Gamma_{\Delta\psi}(r) = \gamma(r)\, r\, \Delta\psi = \gamma(R_1) R_1 \Delta\psi = \text{CONSTANT}.$$

thus

$$\gamma(r) = \frac{R_1}{r}\gamma(R_1)$$

Further the propeller flow field consists of helicoidal trailing vortices. Each trailing vortex line lies on a cylinder of constant diameter (equal to hub or shroud diameter) and has a constant pitch. The effect of the induced velocities on the shape of the helicoidal vortex lines is neglected in the linearized theory.
A sector $\Delta\psi$ of the propeller gives helical vortices starting from the shroud and the hub with a vortex strength per unit of length equal to respectively:

$$T_{\Delta\psi}(R_1) = \gamma(R_1)\, R_1\, \Delta\psi \qquad \text{(shroud)}$$

and $$T_{\Delta\psi}(R_0) = \gamma(R_1) R_1\, \Delta\psi \qquad \text{(hub)}$$

The increase angle of the helical lines is:

$$\epsilon = \operatorname{arctg} \frac{u}{\omega r}$$

The flow around the shroud is represented by a distribution of ring sources and a distribution of ring vortices along a cylinder of constant diameter. The effect of the induced velocities on the shape of the bound vortex system and the sources is neglected. The annular airfoil, representing the shroud, is axi-symmetrical.

Then we have on the shroud:

1. a bound ring vortex distribution with a strength equal to zero at the leading edge of the shroud and equal to the strength of the circumferential component of the helicoidal trailing vortices at the propeller disk. This vortex distribution prevents a drop in the radial induced velocity along the shroud at the screw disk. The vortex distribution $\gamma^*(x, R_1)$ is assumed to have a sinusoidal shape, thus

$$\gamma^*(\xi, R_1) = A \sin \pi \left(\frac{\xi}{c} + a\right)$$

and $\xi = -\frac{a}{\eta}$ $\quad \gamma^*(-\frac{a}{\eta}, R_1) = 0$

$\xi = 0$ $\quad \gamma^*(0, R_1) = \mu\gamma(R_1) = A \sin \pi a$

thus $\gamma^*(\xi, R_1) = \mu\gamma(R_1) \frac{\sin(\frac{\xi}{\eta} + a)}{\sin \pi a}$

2. a source distribution which gives the thickness effect of the shroud. The strength of the source distribution $q(x)$ along the shroud can be calculated in the usual way from the given thickness $H(\xi)$ of the shroud profile.

3. continuous bound ring vortex distributions which are a measure for the loading of the camberline of the shroud, which permits a representation by Fourier Synthesis of other distributions. Since the vortex strengths at the leading- and trailing edges of the shroud are zero, the vortex distributions have sinusoidal shapes.
The strengths of the ring vortex systems are:

$$\gamma_1(R_1) \sin \pi (\frac{\bar{\xi}}{\eta} + a)$$

$$\gamma_2(R_1) \sin 2\pi (\frac{\bar{\xi}}{\eta} + a)$$

$$\gamma_m(R_1) \sin m\pi (\frac{\bar{\xi}}{\eta} + a)$$

The shroud will have shock-free entry because the toal ring vortex strength at the leading edge is equal to zero.

Assume $\bar{\xi} + \eta(a - 0.5) = -\frac{\eta}{2} \cos\theta$

The vortex strength of the various ring vortex systems becomes:

$$\frac{\mu\gamma(R_1)}{\quad} \sin\theta \quad [\text{between} \quad -a\eta \quad \text{and} \quad 0]$$

$\gamma_1(R_1)\sin\theta$	[between $-a\eta$ and $(1-a)\eta$]
$\gamma_2(R_1)\sin 2\theta$	[id]
$\gamma_m(R_1)\sin m\theta$	[id]

The effect of the hub on the flow field is represented by several ring vortex distributions.

The ring vortex distribution $h_0(\xi)$ has the function to compensate the radial induced velocities by the propeller flow field at the hub. The total induced radial velocity along the hub by the propeller flow field and the ring vortex distribution $h_0(\xi)$ must be zero.

The ring vortex distribution $h_{0d}(\xi)$ serves to compensate the radial induced velocities along the hub by the thickness of the shroud.

The ring vortex distributions $h_m(\xi)$ serve to compensate the radial velocities along the hub induced by the sinusoidal ring vortex distributions along the shroud.

The resulting mathematical model is summarized in Figure 2, where $\bar{w}_a$, $\bar{w}_t$ and $\bar{w}_r$ are the dimensionless velocities induced by all the vortices and sources. $\bar{w}_a$, $\bar{w}_t$ and $\bar{w}_r$ are the induced velocities in the axial, circumferential and radial direction respectively.

4.2.2. Calculation of the induced velocities.

The total induced velocites can be calculated according to the law of Biot-Savart.
In the following we give the induced velocities in the point (x,φ,r) of the field by the various vortex systems and source distributions.

The relations are made non-dimensional in the following way:

$$\bar{x} = \frac{x}{R_1} \qquad \bar{\xi} = \frac{\xi}{R_1} \qquad \bar{w} = \frac{w}{u} \qquad \eta = \frac{L}{R_1} \qquad a = \frac{b}{L}$$

$$\bar{r} = \frac{r}{R_1} \qquad \bar{r}_1 = \frac{r_1}{R_1} \qquad \lambda = \frac{R_0}{R_1}$$

$$\mu = \frac{\omega R_1}{u}$$

$$\bar{\gamma} = \frac{\gamma(R_1)}{u} \qquad \bar{\gamma}_1 = \frac{\gamma_1(R_1)}{u} \qquad \bar{\gamma}_m = \frac{\gamma_m(R_1)}{u}$$

$$\bar{g}(\xi) = \frac{g(\xi)}{u}$$

$$\bar{h}_0(\xi) = \frac{h(\xi)}{u} \qquad \bar{h}_{0d}(\xi) = \frac{h_{0d}(\xi)}{u} \qquad \bar{h}_m(\xi) = \frac{h_m(\xi)}{u}$$

1. <u>Induced velocities by the bound vortices of the propeller disk.</u>

$$\bar{w}_a^{(1)}(\bar{x},\bar{r}) = 0$$

$$\bar{w}_r^{(1)}(\bar{x},\bar{r}) = \frac{\bar{\gamma}}{\pi}\int_{\lambda}^{1} d\bar{r}_1 \int_0^{\pi/2} d\psi \, \frac{(\bar{x}-\bar{\xi})\cos 2\psi}{\left[(\bar{x}-\bar{\xi})^2+(\bar{r}_1+\bar{r})^2-4\bar{r}_1\bar{r}\sin^2\psi\right]^{3/2}}$$

$$\bar{w}_r^{(1)}(\bar{x},\bar{r}) = 0$$

2. <u>Induced velocities by the helicoidal vortices starting from the shroud.</u>

$$\bar{w}_a^{(2)}(\bar{x},\bar{r}) = \frac{\mu^3\bar{\gamma}}{\pi}\int_0^{\infty} d\tau \int_0^{\pi/2} d\psi \, \frac{(1+\bar{r}\cos 2\psi)}{\left[\left\{\mu(\bar{x}-\bar{\xi})\right\}^2+\mu^2\left\{(1+\bar{r})^2-4\bar{r}\sin^2\psi\right\}\right]^{3/2}}$$

$$\bar{w}_r^{(2)}(\bar{x},\bar{r}) = \frac{\mu^2\bar{\gamma}}{\pi}\int_0^{\infty} d\tau \int_0^{\pi/2} d\psi \, \frac{(\bar{r}+\cos 2\psi)}{\left[\left\{\mu(\bar{x}-\bar{\xi})\right\}^2+\mu^2\left\{(1+\bar{r})^2-4\bar{r}\sin^2\psi\right\}\right]^{3/2}}$$

$$\bar{w}_r^{(2)}(\bar{x},\bar{r}) = -\frac{\mu^2\bar{\gamma}}{\pi}\int_0^{\infty} d\tau \int_0^{\pi/2} d\psi \, \frac{\left[\mu(\bar{x}-\bar{\xi})-\tau\right]\cos 2\psi}{\left[\left\{\mu(\bar{x}-\bar{\xi})\right\}^2+\mu^2\left\{(1+\bar{r})^2-4\bar{r}\sin^2\psi\right\}\right]^{3/2}}$$

3. Induced velocities by the helicoidal vortices starting from the hub.

$$\bar{W}_a^{(3)}(\bar{x},\bar{r}) = -\frac{\lambda\mu^3\bar{\gamma}}{\pi}\int_0^{\infty} d\tau \int_0^{\pi/2} d\psi \frac{(\lambda+\bar{r}\cos 2\psi)}{\left[\{\mu(\bar{x}-\bar{\xi})-\tau\}^2+\mu^2\{(\lambda+\bar{r})^2-4\lambda\bar{r}\sin^2\psi\}\right]^{3/2}}$$

$$\bar{W}_r^{(3)}(\bar{x},\bar{r}) = -\frac{\mu^2\bar{\gamma}}{\pi}\int_0^{\infty} d\tau \int_0^{\pi/2} d\psi \frac{(\bar{r}+\lambda\cos 2\psi)}{\left[\quad\right]^{3/2}}$$

$$\bar{W}_x^{(3)}(\bar{x},\bar{r}) = \frac{\lambda\mu^2\bar{\gamma}}{\pi}\int_0^{\infty} d\tau \int_0^{\pi/2} d\psi \frac{[\mu(\bar{x}-\bar{\xi})-\tau]\cos 2\psi}{\left[\quad\right]^{3/2}}$$

4. Induced velocities by the discontinuous ring vortex distribution along the shroud.

$$\bar{W}_a^{(4)}(\bar{x},\bar{r}) = \frac{\mu\bar{\gamma}}{2\pi\sqrt{a(1-a)}}\int_{-a\eta}^{0} d\xi \int_0^{\pi/2} d\psi \sin\theta \frac{(1+\bar{r}\cos 2\psi)}{\left[(\bar{x}-\bar{\xi})^2+(1+\bar{r})^2-4\bar{r}\sin^2\psi\right]^{3/2}}$$

$$\bar{W}_r^{(4)}(\bar{x},\bar{r}) = 0$$

$$\bar{W}_x^{(4)}(\bar{x},\bar{r}) = -\frac{\mu\bar{\gamma}}{2\pi\sqrt{a(1-a)}}\int_{-a\eta}^{0} d\xi \int_0^{\pi/2} d\psi \sin\theta \frac{(\bar{x}-\bar{\xi})\cos 2\psi}{\left[\quad\right]^{3/2}}$$

5. Induced velocities by the source distribution along the shroud.

$$\bar{W}_a^{(5)}(\bar{x},\bar{r}) = \frac{1}{\pi}\int_{-a\eta}^{(1-a)\eta} d\bar{\xi} \int_0^{\pi/2} d\psi\, \bar{q}(\xi) \frac{(\bar{x}-\bar{\xi})}{\left[(\bar{x}-\bar{\xi})^2+(1+\bar{r})^2-4\bar{r}\sin^2\psi\right]^{3/2}}$$

$$\bar{W}_r^{(5)}(\bar{x},\bar{r}) = 0$$

$$\bar{W}_x^{(5)}(\bar{x},\bar{r}) = \frac{1}{\pi}\int_{-a\eta}^{(1-a)\eta} d\bar{\xi} \int_0^{\pi/2} d\psi\, \bar{q}(\xi) \frac{(\bar{r}+\cos 2\psi)}{\left[\quad\right]^{3/2}}$$

6. Induced velocities by the sinusoidal ring vortex distributions along the shroud.

$$\bar{W}_a^{(6,m)}(\bar{x},\bar{r}) = \frac{\bar{\gamma}_m}{\pi}\int_{-a\eta}^{(1-a)\eta} d\bar{\xi}\int_0^{\pi/2} d\psi\ \sin m\theta\ \frac{(1+\bar{r}\cos 2\psi)}{\left[(\bar{x}-\bar{\xi})^2+(1+\bar{r})^2-4\bar{r}\sin^2\psi\right]^{3/2}}$$

$$\bar{W}_r^{(6,m)}(\bar{x},\bar{r}) = 0$$

$$\bar{W}_x^{(6,m)}(\bar{x},\bar{r}) = -\frac{\bar{\gamma}_m}{\pi}\int_{-a\eta}^{(1-a)\eta} d\bar{\xi}\int_0^{\pi/2} d\psi\ \sin m\theta\ \frac{(\bar{x}-\bar{\xi})\cos 2\psi}{\left[\quad\right]^{3/2}}$$

7. Induced velocities by the ring vortex distribution $h_o(\xi)$ along the hub.

$$\bar{W}_a^{(7)}(\bar{x},\bar{r}) = -\frac{\lambda}{\pi}\int_{-\infty}^{+\infty} d\bar{\xi}\int_0^{\pi/2} d\psi\ \bar{h}_o(\xi)\frac{[\lambda+\bar{r}\cos 2\psi]}{\left[(\bar{x}-\bar{\xi})^2+\lambda^2+\bar{r}^2+2\bar{r}\lambda\cos 2\psi\right]^{3/2}}$$

$$\bar{W}_r^{(7)}(\bar{x},\bar{r}) = 0$$

$$\bar{W}_x^{(7)}(\bar{x},\bar{r}) = \frac{\lambda}{\pi}\int_{-\infty}^{+\infty} d\bar{\xi}\int_0^{\pi/2} d\psi\ \bar{h}_o(\xi)\frac{(\bar{x}-\bar{\xi})\cos 2\psi}{\left[\quad\right]^{3/2}}$$

8. Induced velocities by the ring vortex distribution $h_{od}(\xi)$ along the hub.

$$\bar{W}_a^{(8)}(\bar{x},\bar{r}) = -\frac{\lambda}{\pi}\int_{-\infty}^{+\infty} d\bar{\xi}\int_0^{\pi/2} d\psi\ \bar{h}_{od}(\xi)\frac{(\lambda+\bar{r}\cos 2\psi)}{\left[(\bar{x}-\bar{\xi})^2+\lambda^2+\bar{r}^2+2\bar{r}\lambda\cos 2\psi\right]^{3/2}}$$

$$\bar{W}_r^{(8)}(\bar{x},\bar{r}) = 0$$

$$\bar{W}_x^{(8)}(\bar{x},\bar{r}) = \frac{\lambda}{\pi}\int_{-\infty}^{+\infty} d\bar{\xi}\int_0^{\pi/2} d\psi\ \bar{h}_{od}(\xi)\frac{(\bar{x}-\bar{\xi})\cos 2\psi}{\left[\quad\right]^{3/2}}$$

9. Induced velocities by the ring vortex distribution $h_m(\xi)$ along the hub.

$$\overline{w}_a^{(s,m)}(\bar{x},\bar{r}) = -\frac{\lambda}{\pi}\int_{-\infty}^{+\infty} d\bar{\xi} \int_0^{\pi/2} d\psi\ \bar{h}_m(\xi)\frac{(\lambda+\bar{r}\cos 2\psi)}{\left[(\bar{x}-\bar{\xi})^2+\lambda^2+\bar{r}^2+2\bar{r}\lambda\cos 2\psi\right]^{3/2}}$$

$$\overline{w}_r^{(s,m)}(\bar{x},\bar{r}) = 0$$

$$\overline{w}_\lambda^{(s,m)}(\bar{x},\bar{r}) = \frac{\lambda}{\pi}\int_{-\infty}^{+\infty} d\bar{\xi} \int_0^{\pi/2} d\psi\ \bar{h}_m(\xi)\frac{(\bar{x}-\bar{\xi})\cos 2\psi}{\left[\quad\quad\quad\quad\quad\quad\right]^{3/2}}$$

The above mentioned relations for the induced velocities can be calculated with the aid of numerical integrations for the chosen data of the design parameters. A numerical program for the N.S.M.B. digital computer based on this theory was made (see Appendix B, Numerical program no. 1).

4.2.3. Calculation of the ring vortex distributions along the hub.

The ring vortex distribution $\bar{h}_o(\xi)$ serves to compensate the radial induced velocities by the propeller flow field and the discontinuous ring vortex distributions along the shroud. The flow field in so far as it depends on the propeller loading consists of:

1. bound vortices of the propeller disk
2. helical vortices starting from hub and shroud
3. discontinuous ring vortex distribution along the shroud

The total induced radial velocity along the hub must be equal to zero, thus:

$$\overline{w}_\lambda^{(1)}(\bar{x},\lambda)+\overline{w}_\lambda^{(2)}(\bar{x},\lambda)+\overline{w}_\lambda^{(3)}(\bar{x},\lambda)+\overline{w}_\lambda^{(4)}(\bar{x},\lambda)+\overline{w}_\lambda^{(5)}(\bar{x},\lambda) = 0$$

The integro-differential equation for the ring vortex distribution has been solved with the aid of numerical calculations (see Appendix B).

In the same way we can determine the ring vortex distributions $\bar{h}_d(\xi)$ and $\bar{h}_m(\xi)$ by the source distribution and the sinusoidal ring vortex distributions respectively along the shroud, with the aid of the following relations:

$$\bar{W}_n^{(s)}(\bar{x},\lambda) + \bar{W}_n^{(s)}(\bar{x},\lambda) = 0$$

$$\bar{W}_n^{(s,m)}(\bar{x},\lambda) + \bar{W}^{(s,m)}(\bar{x},\lambda) = 0$$

4.3. Calculation of the frictionless torque and thrust.

4.3.1. Torque and thrust of the propeller.

The propeller is replaced by a disk with a continuous bound vortex distribution. The strength of the vortices per area unit is:

$$\gamma(r) = \frac{R_1}{r}\,\gamma(R_1)$$

Assume the propeller to possess 2 blades and let each blade be represented by a lifting line. The vortex strength along a lifting line is:

$$\Gamma = \frac{2\pi r}{z}\cdot\frac{R_1}{r}\cdot\gamma(R_1) = \frac{2\pi R_1}{z}\,\gamma(R_1)$$

The relative velocity of the flow with respect to a propeller blade is according to the linearized theory (see also the figure below):

$$V(r) = \left[u^2 + \omega^2 r^2 + 2u\,w_a(o,r) + 2\omega r\,w_t(o,r)\right]^{1/2}$$

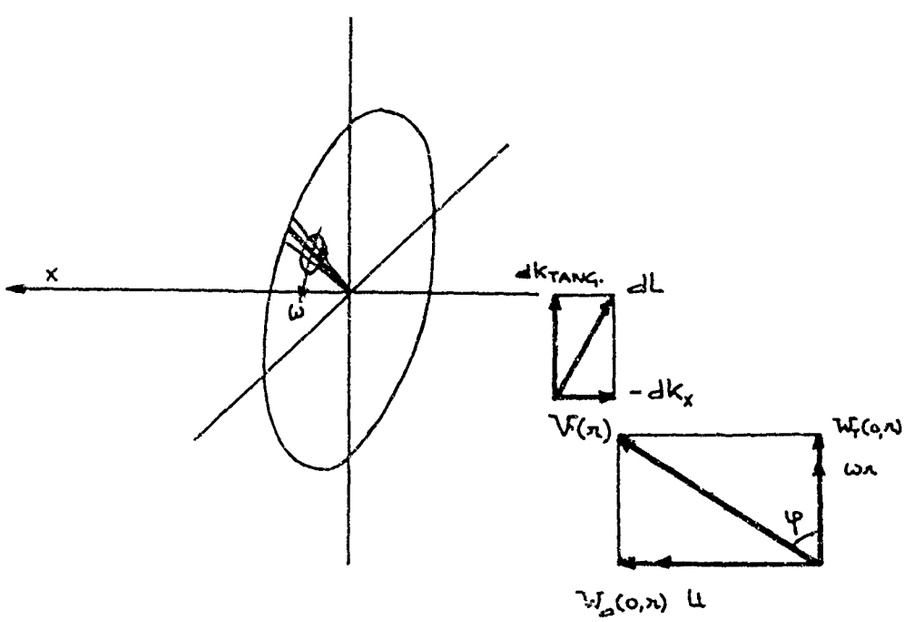

The lift on a propeller blade at a radius r is

$$dL = \varsigma V(r) \frac{2\pi R_1}{z} \gamma(R_1)\, dr$$

thus

$$dK_x = -dL\cos\varphi = -\varsigma \frac{2\pi R_1}{z} \gamma(R_1)\, dr\, [\omega r + w_r(o,r)]$$

$$dk_{TANG} = dL\sin\varphi = \varsigma \frac{2\pi R_1}{z} \gamma(R_1)\, dr\, [U + w_a(o,r)]$$

The total thrust of the propeller is:

$$k^{(i)} = -z \int_{R_o}^{R_1} dk_x$$

or

$$k^{(i)} = \pi\varsigma\omega R_1 \gamma(R_1)(R_1^2 - R_o^2) + 2\pi\varsigma R_1 \gamma(R_1) \int_{R_o}^{R_1} w_r(o,r)\, dr$$

The total torque of the propeller is:

$$M = z \int_{R_o}^{R_1} r\, dk_{TANG}$$

or

$$M = \pi\varsigma R_1 \gamma(R_1)(R_1^2 - R_o^2) U + 2\pi\varsigma R_1 \gamma(R_1) \int_{R_o}^{R_1} w_a(o,r)\, r\, dr$$

$w_a(o,r)$ and $w_r(o,r)$ are the average induced velocities at the point (o,r,φ).

4.3.2. Thrust on the shroud.

In order to calculate the thrust on the shroud it is convenient to consider first the forces on the element $dx R_1 d\varphi$ (see the Figure).

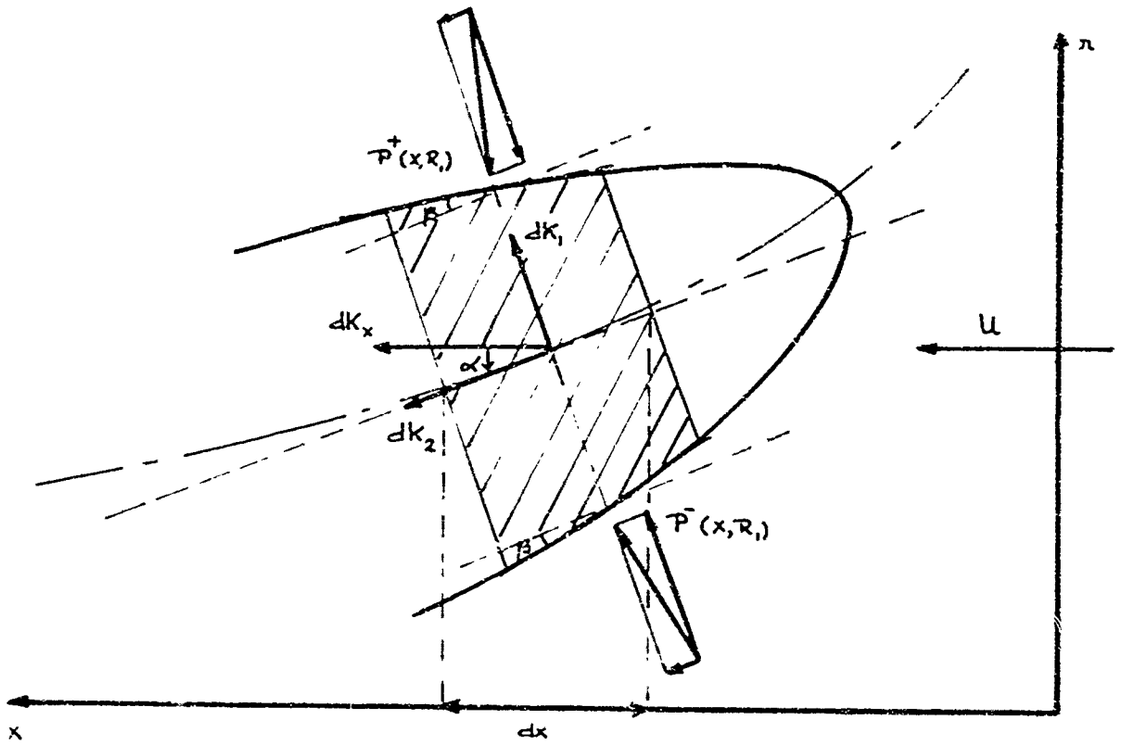

The average radial velocity at the shroud gives the slope of the camberline.

$$\text{Tg } \alpha(x) = \frac{W_r(x,R_1)}{u}$$

According to the linearized theory is

$$\sin \alpha(x) \simeq \frac{W_r(x,R_1)}{u}$$

$$\cos \alpha(x) \simeq 1$$

The thickness form of the shroud is given by $H(x)$
According to the linearized theory is

$$\sin \beta \simeq \frac{dH(x)}{dx}$$

$$\cos \beta \simeq 1$$

The static pressures along the inner- and the outer surface of the shroud are defined by $p^-(x,R_1)$ and $p^+(x,R_1)$ respectively. The forces on the element $dx R_1 d\psi$ of the shroud are:

$$dK_1 = \left[p^-(x,R_1) - p^+(x,R_1)\right] R_1 dx d\psi$$

$$dK_x = \left[p^-(x,R_1) + p^+(x,R_1)\right] \frac{dH(x)}{dx} R_1 dx d\psi$$

The force in the x-direction is:

$$dk_x = - dK_1 \frac{W_a(x,R_1)}{u} + dk_2$$

The total thrust on the shroud is equal to:

$$K^{(2)} = - \int_0^{2\pi} \int_{-b}^{-b+L} dk_x$$

After carrying out the integration over ψ , the thrust on the shroud becomes:

$$K^{(2)} = 2\pi R_1 \int_{-b}^{b+L} \frac{W_a(x,R_1)}{u} \left[p^-(x,R_1) - p^+(x,R_1) \right] dx +$$

$$- 2\pi R_1 \int_{-b}^{b+L} \frac{dH(x)}{dx} \left[p^-(x,R_1) + p^+(x,R_1) \right] dx$$

With the aid of Bernoulli's theorem the pressure distribution can be calculated from the velocity distribution along the shroud.
Derivation of the pressure distribution along the outer and the inner surface of the shroud give respectively:

$$p^+(x,R_1) = p_\infty - \tfrac{1}{2} \rho u^2 \frac{2W_a^+(x,R_1)}{u}$$

$$p^-(x,R_1) = p_\infty + k \rho \omega R_1 \gamma(R_1) - \tfrac{1}{2} \rho u^2 \frac{2W_a^-(x,R_1)}{u}$$

The Bernoulli constant of a streamline changes at the place of the propeller disk. The expression $k \rho \omega R_1 \gamma(R_1)$ mentioned above represents the jump in static pressure at the propeller disk. k satisfies the condition:

$k = 0 \qquad x < 0$

$k = 1 \qquad x > 0$

$W_a^+(x,R_1)$ and $W_a^-(x,R_1)$ are the axial induced velocities along the outer- and the inner surface of the shroud respectively. $W_a^+(x,R_1)$ and $W_a^-(x,R_1)$ are equal to the average axial induced velocities corrected with the drop in the axial velocities induced by the ring vortex distributions along the shroud.

The induced axial velocities are given by

$$W_a^+(x,R_1) = W_a(x,R_1) - \frac{1}{2}\left[\left\{\frac{\mu\gamma(R_1)}{2\sqrt{a(1-a)}}\sin\theta\right\}_{-b\leq x<0}^{+} + \left\{\mu\gamma(R_1)\right\}_{0\leq x\leq -b+L} + \left\{\sum_m \gamma_m(R_1)\sin m\theta\right\}_{-b\leq x\leq -b+L}\right].$$

$$W_a^-(x,R_1) = W_a(x,R_1) + \frac{1}{2}\left[\left\{\frac{\mu\gamma(R_1)}{2\sqrt{a(1-a)}}\sin\theta\right\}_{-b\leq x<0}^{+} + \left\{\mu\gamma(R_1)\right\}_{0\leq x\leq -b+L} + \left\{\sum_m \gamma_m(R_1)\sin m\theta\right\}_{-b\leq x\leq -b+L}\right].$$

The relations for the pressure distributions become:

$$p^-(x,R_1) - p^+(x,R_1) = k\,\rho\omega R_1\gamma(R_1) - \rho u\left[\left\{\frac{\mu\gamma(R_1)}{2\sqrt{a(1-a)}}\sin\theta\right\}_{-b\leq x<0}^{+} + \left\{\mu\gamma(R_1)\right\}_{0\leq x\leq -b+L} + \left\{\sum_m \gamma_m(R_1)\sin m\theta\right\}_{-b\leq x\leq -b+L}\right]$$

and

$$p^-(x,R_1) + p^+(x,R_1) = 2p_\infty + k\,\rho\omega R_1\gamma(R_1) - \rho u\, 2W_a(x,R_1)$$

The total thrust on the shroud becomes:

$$K^{(2)} = -2\pi R_1\rho u\frac{\mu\gamma(R_1)}{2\sqrt{a(1-a)}}\int_{-b}^{0}\frac{W_n(x,R_1)}{u}\sin\theta\,dx + -2\pi R_1\rho u\sum_m\gamma_m(R_1)\int_{-b}^{-b+L}\frac{W_n(x,R_1)}{u}\sin m\theta\,dx +$$

$$+ 2\pi R_1\rho\omega R_1\gamma(R_1)H(0) +$$

$$+ 2\pi R_1\rho u^2\, 2\int_{-b}^{-b+L}\frac{dH(x)}{dx}W_a(x,R_1)\,dx$$

where use is made of the following relations:

$$\int_{-b}^{-b+L}\frac{dH(x)}{dx}\,dx = 0$$

$$\int_{-b}^{-b+L}k\,\frac{dH(x)}{dx}\,dx = -H(0)$$

4.3.3. Thrust on the hub.

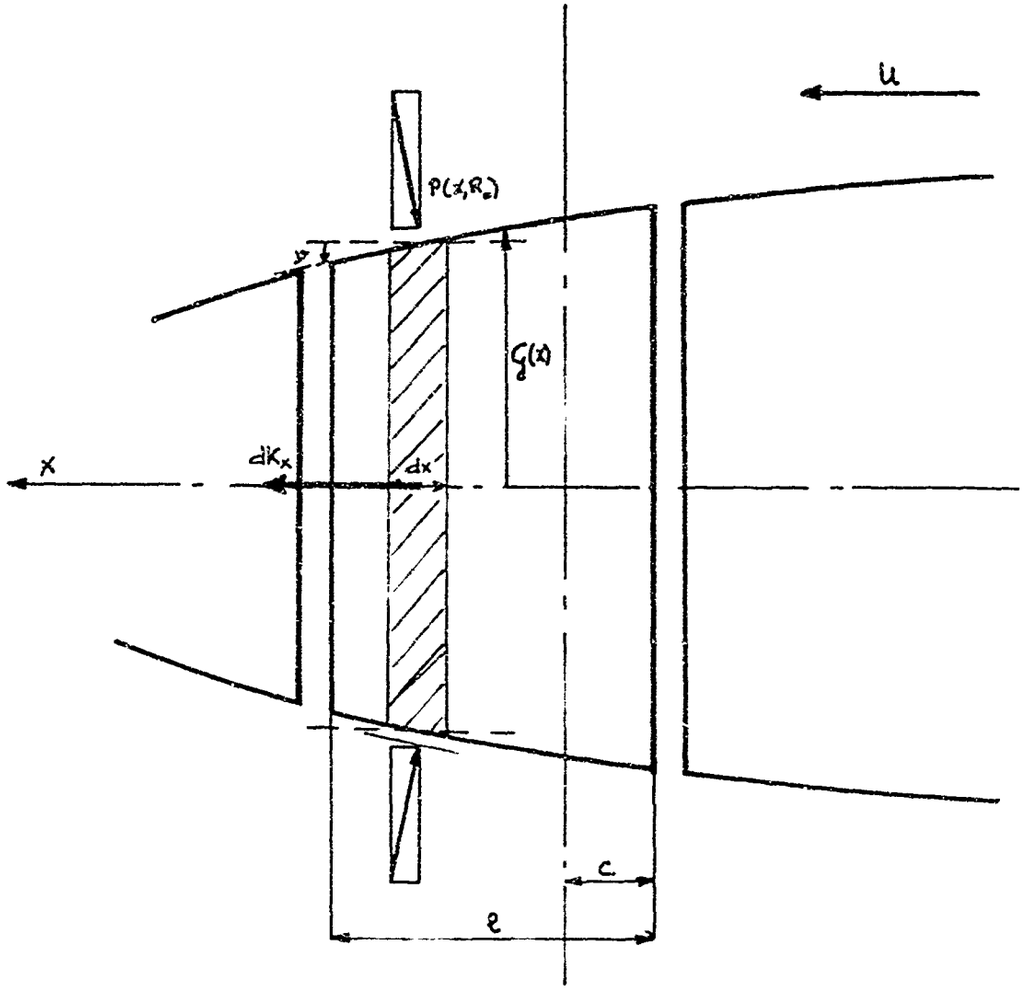

In order to calculate the thrust on the hub it is convenient to consider first the force on the element $dx R_0 d\psi$

The shape of the hub is given by $\zeta(x)$.

According to the linearized theory is:

$$\tan\vartheta \approx \sin\vartheta \approx \frac{d\zeta(x)}{dx}$$

$$\cos\vartheta \approx 1$$

The pressure distribution along the hub is defined by $P(x,R_0)$. The force on the element $\zeta(x)\,d\psi\,dx$ of the hub in the x-direction is than:

$$dK_x = P(x,R_0)\,\frac{d\zeta(x)}{dx}\,\zeta(x)\,d\psi\,dx$$

or after carrying out the integration over ψ:

$$dK_x = 2\pi P(x,R_0)\,\frac{d\zeta(x)}{dx}\,\zeta_j(x)\,dx$$

With the aid of Bernoulli's theorem the pressure distribution can be calculated from the velocity distribution along the hub. The pressure distribution is given by

$$P(x,R_0) = P_\infty + k\,\rho\omega R_1\,\gamma(R_1) - \tfrac{1}{2}\rho u^2\,\frac{2W_a^+(x,R_0)}{u}$$

The expression $k\rho\omega R_1\gamma(R_1)$ represents the effect of the pressure increase along a streamline at the place of the propeller disk. k satisfies the condition mentioned in section 4.3.2.

The axial induced velocity along the hub is defined by $W_a^+(x,R_0)$. The total velocity $W_a^+(x,R_0)$ consists of the average induced axial velocity $W_a(x,R_0)$ and the drop in axial velocity induced by the ring vortex distributions along the hub.
The axial induced velocity is given by:

$$W_a^+(x,R_0) = W_a(x,R_0) + \tfrac{1}{2}\left[\left\{\mu\gamma(R_1)\right\}_{0\le x\le -c+e} + \left\{h_0(x) + h_d(x) + \sum_m h_m(x)\right\}_{-\infty<x<\infty}\right]$$

The thrust on the hub corrected with the force acting on the hub in the case of a non-operating propeller becomes:

$$K^{(1)} = \frac{\pi}{2}\rho\omega R_1\gamma(R_1)\left[\zeta_j^2(0) - \zeta_j^2(-c+e)\right] + 2\pi\rho u\int_{-c}^{-c+e}\frac{d\zeta(x)}{dx}\,\zeta_j(x)\,W_a(x,R_0)\,dx + \pi\rho u\int_{-c}^{-c+e}\frac{d\zeta(x)}{dx}\,\zeta_j(x)\left[h_0(x) + h_d(x) + \sum_m h_m(x)\right]dx$$

where use is made of the following relations:

$$\int_{-c}^{-c+\ell} \frac{dG(x)}{dx}\, G(x)\, dx = \frac{1}{2}\left[G^2(-c+\ell) - G^2(-c)\right]$$

$$\int_{-c}^{-c+\ell} x \frac{dG(x)}{dx}\, G(x)\, dx = \frac{1}{2}\left[G^2(-c+\ell) - G^2(0)\right]$$

and $\quad G(0) = R_0$

4.3.4. Calculation of torque, total thrust and efficiency.

The relations for the torque and thrust as derived in the previous sections are made non-dimensional in the way as described in section 4.2.2. and further with

$$\bar{H}(x) = \frac{H(x)}{R_1} \qquad \bar{G}(x) = \frac{G(x)}{R_1}$$

$$\alpha = \frac{c}{\ell} \qquad \xi = \frac{\ell}{R_1}$$

The non-dimensional torque and thrust coefficients are defined by

$$K_T = \frac{k}{\rho n^2 D^4} = \frac{\pi^2}{4} \cdot \frac{k}{\rho \omega^2 R_1^4}$$

$$K_Q = \frac{M}{\rho n^2 D^5} = \frac{\pi^2}{8} \cdot \frac{M}{\rho \omega^2 R_1^5}$$

The torque coefficient becomes:

$$K_Q^{(1)} = \frac{\pi^3}{8} \cdot \frac{(1-\bar{X}^2)\bar{\gamma}}{\mu^2} + \frac{\pi^3}{4} \cdot \frac{\bar{\gamma}}{\mu^2} \int_{\lambda}^{1} \bar{W}_a(0,\bar{r})\, \bar{r}\, d\bar{r}$$

The thrust coefficients of propeller, shroud and hub become respectively:

$$K_T^{(1)} = \frac{\pi^3}{4} \cdot \frac{\bar{\gamma}(1-\bar{X})}{\mu} + \frac{\pi^3}{2} \cdot \frac{\bar{\gamma}}{\mu^2} \int_{\lambda}^{1} \bar{W}_T(0,\bar{r})\, d\bar{r}$$

$$K_T^{(2)} = -\frac{\pi^3}{4} \cdot \frac{\bar{\gamma}}{\mu\sqrt{a(1-a)}} \int_{-a\gamma}^{0} \bar{W}_n(\bar{x},1) \sin\theta\, d\bar{x} +$$

$$- \frac{\pi^3}{2} \sum_m \frac{\bar{\gamma}_m}{\mu^2} \int_{-a\eta}^{(1-a)\eta} \overline{W}_n(\bar{x},1) \sin m\theta \, d\bar{x} +$$

$$+ \frac{\pi^3}{2} \cdot \frac{\bar{\gamma}}{\mu} \bar{H}(0) + \frac{\pi^3}{\mu^2} \int_{-a\eta}^{(1-a)\eta} \frac{d\bar{H}(\bar{x})}{d\bar{x}} \overline{W}_a(\bar{x},1) \, d\bar{x}$$

$$K_T^{(3)} = + \frac{\pi^3}{8} \cdot \frac{\bar{\gamma}\{\bar{\lambda}^2 - \bar{G}_\gamma^2[(1-d)\zeta]\}}{\mu} +$$

$$+ \frac{\pi^3}{2\mu^2} \int_{-d\zeta}^{(1-d)\zeta} \frac{d\bar{G}_\gamma(\bar{x})}{d\bar{x}} \bar{G}_\gamma(\bar{x}) \overline{W}_a(\bar{x},\lambda) \, d\bar{x} +$$

$$+ \frac{\pi^3}{4} \cdot \frac{1}{\mu^2} \cdot \int_{-d\zeta}^{(1-d)\zeta} \frac{d\bar{G}_\gamma(\bar{x})}{d\bar{x}} \bar{G}_\gamma(\bar{x}) \left[\bar{h}_0(\bar{x}) + \bar{h}_d(\bar{x}) + \sum_m \bar{h}_m(x)\right] d\bar{x}$$

The total thrust coefficients becomes:

$$K_T = K_T^{(1)} + K_T^{(2)} + K_T^{(3)}$$

The efficiency of the propulsion device is defined by :

$$\eta_o = \frac{1}{2\mu} \cdot \frac{K_T}{K_Q}$$

A numerical program for the N.S.M.B.-digital computer has been made to calculate the thrust and torque coefficients and the efficiency of the large hub to diameter ratio propeller based on the above derived expressions. (see Appendix B, Numerical program no. 2).

4.3.5. Calculation of the camberline of the shroud.

The shape of the camberline of the shroud can be derived from the average radial velocities along the shroud.
The shape of the shroud is defined by $\bar{s}(\bar{x})$, the distance between a cylinder of constant diameter (radius R_1) and the camberline. (see also the Figure)

The function $\bar{S}(\bar{x})$ is given by

$$\frac{d\bar{S}(\bar{x})}{d\bar{x}} = \overline{W}_{s}(\bar{x},1)$$

OR

$$\bar{S}(x_1) = \int_0^{x_1} \overline{W}_{s}(\bar{x},1)\, d\bar{x}$$

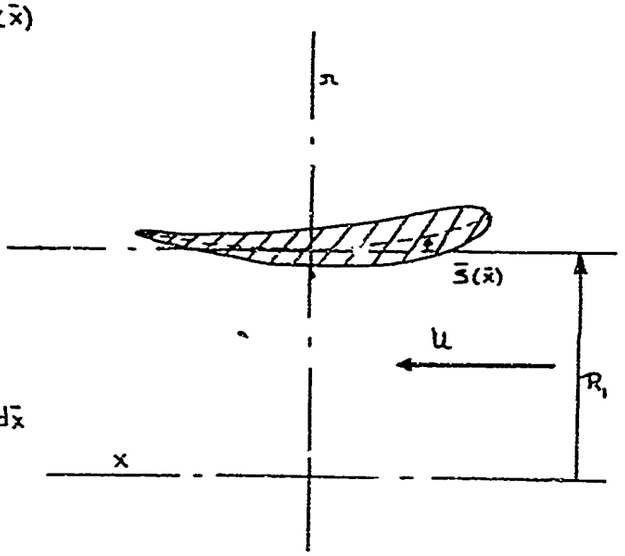

The values of x_1 are situated between $-a\eta$ and $(1-a)\eta$.

4.3.6. Pressure distribution along the shroud.

The pressure distributions along the inner- and the outer surface of the shroud are derived in section 4.3.2. The expressions for the pressure distributions are made non-dimensional in the usual way (see sections 4.2.2. and 4.3.4.).
The pressure coefficients $\Delta\bar{p}^{+}(x)$ and $\Delta\bar{p}^{-}(x)$ are defined by:

$$\Delta\bar{p}^{+}(\bar{x}) = \frac{\bar{p}^{+}(\bar{x},1) - p_{\infty}}{\frac{1}{2}\rho u^2}$$

$$\Delta\bar{p}^{-}(\bar{x}) = \frac{\bar{p}^{-}(\bar{x},1) - p_{\infty}}{\frac{1}{2}\rho u^2}$$

The pressure coefficients become:

$$\Delta\bar{p}^{+}(\bar{x}) = -2\overline{W}_{a}(\bar{x},1) + \left[\frac{\mu\bar{\gamma}}{2\sqrt{a(1-a)}}\sin\theta\right]_{-a\eta \le \bar{x} < 0} +$$

$$+ \left[\mu\bar{\gamma}\right]_{0 < \bar{x} \le (1-a)\eta} + \left[\sum_m \bar{\gamma}_m \sin m\theta\right]_{-a\eta \le \bar{x} \le (1-a)\eta}$$

$$\Delta\bar{p}^{-}(\bar{x}) = -2\overline{W}_{a}(\bar{x},1) - \left[\frac{\mu\bar{\gamma}}{2\sqrt{a(1-a)}}\sin\theta\right]_{-a\eta \le \bar{x} < 0} +$$

$$+ \left[\mu\bar{\gamma}\right]_{0 < \bar{x} \le (1-a)\eta} - \left[\sum_m \bar{\gamma}_m \sin m\theta\right]_{-a\eta \le \bar{x} \le (1-a)\eta}$$

A numerical program for the N.S.M.B.-digital computer has been made to calculate the camberline and the pressure coefficients with the above derived relations (see Appendix B).

4.4. Effect of drag on torque, thrust and efficiency.

4.4.1. Drag of the propeller.

The average relative velocity of the flow with respect to a propeller blade is according to the linearized theory.

$$V(r) = \left(u^2+\omega^2r^2\right)^{1/2}\cdot\left[1+\frac{u}{u^2+\omega^2r^2}w_a(o,r)+\frac{\omega r}{u^2+\omega^2r^2}w_t(o,r)\right].$$

The number of blades of the propeller is assumed to be equal to Z. The vortex strength along a lifting line by which a propeller blade can be replaced is

$$\Gamma = \frac{2\pi R_1}{z}\gamma(R_1)$$

The chord length and the maximum thickness of a section of a propeller blade are defined by $c(r)$ and $s^{(1)}(r)$ respectively.
The lift on a blade section at a radius r is per unit span:

$$L(r) = \rho V(r)\frac{2\pi R_1}{z}\gamma(R_1)$$

The lift coefficient becomes:

$$C_L(r) = \frac{L(r)}{\frac{1}{2}\rho V^2(r)\,c(r)} = \frac{4\pi R_1\gamma(R_1)}{zV(r)\,c(r)}$$

The value of the drag coefficient $C_d^{(1)}(r)$ as a function of the Reynolds number, the lift coefficient and the maximum thickness of the blade section, can be obtained from the experimental results on two dimensional streamlined foils as collected by Hoerner [2] . (see section 4.4.4.)

The drag of a blade section at a radius r is:

$$dW(r) = \tfrac{1}{2}\rho V^2(r)\, c(r)\, c_d^{(i)}(r)\, dr$$

The drag of the blade section in axial- and in circumferential direction are according to the linearized theory.

$$dW_{AX}(r) = \tfrac{1}{2}\rho u^2 c(r) c_d^{(i)}(r) \left(1+\frac{\mu^2 r^2}{R_1^2}\right)^{1/2} \cdot \left[1 + \frac{2+\frac{\mu^2 r^2}{R_1^2}}{1+\frac{\mu^2 r^2}{R_1^2}} \cdot \frac{w_a(0,r)}{u} + \right.$$
$$\left. + \frac{\frac{\mu r}{R_1}}{1+\frac{\mu^2 r^2}{R_1^2}} \cdot \frac{w_t(0,r)}{u} \right] dr$$

$$dW_{TANG.}(r) = \tfrac{1}{2}\rho u^2 c(r) c_d^{(i)}(r) \left(1+\frac{\mu^2 r^2}{R_1^2}\right)^{1/2} \left[1 + \frac{1}{1+\frac{\mu^2 r^2}{R_1^2}} \cdot \frac{w_a(0,r)}{u} + \right.$$
$$\left. + \frac{1+2\frac{\mu^2 r^2}{R_1^2}}{1+\frac{\mu^2 r^2}{R_1^2}} \cdot \frac{w_t(0,r)}{u} \right] dr$$

The decrease of the propeller thrust by the drag is:

$$K_W^{(i)} = z \int_{R_0}^{R_1} dW_{AX}(r)$$

or

$$K_W^{(i)} = z \cdot \tfrac{1}{2}\rho u^2 \int_{R_0}^{R_1} c(r) c_d^{(i)}(r) \left(1+\frac{\mu^2 r^2}{R_1^2}\right)^{1/2} \left[1 + \frac{2+\frac{\mu^2 r^2}{R_1^2}}{1+\frac{\mu^2 r^2}{R_1^2}} \cdot \frac{w_a(0,r)}{u} + \right.$$
$$\left. + \frac{\frac{\mu r}{R_1^2}}{1+\frac{\mu^2 r^2}{R_1^2}} \cdot \frac{w_t(0,r)}{u} \right] dr$$

The increase of the propeller torque due to the drag is:

$$M_W^{(i)} = z \int_{R_0}^{R_1} r\, dW_{TANG.}(r)$$

or

$$M_w^{(1)} = -\tfrac{1}{2}\rho U^2 \int_{R_0}^{R_1} c(r)\, c_d^{(1)}(r)\, \frac{\mu r}{R_1}\left(1+\frac{\mu^2 r^2}{R_1^2}\right)^{1/2}\left[1+\frac{1}{1+\frac{\mu^2 r^2}{R_1^2}}\cdot\frac{W_a(0,r)}{U}+\right.$$
$$\left.+\frac{1+2\frac{\mu^2 r^2}{R_1^2}}{1+\frac{\mu^2 r^2}{R_1^2}}\cdot\frac{W_T(0,r)}{U}\right] r\,dr$$

4.4.2. Drag of the shroud.

The average axial velocity along the shroud is according to the linearized theory:

$$V_{gem} = U + \frac{1}{L}\int_{-b}^{-b+L} W_a(x,R_1)\,dx$$

The value of the drag coefficient $c_d^{(2)}$ of the shroud as a function of the Reynolds number and the maximum thickness of the shroud profile can be obtained from the experimental results, collected by Hoerner [2] (see section 4.4.4.).
The induced drag is already taken into account, because in 4.3. the pressure on the shroud has been calculated.
The drag of the shroud becomes:

$$K_w^{(2)} = \tfrac{1}{2}\rho V_{gem}^2\, c_d^{(2)}\, L\, 2\pi R_1 = \pi\rho c_d^{(2)} L R_1 U^2\left[1+\frac{2}{L}\int_{-b}^{-b+L}\frac{W_a(x,R_1)}{U}\,dx\right]$$

4.4.3. Drag of the hub.

The axial velocity along the hub at the place of the propeller disk is:

$$V = U + W_a(0,\lambda)$$

The wetted area (o) of the hub is given by the following relation:

$$O = 2\pi\int_{-c}^{-c+\ell} G_g(x)\sqrt{1+\left[\frac{dG_g(x)}{dx}\right]^2}\,dx$$

Only the skin friction drag coefficient $c_d^{(3)}$ has to be taken into account for the calculation of the drag of the hub (see section 4.4.4.).

The drag of the hub due to the skin friction becomes:

$$K_w^{(3)} = \tfrac{1}{2}\rho u^2 . c_d^{(3)} . O \left[1 + 2\frac{w_a(o,\lambda)}{u}\right]$$

4.4.4. Calculation of the drag coefficients.

The values of the drag coefficients $c_d^{(1)}(r)$; $c_d^{(2)}$ and $c_d^{(3)}$ can be obtained from the experimental results collected by Hoerner.

The flow around propeller blades and along hub and shroud is fully turbulent because the value of the Reynolds number based on the profile length is beyond 10^7.

The drag coefficient in this region of Reynolds numbers is expressed by the following empiric relation (see Hoerner):

$$c_d = 2 c_f \left\{1 + 2s + \frac{c_l^2}{16}\right\}$$

The parameter c_f is the turbulent skin-friction drag coefficient.

The drag coefficient $c_d^{(1)}(r)$ as mentioned in section 4.4.1. becomes:

$$c_d^{(1)}(r) = 2 c_f^{(1)}(r) \left\{1 + 2s^{(1)}(r) + \frac{c_l^2(r)}{16}\right\}$$

The skin-driction drag coefficient $c_f^{(1)}(r)$ can be obtained with the aid of the following empiric relation:

$$c_f^{(1)}(r) = 0.455 \left[\log\left\{(1+\eta^2 r^2)^{1/2} c(r) \frac{uR_1}{\nu}\right\}\right]^{-2.58}$$

The effect of the induced velocities on the value of the Reynolds number is neglected.

The drag coefficient $c_d^{(2)}$ becomes:

$$c_d^{(2)} = 2 c_f^{(2)} \left[1 + 2s^{(2)}\right]$$

$C_f^{(2)}$ can be obtained with the following empiric relation:

$$C_f^{(2)} = 0.455 \left[\log \left(\eta \frac{uR_1}{\nu} \right) \right]^{-2.58}$$

The effect of the induced velocities on the value of the Reynolds number is neglected.

The drag coefficient $C_d^{(3)}$ becomes:

$$C_d^{(3)} = C_f^{(3)} = 0.455 \left[\log \left\{ \zeta \frac{uR_1}{\nu} \right\} \right]^{-2.58}$$

4.4.5. Effect of drag on torque, thrust and efficiency.

The relations for the torque and thrust due to the drag as derived in the previous sections are made non-dimensional in the way as described in the sections 4.2.2. and 4.3.4.
The non-dimensional torque and thrust coefficients due to drag are defined by

$$K_{T_W} = \frac{\pi^2}{4} \cdot \frac{K_W}{\rho \omega^2 R_1^4}$$

$$K_{Q_W} = \frac{\pi^2}{8} \cdot \frac{M_W}{\rho \omega^2 R_1^5}$$

The torque coefficient of the propeller due to drag becomes:

$$K_{Q_W} = \frac{\pi^2}{16} \cdot \frac{z}{\mu} \int_\lambda^1 \bar{c}(r)\, C_d^{(1)}(r) \left(1+\mu^2\bar{r}^2\right)^{1/2} \cdot \left[1 + \frac{1}{1+\mu^2\bar{r}^2} \overline{W_a}(0,\bar{r}) + \right.$$

$$\left. + \frac{1+2\mu^2\bar{r}^2}{1+\mu^2\bar{r}^2} \cdot W_t(0,\bar{r}) \right] dr$$

The thrust coefficients of the propeller, shroud and hub due to drag become:

$$K_{S_w}^{(1)} = \frac{\pi^2}{8}\frac{z}{\mu^2}\int_{\lambda}^{1} \bar{c}(\bar{r})\, c_d^{(1)}(\bar{r})\,(1+\mu^2\bar{r}^2)^{1/2}\left[1+\frac{2+\mu^2\bar{r}^2}{1+\mu^2\bar{r}^2}\,\overline{w}_a(0,\bar{r}) + \frac{\mu\bar{r}}{1+\mu^2\bar{r}^2}\,\overline{w}_T(0,\bar{r})\right] d\bar{r}$$

$$K_{S_w}^{(2)} = \frac{\pi^3}{4}\frac{\eta c_d^{(2)}}{\mu^2}\left[1+\frac{2}{\eta}\int_{-a\eta}^{(1-a)\eta}\overline{w}_a(\bar{x},1)\,d\bar{x}\right]$$

$$K_{S_w}^{(3)} = \frac{\pi^3}{4}\frac{c_d^{(3)}}{\mu^2}\left[1+2\overline{w}_a(0,\lambda)\right]\int_{-d\zeta}^{(1-d)\zeta}\bar{\zeta}_d(\bar{x})\sqrt{1+\bar{\zeta}_d^2(\bar{x})}\,d\bar{x}.$$

The total thrust of the propulsion device including the effect of the drag is:

$$K_{S_{TOT}} = K_S^{(1)} + K_S^{(2)} + K_S^{(3)} - K_{S_w}^{(1)} - K_{S_w}^{(2)} - K_{S_w}^{(3)}$$

The torque becomes:

$$K_{Q_T} = K_{Q_0}^{(1)} + K_{Q_w}^{(1)}$$

The efficiency of the propulsion device including the effect of the drag is defined by η_ω, thus

$$\eta_\omega = \frac{1}{2\mu}\,\frac{K_{T_{TOT.}}}{K_{Q_{TOT.}}}$$

A numerical program for the N.S.M.B.-digital computer has been made to calculate the thrust, torque and efficiency of the propeller including the effect of the drag based on the relations as derived in the previous sections. (see Appendix B, Numerical program no. 3).

4.5. Presentation and discussion of the computation results.

With the aid of the theoretical analysis developed by the N.S.M.B. the propeller torque, thrust and efficiency, the camberline of the shroud and the pressure distribution along the shroud can be calculated for the chosen values of design parameters.
The design of the propeller can be optimized with respect to efficiency for instance by a systematical variation of the design parameters.

The numerical program for the N.S.M.B. digital computer based on this theory was divided into the following parts:
part 1. Calculation of the propeller flow field
part 2. Calculation of the torque, thrust and efficiency
part 3. Calculation of the effect of drag on the torque, thrust and efficiency.

At this moment only part 1 of the numerical program is finished. The camberline of the shroud and the pressure distribution along the shroud can be calculated easily if the propeller flow field is known.

To illustrate the possibilities of part 1 of the numerical program we will give a series of shroud shapes for which the velocities at the propeller disk increases. In order to increase systematically the velocities at the propeller disk, the loading of the shroud was varied. The data used for the design parameters and the assumed propeller loading are:

1. $\eta = 0.36$
2. $a = 0.60$
3. $\Lambda = 1.35$
4. $K_T = 0.10$
5. $\lambda = 0.80$
6. the shroud has a NASA 0007 basic thickness form.

These data are chosen similar to the propellers of the T.P.S.
The strength of the continuous bound vortex distribution representing the propeller, is chosen in accordance with the value of the thrust coefficient K_T.

The strength of the vortex distribution along the shroud is chosen sinusoidal (see $\gamma_1(R_1)$ in Figure 4.2.). The amplitude of the vortex strength is varied systematically. Shroud no. 1 (see the Figures 4.3 and 4.4) has an unloaded camber. Shrouds no. 2 and no. 3 have systematically increasing loadings of the camber lines, resulting in increasing velocities and a decreasing static pressure at the propeller location.

The calculations, carried out according to the theory developed by the N.S.M.B., lead to results which are given in the Figures 4.3 and 4.4 and table 4.1.

The shape of the camberline according to the loading of the shroud is given in Figure 4.3 and tabulated in table 4.1. The shape of the camberlines is given with respect to a cylinder of constant diameter representing the shroud of the mathematical model.

Figure 4.4. shwos the static pressure coefficients $C_p^+(x)$ and $C_p^-(x)$ along the nozzle with the loading of the nozzle as parameter. The static pressure coefficients $C_p^+(x)$ and $C_p^-(x)$ are defined by:

$$C_p^+(x) = \frac{p^+(x) - p_\infty}{\frac{1}{2}\rho U^2}$$

$$C_p^-(x) = \frac{p^-(x) - p_\infty}{\frac{1}{2}\rho U^2}$$

p_∞ and U are the static pressure and the velocity of the undisturbed flow respectively. $p^+(x)$ and $p^-(x)$ are the static pressure at respectively the inner and the outer side of the shroud at a location x.

The shrouds have shock-free entry because the vortex strength at the leading edge of the shroud equals zero.

The shroud shape of the T.P.S. propeller is, for comparison with the calculated series of shroud shapes, also given in Figure 4.3. The shrouded forward- and the shrouded aft propeller configurations of the T.P.S. are given in the Figures 4.5 and 4.6. In these figures is also given the calculated shroud shape.

After completion of parts 2 and 3 of the numerical program we can define the propeller characteristics (thrust, torque and efficiency) and judge the characteristics of the T.P.S. propellers.

5. Conclusions and suggestions for further research.

The most important conclusions which can be drawn from the experimental results are:

1. the magnitude of the transverse forces is for low values of Λ equal to around 10 % of the thrust and increases by an appreciable amount if the velocity is increased.
2. the direction of the transverse force changes by an appreciable amount if the velocity is increased.
3. side forces opposed to those generated by the propeller are experienced by the body as a consequence of the sideways deflection of the propeller yet.
   Especially in the case of the forward propeller therefore a drastic reduction in the generated side forces has been found if compared with the aft propeller.
4. the generation of the side forces is accompanied by a decrease in thrust and an increase in propeller torque.
   For low values of the propeller torque the increase in the torque due to cyclic pitch appeared to be large and for large values of the propeller torque the increase in torque due to cyclic pitch appeared to be small.
   Thus the required power for the propellers of the submarine will not be primarily defined by requirements concerning the maneuvrability.
5. the presence of a shroud does not have a large effect on the magnitude of the side forces. The direction of the side forces is somewhat effected by the presence of a shroud.

It seems advisible to extend the research in the following directions:

1. more detailed experiments must be carried out to examine the characteristics of the propellers as a manoeuvring device by low speed and large angles of attack of the submarine.
2. a more detailed determination of the interaction effects between propellers and submarine body and the mutual interaction effects between the propellers.

It has been concluded that it might be very difficult to determine ad hoc the shroud shapes for large hub to diameter ratio propellers. As starting point for further research it seems also advisible to optimize the shape of the shroud with respect to efficiency as a function of the design variables and the kind of body in combination with which the propeller will be used. Investigations to optimize the design of the shrouded large hub to diameter ratio propeller can be based on the theory developed by the N.S.M.B.

Wageningen, July 1964

Prof.Dr. J.D. van Manen
Principal Investigator.

References:

1. Joosen, W.P.A., J.D. van Manen and F. van der Walle:
"Large hub to diameter ratio propellers with programmed blade control".
Int. Shipbuilding Progress, January 1963.

2. Hoerner, S.F.:
"Aerodynamic Drag", Published by the author, 1951.

3. Manen, J.D. van:
"Effect of radial load distribution on the performance of shrouded propellers".
Int. Shipbuilding Progress, May 1962.

4. Joosen, W.P.A.:
"The induced velocities at the blade of a tandem propeller with programmed blade control in a shroud".
N.S.M.B. Laboratory memorandum no. 3 (January 1962).

Appendix A.

Qualitative theoretical analysis of the side force direction.

Calculation of the flow field.

The calculation of the flow field of the large hub to diameter ratio propeller can be based on the following assumptions. The propeller moves steadily forward. The forward velocity is assumed to be sufficiently large and the blade loading sufficiently low to permit the application of linearized theory. The propeller is assumed to have an infinite number of blades. The mathematical model of the screw configuration can be composed by means of vortex distributions.

The propeller flow field is represented by a disk with a continuous bound vortex distribution of variable strength in circumferential direction. The vortex strength is constant along lifting lines in which we can split up the bound vorfex distribution. Assume the vortex strength per unit of area to be equal to:

$$\gamma(r,\varphi) = \gamma_0(r) + \gamma_1(r)\sin\varphi$$

and

$$\Gamma(r,\varphi) = \gamma(r,\varphi)\, r\, \Delta\varphi =$$

$$= \gamma(R_1,\varphi) R_1 \Delta\varphi = \text{const.}$$

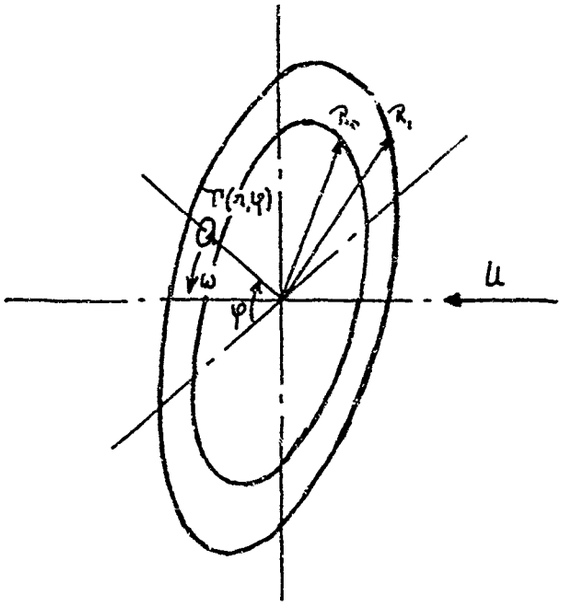

thus

$$\gamma(r,\varphi) = \frac{R_1}{r}\gamma(R,\varphi) = \frac{R_1}{r}\left[\gamma_0(R_1) + \gamma_1(R_1)\sin\varphi\right]$$

Further the propeller flow field consists of helical trailing vortices. Each trailing vortex line lies on a cylinder of constant diameter (equal to blade tips- or hub diameter) and has a constant pitch.

The effects of the helical trailing vortices and the vortex systems by which the hub and shroud can be replaced are not taken into account for the calculation of the induced velocities at the propeller disk. This analysis has only the intention to determine qualitatively side force direction. The most important contribution to the induced velocities at the propeller plane is given by the bound vortices for large values of Λ $[1.0 < \Lambda < 2.0]$.

According to the law of Biot and Savart, the axial- and circumferential induced velocities at the propeller due to the bound vortices can be calculated:

$$W_a(r,\varphi) = -\frac{1}{4\pi}\int_{R_0}^{R_1} dr_1 \int_{\varphi}^{\varphi+\pi} d\theta \; \frac{R_1\{\gamma_0(R_1)+\gamma_1(R_1)\sin\theta\}\, r\sin(\varphi-\theta)}{[r_1^2+r^2-2rr_1\cos(\varphi-\theta)]^{3/2}}$$

$$W_r(r,\varphi) = 0$$

The average induced velocity in axial direction becomes:

$$W_a(r,\varphi) = -\gamma_1(R_1)\cos\varphi \; C_1(r)$$

with

$$C_1(r) = \frac{1}{\pi}\int_{R_0}^{R_1} dr_1 \int_{0}^{\pi/2} d\psi \; \frac{rR_1\sin^2 2\psi}{[r_1^2+r^2+2rr_1\cos 2\psi]^{3/2}} \longrightarrow C_1(r) > 0$$

The parameter $C_1(r)$ is only a function of the propeller geometry.

<u>Calculation of the vortex strength distribution due to a given pitch variation.</u>

Assume, the (collective and cyclic) pitch of a propeller blade is given by:

$$\alpha = \alpha_0 + \alpha_1 \sin\varphi$$

The inclination angle of a propeller blade at a radius R_g $\left[R_g \approx \frac{R_1+R_0}{2}\right]$ is assumed to be decisive for the vortex strength along the lifting line by which the propeller is replaced. The vortex strength along the lifting line is assumed to be constant.

The mentioned assumptions are only permitted as $\frac{R_1 - R_2}{R_1} \ll 1$

The inclination angle $[\beta^{(i)}_{eff}]$ of a propeller blade at radius R_g becomes:

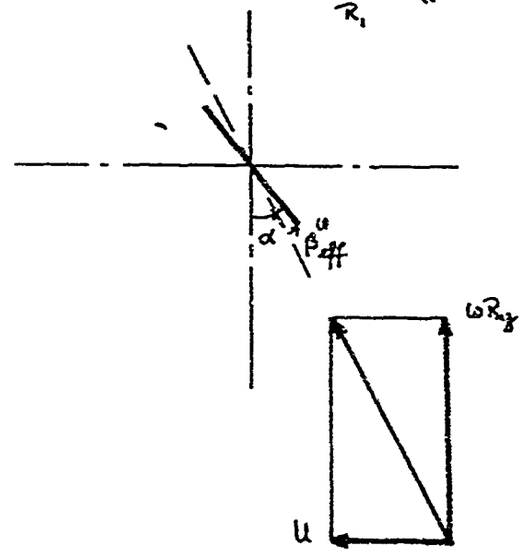

$$\beta^{(i)}_{eff} = \alpha_0 + \alpha_1 \sin\varphi - \operatorname{arctg} \frac{u}{\omega R_g}$$

The vortex strength is in first approximation and according to the two-dimensional theory:

$$\Gamma^{(i)}(R_g, \varphi) = \pi c V \left[\alpha_0 + \alpha_1 \sin\varphi - \operatorname{ARCTG} \frac{u}{\omega R_g}\right]$$

with $V = \sqrt{u^2 + \omega^2 R_g^2}$

The chord length and the number of propeller blades are defined by c and z respectively.

The vortex strength per area unit of the propeller disk becomes:

$$\gamma^{(i)}(R_1, \varphi) = \frac{z}{R_1} \gamma^{(i)}(r, \varphi) = \frac{R_g}{R_1} \gamma^{(i)}(R_g, \varphi) =$$

$$= \frac{z}{2\pi R_1} \Gamma^{(i)}(R_g, \varphi) = \frac{zcV}{2R_1} \left[\alpha_0 + \alpha_1 \sin\varphi - \operatorname{ARCTG} \frac{u}{\omega R_g}\right]$$

or

$$\gamma^{(i)}(R_1, \varphi) = \gamma^{(i)}_0(R_1) + \gamma^{(i)}_1(R_1) \sin\varphi$$

with

$$\gamma^{(i)}_0(R_1) = \frac{zcV}{2R_1} \left[\alpha_0 - \operatorname{ARCTG} \frac{u}{\omega R_g}\right]$$

$$\gamma^{(i)}_1(R_1) = \frac{zcV\alpha_1}{2R_1}$$

The bound vortex distribution $\gamma^{(1)}(r,\varphi)$ gives the following induced velocities at the propeller plane:

$$w_a(r,\varphi) = -\gamma_1^{(1)}(R_1)\cos\varphi\; C_1(r) = -\frac{zcV\alpha_1 C_1(r)}{2R_1}\cos\varphi$$

$$w_t(r,\varphi) = 0$$

With the aid of the calculated induced velocities and the given pitch variation, the bound vortex distribution at the propeller disk can be calculated in second approximation.
The effective inclination angle of a propeller blade becomes:

$$\beta_{eff.}^{(2)} = \alpha_0 + \alpha_1 \sin\varphi - \operatorname{arctg}\left[\frac{u+w_a(R_g,\varphi)}{\omega R_g}\right] =$$

$$\approx \alpha_0 + \alpha_1 \sin\varphi - \operatorname{arctg}\frac{u}{\omega R_g} - \frac{\omega R_g}{V^2}\cdot w_a(R_g,\varphi).$$

The vortex strength becomes according to the two-dimensional theory:

$$\Gamma^{(2)}(R_g,\varphi) = \pi c\left[\left\{u+w_a(R_g,\varphi)\right\}^2 + \omega^2 R_g^2\right]^{1/2}\cdot\left[\alpha_0 - \operatorname{arctg}\frac{u}{\omega R_g} + \right.$$

$$\left. + \alpha_0\sin\varphi + \frac{zc\omega R_g C_1(R_g)\alpha_1}{2VR_1}\cos\varphi\right].$$

or

$$\gamma^{(2)}(R_1,\varphi) = \gamma_0^{(2)}(R_1) + \gamma_1^{(2)}(R_1)\sin\varphi + \gamma_2^{(2)}(R_1)\cos\varphi$$

with

$$\gamma_0^{(2)}(R_1) = \gamma_0^{(1)}(R_1) = \frac{zcV}{2R}\left[\alpha_0 - \operatorname{arctg}\frac{u}{\omega R_g}\right]$$

$$\gamma_1^{(2)}(R_1) = \gamma_1^{(1)}(R_1) = \frac{zcV}{2R_1}\alpha_1$$

$$\gamma_2^{(2)}(R_1) = \frac{z^2c^2\omega R_g C_1(R_g)}{4R_1^2}\alpha_1$$

Calculation of the side forces due to cyclic pitch.

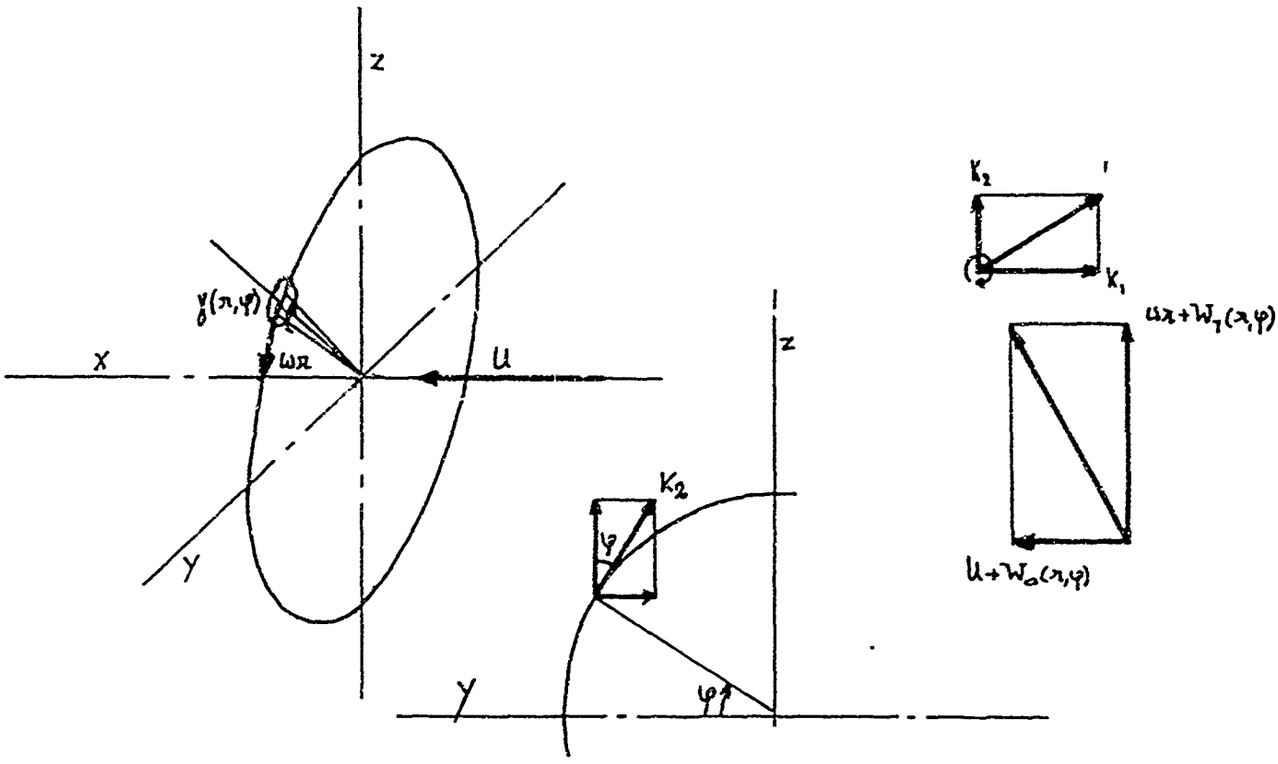

The vortex strength is assumed to be equal to:

$$\gamma(r,\varphi) = \frac{R_1}{\pi}\left[\gamma_0(R_1)+\gamma_1(R_1)\sin\varphi+\gamma_2(R_1)\cos\varphi\right]$$

The force L on an area $r\,d\varphi\,dr$ of the propeller plane due to the bound vortices is equal to:

$$L = \rho\sqrt{\left[U+W_a(r,\varphi)\right]^2+\left[\omega r+W_T(r,\varphi)\right]^2}\;\gamma(r,\varphi)$$

The bound vortices $\left[\gamma_0(R_1)\;;\;\gamma_1(R_1)\right.$ and $\left.\gamma_2(R_1)\right]$ and the induced velocities $W_a(r,\varphi)$ and $W_T(r,\varphi)$ are of the same magnitude and small with respect to the undisturbed flow velocity U.
Thus,

$$L \simeq \rho V\frac{R_1}{\pi}\left[\gamma_0(R_1)+\gamma_1(R_1)\sin\varphi+\gamma_2(R_1)\cos\varphi\right]$$

and

$$K_y = -\int_0^{2\pi}d\varphi\int_{R_0}^{R_1}dr\;\rho U R_1\left[\gamma_0(R_1)+\gamma_1(R_1)\sin\varphi+\gamma_2(R_1)\cos\varphi\right]\sin\varphi$$

$$K_z = \int_0^{2\pi}d\varphi\int_{R_0}^{R_1}dr\;\rho U R_1\left[\gamma_0(R_1)+\gamma_1(R_1)\sin\varphi+\gamma_2(R_1)\cos\varphi\right]\cos\varphi$$

or after carrying out the integrations over φ and r.

$$K_y = -\pi\varsigma u\, \gamma_1(R_1)\, R_1 (R_1 - R_0)$$

$$K_z = \pi\varsigma u\, \gamma_2(R_1)\, R_1 (R_1 - R_0)$$

The moments around the y and z axes becomes:

$$Q_y = -\frac{\pi}{3}\varsigma\omega R_1\, \gamma_1(R_1)\,(R_1^3 - R_0^3)$$

$$Q_z = \frac{\pi}{3}\varsigma\omega R_1\, \gamma_2(R_1)\,(R_1^3 - R_0^3)$$

Discussion of the result.

A pitch variation of the propeller given by

$$\alpha = \alpha_0 + \alpha_1 \sin\varphi$$

results in the following vortex distribution:

$$\gamma(r,\varphi) = \gamma_0(R_1) + \gamma_1(R_1)\sin\varphi + \gamma_2(R_1)\cos\varphi$$

with

$$\gamma_0(R_1) = \frac{zcV}{2R_1}\cdot\left[\alpha_0 - \operatorname{arctg}\frac{u}{\omega R_g}\right]$$

$$\gamma_1(R_1) = \frac{zcV}{2R_1}\alpha_1$$

$$\gamma_2(R_1) = \frac{z^2c^2\omega R_g\, C_1(R_g)}{4R_1^2}\alpha_1$$

The side forces K_y and K_z according to these vortex distributions are equal to:

$$K_y = -\frac{\pi\varsigma}{2}\, zc\, uV\,(R_1 - R_0)\,\alpha_1$$

$$K_z = \frac{\pi\varsigma}{4}\, z^2c^2\, u\,\omega R_g \cdot \frac{(R_1 - R_0)}{R_1}\cdot C_1(R_g)\,\alpha_1$$

The angle between the total side force and the positive y axis is defined by X.

For a clockwise rotating propeller (looking forward) is the angle X_1 equal to:

$$X_1 = \operatorname{arctg}\frac{K_z}{K_y} = \operatorname{arctg}\left[-\frac{A}{\sqrt{\left(\frac{u}{\omega R_1}\right)^2 B + 1}}\right]$$

with

$$A = \frac{zc\,C_1(R_g)}{2R_1}$$

$$B = \left(\frac{R_1}{R_g}\right)^2$$

For a counter clockwise rotating propeller becomes the angle χ_2 :

$$\chi_2 = \text{ARCTG}\left[\frac{A}{\sqrt{\left(\frac{u}{\omega R_1}\right)^2 B + 1}}\right]$$

The parameters A and B are only functions of the propeller geometry. For the tested propeller configurations applies:

$A = 0.86$

$B = 1.24$

The angles χ_1 and χ_2 have been calculated for some values of Λ $\left[\Lambda = \frac{u}{n D}\right]$ and the results are listed below.

Λ	χ_1	χ_2
0.50	138°	42°
1.00	141°	39°
1.50	143°	37°

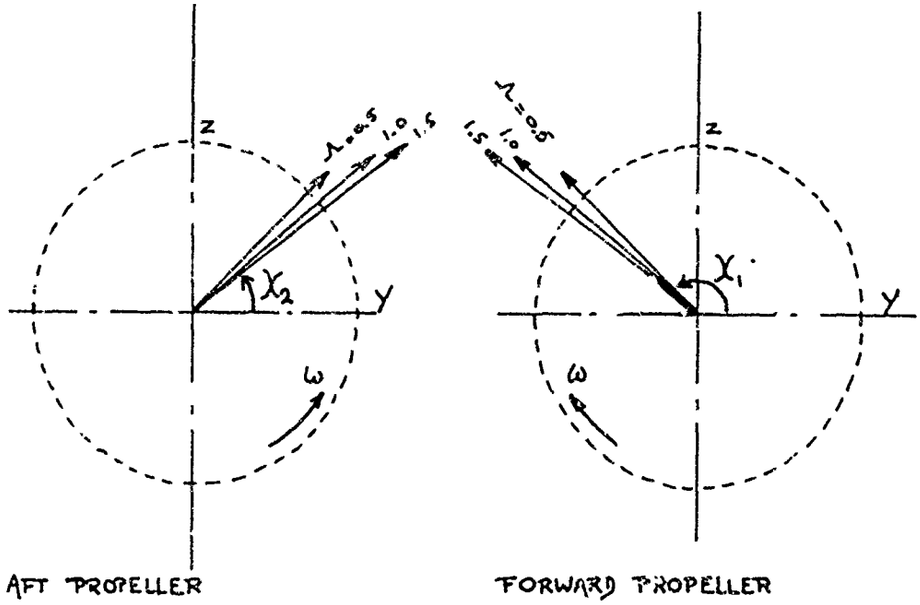

The side force directions obtained from the qualitative theoretical analyse and the measurements with the T.P.S. agree with each other for large values of Λ (see Figure 3,23.) (Λ around 1.0-2.0). The contribution of the helical vortices to the induced velocities at the propeller plane becomes more important for small values of Λ . In consequence it is not permitted to neglect the effects of the helical vortices. Probably the rotation of the side force can be explained by means of a qualitative analysis of the effects of the helical vortices for small values of Λ.

Appendix B.

Large hub to diameter ratio propellers.

Numerical programs for the calculation of the induced velocities, the frictionless torque, thrust and efficiency and the effect of friction on torque, thrust and efficiency.

Contents.

1. Definitions of the various parameters

The various parameters are summarised in the figure below

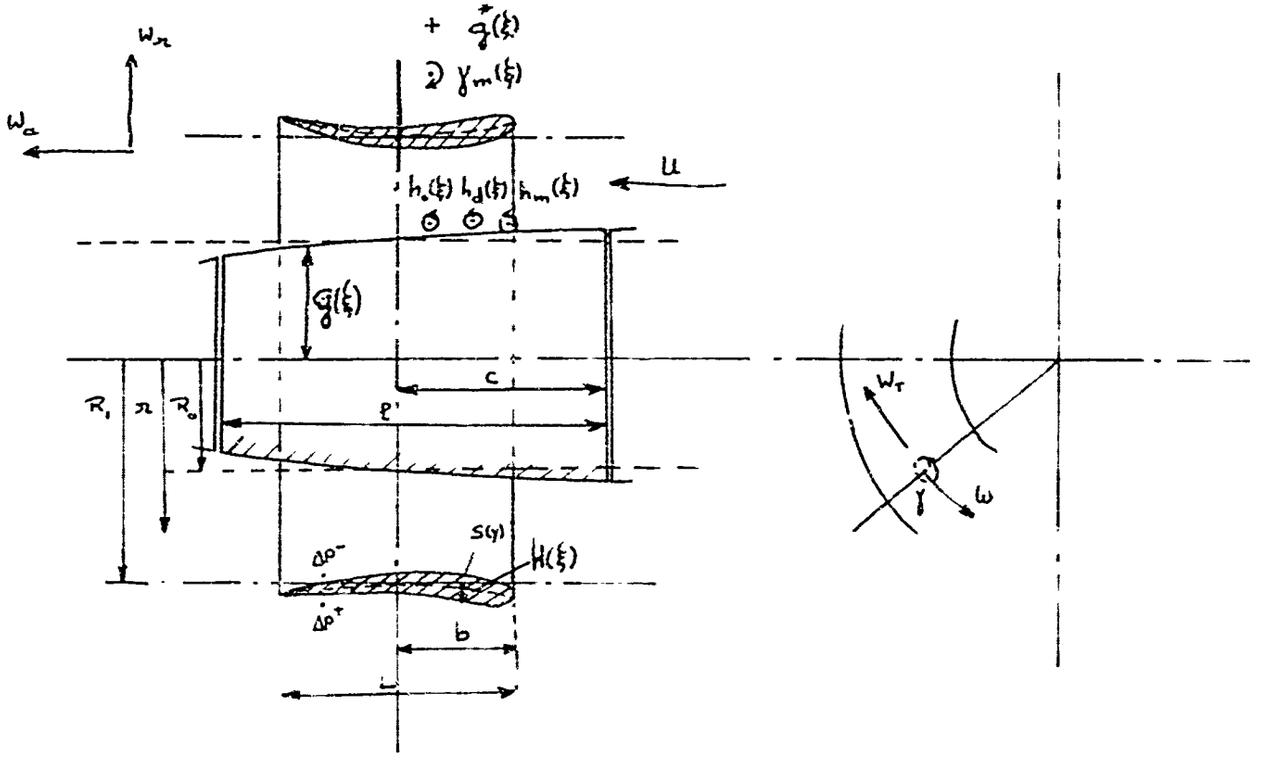

$w^{(1)}$ = average induced velocity by bound vortices propeller disk

$w^{(2)}$ = id helical vortices starting from shroud

$w^{(3)}$ = id helical vortices starting from hub

$w^{(4)}$ = id discontinuous bound vortices along the shroud

$w^{(5)}$ = id sources along the shroud

$w^{(6,m)}$ = id sinusoidal bound vortices along the shroud

$w^{(7)}$ = average induced velocity by ring vortex distribution $h_0(\xi)$

$w^{(8)}$ = id id $h_d(\xi)$

$w^{(am)}$ = id id $h_m(\xi)$

The parameters are made non-dimensional in the following way

$$\lambda = \frac{R_0}{R_1} \qquad \eta = \frac{L}{R_1} \qquad \xi = \frac{\rho}{R_1} \qquad a = \frac{b}{L} \qquad d = \frac{c}{L}$$

$$\bar{\xi} = \frac{\xi}{R_1} \qquad \bar{x} = \frac{x}{R_1} \qquad \bar{r} = \frac{r}{R_1} \qquad \bar{r}_1 = \frac{r_1}{R_1}$$

$$\bar{H}(\xi) = \frac{H(\xi)}{R_1} \qquad \bar{G}(\xi) = \frac{G(\xi)}{R_1}$$

$$\bar{w} = \frac{w}{u} \qquad \gamma = \frac{\gamma_1(r_1)}{u} \qquad \gamma_m = \frac{\gamma_m(R_1)}{u} \qquad \bar{g}(\bar{\xi}) = \frac{g(\xi)}{u}$$

$$\bar{h}_0(\bar{\xi}) = \frac{h_0(\xi)}{u} \qquad \bar{h}_d(\bar{\xi}) = \frac{h_d(\xi)}{u} \qquad \bar{h}_m(\bar{\xi}) = \frac{h_m(\xi)}{u}$$

$$\bar{h}_{od}(\bar{\xi}) = \frac{h_{od}(\xi)}{u}$$

$$\mu = \frac{\omega R_1}{u}$$

and further

$$\bar{\xi} + \eta\left(a - \frac{1}{2}\right) = -\frac{\eta}{2}\cos\theta$$

$$\bar{g}(\bar{\xi}) = \frac{d\bar{H}(\bar{\xi})}{d\bar{\xi}} = \frac{a_0}{\sqrt{a\eta + \bar{\xi}}} + \bar{f}(\bar{\xi}) \qquad a_0 = \left[\frac{\text{fronteshaal}}{2R_1}\right]^{1/2}$$

and

$s^{(1)}(r)$ = thickness ratio of propeller blade profile

$s^{(2)}$ = thickness ratio of the shroud profile

ν = kinematic viscosity

z = number of propeller blades

$\bar{c}(\bar{r}) = \frac{c(r)}{R_1}$ = chord length of propeller blade profile.

and

$$X_a^{(1)}(0,\bar{r}) = \frac{\bar{w}_a^{(1)}(0,\bar{r}) + \bar{w}_a^{(2)}(0,\bar{r}) + \bar{w}_a^{(3)}(0,\bar{r}) + \bar{w}_a^{(4)}(0,\bar{r}) + \bar{w}_a^{(7)}(0,\bar{r})}{\mu\bar{\gamma}}$$

$$X_a^{(2)}(0,\bar{r}) = \bar{w}_a^{(5)}(0,\bar{r}) + \bar{w}_a^{(8)}(0,\bar{r})$$

$$X_a^{(3,m)}(0,\bar{r}) = \frac{\bar{w}_a^{(6,m)}(0,\bar{r}) + \bar{w}_a^{(9,m)}(0,\bar{r})}{\gamma_m}$$

$$X_T^{(1)}(0,\bar{r}) = \frac{\bar{w}_T^{(1)}(0,\bar{r}) + \bar{w}_T^{(2)}(0,\bar{r}) + \bar{w}_T^{(3)}(0,\bar{r})}{\gamma}$$

$$X_r^{(1)}(\bar{x},1) = \frac{\bar{w}_r^{(1)}(\bar{x},1) + \bar{w}_r^{(2)}(\bar{x},1) + \bar{w}_r^{(3)}(\bar{x},1) + \bar{w}_r^{(4)}(\bar{x},1) + \bar{w}_r^{(7)}(\bar{x},1)}{\mu\gamma}$$

$$X_r^{(2)}(\bar{x},1) = \bar{w}_r^{(5)}(\bar{x},1) + \bar{w}_r^{(8)}(\bar{x},1)$$

$$X_r^{(3,m)}(\bar{x},1) = \frac{\bar{w}_r^{(6,m)}(\bar{x},1) + \bar{w}_r^{(9,m)}(\bar{x},1)}{\gamma_m}$$

$$X_a^{(1)}(\bar{x},1) = \frac{\bar{w}_a^{(1)}(\bar{x},1) + \bar{w}_a^{(2)}(\bar{x},1) + \bar{w}_a^{(3)}(\bar{x},1) + \bar{w}_a^{(4)}(\bar{x},1) + \bar{w}_a^{(7)}(\bar{x},1)}{\mu\gamma}$$

$$X_a^{(2)}(\bar{x},1) = \bar{w}_a^{(5)}(\bar{x},1) + \bar{w}_a^{(8)}(\bar{x},1)$$

$$X_a^{(3,m)}(\bar{x},1) = \frac{\bar{w}_a^{(6,m)}(\bar{x},1) + \bar{w}_a^{(9,m)}(\bar{x},1)}{\gamma_m}$$

$$X_a^{(1)}(\bar{x},\lambda) = \frac{\bar{w}_a^{(1)}(\bar{x},\lambda) + \bar{w}_a^{(2)}(\bar{x},\lambda) + \bar{w}_a^{(3)}(\bar{x},\lambda) + \bar{w}_a^{(4)}(\bar{x},\lambda) + \bar{w}_a^{(7)}(\bar{x},\lambda)}{\mu\gamma}$$

$$X_a^{(2)}(\bar{x},\lambda) = \bar{w}_a^{(5)}(\bar{x},\lambda) + \bar{w}_a^{(8)}(\bar{x},\lambda)$$

$$X_a^{(3)}(\bar{x},\lambda) = \frac{\bar{w}_a^{(6m)}(\bar{x},\lambda) + \bar{w}_a^{(9,m)}(\bar{x},\lambda)}{\gamma_m}$$

$$X_o(\bar{x}) = \frac{\bar{h}_o(\bar{x})}{\mu\gamma}$$

$$X_d(\bar{x}) = \bar{h}_d(\bar{x})$$

$$X_m(\bar{x}) = \frac{\bar{h}_m(\bar{x})}{\gamma_m}$$

and

K_S = thrust coefficient

K_Φ = torque coff.-cient

η^* = efficiency

$K_{S_{TOT}}$ = thrust coefficient including friction effect.

$K_{\Phi_{TOT}}$ = torque coefficient including friction effect

η_w = efficiency including friction effect.

2 Numerical program for the calculations of the induced velocities

2,1 Data for the calculations

2,2 Calculation of the induced velocities by
- a the propeller with the helical trailing vortices and discontinuous vortex distribution along the shroud
- b the distribution of sources along the shroud.
- c the sinusoidal ring vortex distributions along the shroud.

2,3 Calculation of the ring vortex distributions along the hub in order to compensate the induced radial velocities along the hub by the vortex systems as mentioned under items 3a, 3b and 3c

2,4 Calculation of the induced velocities by the ring vortex distributions along the hub.

2,1 Data for the calculations

$\lambda, \eta, \sigma, \mu, a_0$

$\bar{h}(\bar{\xi})$ for some values of $\bar{\xi}$ $\quad [-a\eta \leq \xi \leq (1-a)\eta]$

m

$\bar{x}$ and $\bar{r}$

2,2 Calculation of the induced velocities

A Radial induced velocities along the hub

$[r=\lambda\ ,\ x=\ldots\ldots]$

$$\frac{W_r^{(1)}+W_r^{(2)}+W_r^{(3)}+W_r^{(4)}}{\gamma} = \left[R_{L_0}-\text{idtc}\right]_{r=\lambda} =$$

$$= S_4(\bar{x}) - \frac{\mu}{2\sqrt{a(1-a)}}\int_{-a\eta}^{0} \sin\theta\ S_6(\bar{x},\bar{\xi})\,d\bar{\xi} - \frac{1}{\pi}\int_{-a\eta}^{(1-a)\eta} \bar{g}(\bar{\xi})\,\frac{\lambda G_0(R_2^2)+G_1(R_2^2)}{[(\bar{x}-\bar{\xi})^2+(\lambda+1)^2]^{3/2}}\,d\bar{\xi}$$

$$\frac{W_r^{(1)}+W_r^{(2)}+W_r^{(3)}+W_r^{(4)}}{\left[\frac{\gamma}{\delta}\right]_{\gamma=1}} + W_r^{(5)} = \left[R_{L_0}\right]_{r=\lambda} =$$

$$= S_4(\bar{x}) - \frac{\mu}{2\sqrt{a(1-a)}}\int_{-a\eta}^{(1-a)\eta} \sin\theta\ S_5(\bar{x},\bar{\xi})\,d\bar{\xi}$$

$$\frac{W_r^{(6,m)}}{\gamma_m} = \left[R_{L_m}\right]_{r=\lambda} =$$

$$= -\frac{1}{\pi}\int_{-a\eta}^{(1-a)\eta} \sin m\theta\ S_5(\bar{x},\bar{\xi})\,d\bar{\xi}$$

B Radial induced velocities along the shroud.

$[r=1\ ,\ x=\ldots\ldots]$

$$\frac{W_r^{(1)}+W_r^{(2)}+W_r^{(3)}+W_r^{(4)}}{\gamma} = \left[\bar{r}_0-\text{idtc}\right]_{r=1} =$$

$$= S_1(\bar{x}) - \frac{\mu}{2\sqrt{a(1-a)}}\int_{-a\eta}^{0} \sin\theta\ S_2(\bar{x},\bar{\xi})\,d\bar{\xi} - \frac{1}{\pi}\int_{-a\eta}^{(1-a)\eta} \bar{g}(\bar{\xi})\,\frac{G_0(R_1^2)+G_1(R_1^2)}{[(\bar{x}-\bar{\xi})^2+4]^{3/2}}\,d\bar{\xi}$$

$$\frac{W_r^{(1)}+W_r^{(2)}+W_r^{(3)}+W_r^{(4)}}{[\gamma]_{\gamma=1}} + W_r^{(5)} =$$

$$= S_1(\bar{x}) - \frac{\mu}{2\sqrt{a(1-a)}}\int_{-a\eta}^{0} \sin\theta\ S_2(\bar{x},\bar{\xi})\,d\bar{\xi}$$

$$\frac{w_x^{(6,m)}}{\gamma_m} = \left[F_m\right]_{x=1} =$$

$$= -\frac{1}{\pi}\int_{-a\eta}^{(1-a)\eta} \sin m\theta \; S_2(\bar{x},\bar{\xi})\, d\bar{\xi}$$

C Axial induced velocities along the hub

$\left[x=\lambda,\ x=\text{----}\right]$

$$\frac{w_a^{(1)}+w_a^{(2)}+w_a^{(3)}}{\gamma} = \left[W_a \text{ schroef}\right]_{x=\lambda} =$$

$$= \frac{\mu}{\pi}\int_0^{\pi/2}\left[1+\frac{(1+\lambda\cos 2\psi)}{(\lambda+1)^2-4\lambda\sin^2\psi}\cdot\frac{\bar{x}}{\left[\bar{x}^2+(\lambda+1)^2-4\lambda\sin^2\psi\right]^{1/2}}\right]d\psi +$$

$$-\frac{\mu}{2\pi}\int_0^{\pi/2}\left[1+\frac{\bar{x}}{\left[\bar{x}^2+4\lambda^2\cos^2\psi\right]^{1/2}}\right]d\psi$$

$$\frac{w_a^{(4)}}{\gamma} = \left[W_a \text{ wervel}\right]_{x=\lambda} =$$

$$= \frac{\mu}{2\sqrt{a(1-a)}}\int_{-a\eta}^{0} \sin\theta \;\frac{G_0(k_2^2)+\lambda G_1(k_2^2)}{\left[(\bar{x}-\bar{\xi})^2+(\lambda+1)^2\right]^{3/2}}\, d\bar{\xi}$$

$$w_a^{(5)} = \left[W_a \text{ dikte}\right]_{x=\lambda} =$$

$$= \frac{1}{\pi}\int_{-a\eta}^{(1-a)\eta} \bar{g}(\bar{\xi})\,\frac{(\bar{x}-\bar{\xi})\,G_0(k_2^2)}{\left[(\bar{x}-\bar{\xi})^2+(\lambda+1)^2\right]^{3/2}}\, d\bar{\xi}$$

$$\frac{w_a^{(6,m)}}{\gamma_m} = \left[W_{am} \text{ wervel}\right]_{x=\lambda} =$$

$$= \frac{1}{\pi}\int_{-a\eta}^{(1-a)\eta} \sin m\theta \;\frac{G_0(k_2^2)+\lambda G_1(k_2^2)}{\left[(\bar{x}-\bar{\xi})^2+(\lambda+1)^2\right]^{3/2}}\, d\bar{\xi}$$

D Axial induced velocities along the shroud

$\left[x=1,\ x=\text{----}\right]$

$$\frac{w_a^{(1)}+w_a^{(2)}+w_a^{(3)}}{\gamma} = \left[w_a \text{ schroef}\right]_{r=1} =$$

$$= \frac{\mu}{2\pi}\int_0^{\pi/2}\left[1+\frac{\bar{x}}{[\bar{x}^2+4\cos^2\psi]^{1/2}}\right]d\psi +$$

$$-\frac{\lambda\mu\bar{x}}{\pi}\int_0^{\pi/2}\frac{(\lambda+\cos 2\psi)}{[(\lambda+1)^2-4\lambda\sin^2\psi]}\cdot\frac{1}{[\bar{x}^2+(\lambda+1)^2-4\lambda\sin^2\psi]^{1/2}}\,d\psi.$$

$$\frac{w_a^{(4)}}{\gamma} = \left[w_{a_0} \text{ wervel}\right]_{r=1} =$$

$$= \frac{\mu}{2\pi\sqrt{a(1-a)}}\cdot\int_{-a\eta}^{\infty}\sin\theta\;\frac{G_0(\bar{R}_1^2)+G_1(\bar{R}_1^2)}{[(\bar{x}-\bar{\xi})^2+4]^{3/2}}\,d\bar{\xi}$$

$$w_a^{(5)} = \left[w_a \text{ delta}\right]_{r=1} =$$

$$= \frac{1}{\pi}\int_{-a\eta}^{(1-a)\eta}\dot{g}(\bar{\xi})\,\frac{(\bar{x}-\bar{\xi})G_0(\bar{R}_1^2)}{[(\bar{x}-\bar{\xi})^2+4]^{3/2}}\,d\bar{\xi}.$$

$$\frac{w_a^{(6,m)}}{\gamma_m} = \left[w_{am} \text{ wervel}\right]_{r=1} =$$

$$= \frac{1}{\pi}\int_{-a\eta}^{(1-a)\eta}\sin m\theta\;\frac{G_0(\bar{R}_1^2)+G_1(\bar{R}_1^2)}{[(\bar{x}-\bar{\xi})^2+4]^{3/2}}\,d\bar{\xi}$$

Σ Axial induced velocities at the screw disk

[$r = \ldots\ldots$, $\bar{x}=1$ or $\ldots\ldots$]

$$\frac{w_a^{(1)}+w_a^{(2)}+w_a^{(3)}}{\gamma} = \left[w_a \text{ schroef}\right]_{r=r_0} =$$

$$= \frac{\mu}{\pi}\int_0^{\pi/2}\frac{(1+\bar{r}_0\cos 2\psi)}{[(1+\bar{r}_0)^2-4\bar{r}_0\sin^2\psi]}\cdot\left[1+\frac{\bar{x}}{[\bar{x}^2+(\bar{r}_0+1)^2-4\bar{r}_0\sin^2\psi]^{1/2}}\right]d\psi +$$

$$-\frac{\lambda\mu}{\pi}\int_0^{\pi/2}\frac{(\lambda+r_0\cos 2\psi)}{[(\lambda+\bar{r}_0)^2-4\lambda\bar{r}_0\sin^2\psi]}\left[1+\frac{\bar{x}}{[\bar{x}^2+(\bar{r}_0+\lambda)^2-4\bar{r}_0\lambda\sin^2\psi]^{1/2}}\right]d\psi$$

$$\frac{w_a^{(4)}}{\gamma} = \left[w_{a_0 \text{ wond}} \right]_{r=r_0} =$$

$$= \frac{\mu}{2\sqrt{a(1-a)}} \int_{-a\eta}^{\infty} \sin\theta \; \frac{G_0(k_4^2) + r_0 G_1(k_4^2)}{\left[(\bar{x}-\bar{\xi})^2 + (\bar{r}_0+1)^2\right]^{3/2}} \, d\bar{\xi}$$

$$w_a^{(5)} = \left[w_a \text{ dilate} \right]_{r=r_0} =$$

$$= \frac{1}{\pi} \int_{-a\eta}^{(1-a)\eta} \bar{q}_j(\bar{\xi}) \frac{(\bar{x}-\bar{\xi}) G_0(k_4^2)}{\left[(\bar{x}-\bar{\xi})^2 + (\bar{r}_0+1)^2\right]^{3/2}} \, d\bar{\xi}$$

$$\frac{w_a^{(6,m)}}{\gamma_m} = \left[w_{a_m \text{ wond}} \right]_{r=r_0} =$$

$$= \frac{1}{\pi} \int_{-a\eta}^{(1-a)\eta} \sin m\theta \; \frac{G_0(k_4^2) + r_0 G_1(k_4^2)}{\left[(\bar{x}-\bar{\xi})^2 + (r_0+1)^2\right]^{3/2}} \, d\bar{\xi}$$

∓ Circumferential induced velocities at the screw disk [r = ----, x = 1 or ----]

$$\frac{w_T^{(1)} + w_T^{(2)} + w_T^{(3)}}{\gamma} = \left[w_{T \text{ schroef}} \right]_{r=r_0} =$$

$$= \frac{1}{\pi} \int_0^{\pi/2} \frac{(r_0 + \cos 2\psi)}{\left[(r_0+1)^2 - 4r_0 \sin^2\psi\right]} \left[1 + \frac{\bar{x}}{\left[\bar{x}^2 + (r_0+1)^2 - 4r_0 \sin^2\psi\right]^{1/2}} \right] d\psi +$$

$$- \frac{1}{\pi} \int_0^{\pi/2} \frac{(r_0 + \lambda \cos 2\psi)}{\left[(r_0+\lambda)^2 - 4r_0\lambda \sin^2\psi\right]} \left[1 + \frac{\bar{x}}{\left[\bar{x}^2 + (r_0+\lambda)^2 - 4r_0\lambda \sin^2\psi\right]^{1/2}} \right] d\psi$$

2.3 Calculation of the ring vortex distributions along the hub

$\bar{h}_{od}(\bar{\xi})$

$$S_4(\bar{x},\bar{\xi}) - \frac{\mu}{2\sqrt{a(1-a)}} \int_{-a\eta}^{\infty} \sin\theta \; S_6(\bar{x},\bar{\xi}) \, d\bar{\xi} + \int_{\infty}^{+\infty} \bar{h}_{od}(\bar{\xi}) \, S_4(\bar{x},\bar{\xi}) \, d\bar{\xi} = 0$$

$\bar{h}_o(\bar{\xi})$

$$S_4(\bar{x},\bar{\xi}) - \frac{1}{\pi}\int_{-a\eta}^{(1-a)\eta} \bar{q}(\bar{\xi})\,\frac{\lambda G_0(\lambda\bar{\xi}_i)+G_1(\lambda\bar{\xi}_i)}{[(\bar{x}-\bar{\xi})^2+(\lambda+1)^2]^{3/2}}\,d\bar{\xi} - \frac{\mu}{2\sqrt{a(1-a)}}\int_{-a\eta}^{0} \sin\theta\; S_5(\bar{x},\bar{\xi})\,d\bar{\xi} +$$
$$+\int_{-\infty}^{+\infty} \bar{h}_o(\bar{\xi})\; S_6(\bar{x},\bar{\xi})\,d\bar{\xi} = 0$$

$\bar{h}_m(\bar{\xi})$.

$$-\int_{-a\eta}^{(1-a)\eta} \sin m\theta\; S_5(\bar{x},\bar{\xi})\,d\bar{\xi} + \int_{-\infty}^{+\infty} \bar{h}_m(\bar{\xi})\; S_6(\bar{x},\bar{\xi})\,d\bar{\xi} = 0$$

2,4 Calculation of the induced velocities by the ring vortex distributions along the hub.

A Radial induced velocities along the hub.

$[r=\lambda\ ;\ \bar{x} = \text{----}]$

$$\bar{W}_r^{(q)} = \left[\bar{W}_r\{\bar{h}_o(\bar{\xi})\}\right]_{r=\lambda} = \int_{-\infty}^{+\infty} \bar{h}_o(\bar{\xi})\; S_6(\bar{x},\bar{\xi})\,d\bar{\xi}$$

$$\bar{W}_r^{(\beta)} = \left[\bar{W}_r\{\bar{h}_d(\bar{\xi})\}\right]_{r=\lambda} = \int_{-\infty}^{+\infty} \left[\bar{h}_{od}(\bar{\xi}) - \bar{h}_o(\bar{\xi})\right] S_6(\bar{x},\bar{\xi})\,d\bar{\xi}$$

$$\bar{W}_r^{(q,m)} = \left[\bar{W}_r\{\bar{h}_m(\bar{\xi})\}\right]_{r=\lambda} = \int_{-\infty}^{+\infty} \bar{h}_m(\bar{\xi})\; S_6(\bar{x},\bar{\xi})\,d\bar{\xi}$$

B Radial induced velocities along the shroud

$[r=1\ ,\ \bar{x} = \text{----}]$

$$\bar{W}_r^{(q)} = \left[W_r\{\bar{h}_o(\bar{\xi})\}\right]_{r=1} = \int_{-\infty}^{+\infty} \bar{h}_o(\bar{\xi})\; S_3(\bar{x},\bar{\xi})\,d\bar{\xi}$$

$$\bar{W}_r^{(\beta)} = \left[W_r\{\bar{h}_d(\bar{\xi})\}\right]_{r=1} = \int_{-\infty}^{+\infty} \left[\bar{h}_{od}(\bar{\xi}) - \bar{h}_o(\bar{\xi})\right] S_3(\bar{x},\bar{\xi})\,d\bar{\xi}$$

$$\bar{w}_r^{(q,m)} = \left[\bar{w}_r\{\bar{h}_m(\bar{\xi})\}\right]_{r=1} = \int_{-\infty}^{+\infty} \bar{h}_m(\bar{\xi})\, s_3(\bar{x},\bar{\xi})\, d\bar{\xi}$$

C Axial induced velocities along the hub

$[r=\lambda\ ,\ \bar{x}=\text{----}]$

$$\bar{w}_a^{(\gamma)} = \left[\bar{w}_a\{\bar{h}_o(\bar{\xi})\}\right]_{r=\lambda} = -\frac{\lambda^2}{\pi}\int_{-\infty}^{+\infty} \bar{h}_o(\bar{\xi})\ \frac{\zeta_o(k_3^2)+\zeta_1(k_3^2)}{[(\bar{x}-\bar{\xi})^2+4\lambda^2]^{3/2}}\, d\bar{\xi}$$

$$\bar{w}_a^{(\beta)} = \left[\bar{w}_a\{\bar{h}_d(\bar{\xi})\}\right]_{r=\lambda} = -\frac{\lambda^2}{\pi}\int_{-\infty}^{+\infty} \left[\bar{h}_{od}(\bar{\xi}) - \bar{h}_o(\bar{\xi})\right] \frac{\zeta_o(k_3^2)+\zeta_1(k_3^2)}{[(\bar{x}-\bar{\xi})^2+4\lambda^2]^{3/2}}\, d\bar{\xi}$$

$$\bar{w}_a^{(q,m)} = \left[\bar{w}_a\{\bar{h}_m(\bar{\xi})\}\right]_{r=\lambda} = -\frac{\lambda^2}{\pi}\int_{-\infty}^{+\infty} \bar{h}_m(\bar{\xi})\ \frac{\zeta_o(k_3^2)+\zeta_1(k_3^2)}{[(\bar{x}-\bar{\xi})^2+4\lambda^2]^{3/2}}\, d\bar{\xi}$$

D Axial induced velocities along the shroud

$[r=1\ ,\ x=\text{----}]$

$$\bar{w}_a^{(\gamma)} = \left[\bar{v}_a\{\bar{h}_o(\bar{\xi})\}\right]_{r=1} = -\frac{\lambda}{\pi}\int_{-\infty}^{+\infty} \bar{h}_o(\bar{\xi})\ \frac{\lambda\zeta_o(k_2^2)+\zeta_1(k_2^2)}{[(\bar{x}-\bar{\xi})^2+(\lambda+1)^2]^{3/2}}\, d\bar{\xi}$$

$$\bar{w}_a^{(\beta)} = \left[\bar{w}_a\{\bar{h}_d(\bar{\xi})\}\right]_{r=1} = -\frac{\lambda}{\pi}\int_{-\infty}^{+\infty} \left[\bar{h}_{od}(\bar{\xi}) - \bar{h}_o(\bar{\xi})\right] \frac{\lambda\zeta_o(k_2^2)+\zeta_1(k_2^2)}{[(\bar{x}-\bar{\xi})^2+(\lambda+1)^2]^{3/2}}\, d\bar{\xi}$$

$$\bar{w}_a^{(q,m)} = \left[\bar{w}_a\{\bar{h}_m(\bar{\xi})\}\right]_{r=1} = -\frac{\lambda}{\pi}\int_{-\infty}^{+\infty} \bar{h}_m(\bar{\xi})\ \frac{\lambda\zeta_o(k_2^2)\ \ \zeta_1(k_2^2)}{[(\bar{x}-\bar{\xi})^2+(\lambda+1)^2]^{3/2}}\, d\bar{\xi}$$

E Axial induced velocities at the screw disk

$[r=\text{----}\ ,\ \bar{x}=1\ \text{or}\ \text{----}]$

$$\bar{w}_a^{(\gamma)} = \left[w_a\{\bar{h}_o(\bar{\xi})\}\right]_{r=\bar{r}_o} = -\frac{\lambda}{\pi}\int_{-\infty}^{+\infty} h_o(\bar{\xi})\ \frac{\lambda\zeta_o(k_5^2)+\bar{r}_o\zeta_1(k_5^2)}{[(\bar{x}-\bar{\xi})^2+(\lambda+\bar{r}_o)^2]^{3/2}}\, d\bar{\xi}$$

$$\bar{w}_a^{(\beta)} = \left[w_a\{\bar{h}_d(\bar{\xi})\}\right]_{r=\bar{r}_o} = -\frac{\lambda}{\pi}\int_{-\infty}^{+\infty} \left[\bar{h}_{od}(\bar{\xi}) - \bar{h}_o(\bar{\xi})\right] \frac{\lambda\zeta_o(k_5^2)+\bar{r}_o\zeta_1(k_5^2)}{[(\bar{x}-\bar{\xi})^2+(\lambda+\bar{r}_o)^2]^{3/2}}\, d\bar{\xi}$$

$$\bar{w}_a^{(q,m)} = \left[w_a\{\bar{h}_m(\bar{\xi})\}\right]_{r=\bar{r}_o} = -\frac{\lambda}{\pi}\int_{-\infty}^{+\infty} h_m(\bar{\xi})\ \frac{\lambda\zeta_o(k_5^2)+\bar{r}_o\zeta_1(k_5^2)}{[(\bar{x}-\bar{\xi})^2+(\lambda+\bar{r}_o)^2]^{3/2}}\, d\bar{\xi}$$

S, γ, k and G are defined by

$$S_1(\bar{x}) = \frac{\mu^2}{\pi}\int_0^{\pi/2} \cos 2\psi\, \gamma_{co}^{(1)}\, d\psi - \frac{\lambda\mu^2}{\pi}\int_0^{\pi/2} \cos 2\psi\, \gamma_{co}^{(2)}\, d\psi + \frac{1}{\pi}\int_{-a\eta}^{(1-a)\eta} \bar{q}(\bar{\xi})\, \frac{G_0(k_1^2)+G_1(k_1^2)}{[(\bar{x}-\bar{\xi})^2+4]^{3/2}}\, d\bar{\xi}$$

$$S_2(\bar{x}) = \frac{1}{\pi}\cdot\frac{(\bar{x}-\bar{\xi})\, G_1(k_1^2)}{[(\bar{x}-\bar{\xi})^2+4]^{3/2}}$$

$$S_3(\bar{x}) = \frac{\lambda}{\pi}\,\frac{(\bar{x}-\bar{\xi})\, G_1(k_2^2)}{[(\bar{x}-\bar{\xi})^2+(\lambda+1)^2]^{3/2}}$$

$$S_4(\bar{x}) = \frac{\mu^2}{\pi}\int_0^{\pi/2} \cos 2\psi\, \gamma_{co}^{(2)}\, d\psi - \frac{\lambda\mu^2}{\pi}\int_0^{\pi/2} \cos 2\psi\, \gamma_{co}^{(3)}\, d\psi + \frac{1}{\pi}\int_{-a\eta}^{(1-a)\eta} \bar{q}(\bar{\xi})\, \frac{\lambda G_0(k_2^2)+G_1(k_2^2)}{[(\bar{x}-\bar{\xi})^2+(\lambda+1)^2]^{3/2}}\, d\bar{\xi}$$

$$S_5(\bar{x}) = \frac{1}{\pi}\,\frac{(\bar{x}-\bar{\xi})\, G_1(k_2^2)}{[(\bar{x}-\bar{\xi})^2+(\lambda+1)^2]^{3/2}}$$

$$S_6(\bar{x}) = \frac{\lambda}{\pi}\,\frac{(\bar{x}-\bar{\xi})\, G_1(k_3^2)}{[(\bar{x}-\bar{\xi})^2+4\lambda^2]^{3/2}}$$

$$\gamma_{co}^{(1)} = \frac{1}{\mu[\bar{x}^2+4\cos^2\psi]^{1/2}}$$

$$\gamma_{co}^{(2)} = \frac{1}{\mu[\bar{x}^2+(\lambda+1)^2-4\lambda\sin^2\psi]^{1/2}}$$

$$\gamma_{co}^{(3)} = \frac{1}{\mu[\bar{x}^2+4\lambda^2\cos^2\psi]^{1/2}}$$

$$k_1^2 = \frac{4}{(\bar{x}-\bar{\xi})^2+4} \qquad k_4^2 = \frac{4\bar{n}_0}{(\bar{x}-\bar{\xi})^2+(\bar{n}_0+1)^2}$$

$$k_2^2 = \frac{4\lambda}{(\bar{x}-\bar{\xi})^2+(\lambda+1)^2} \qquad k_5^2 = \frac{4\bar{n}_0\lambda}{(\bar{x}-\bar{\xi})^2+(\bar{n}_0+\lambda)^2}$$

$$k_3^2 = \frac{4\lambda^2}{(\bar{x}-\bar{\xi})^2+4\lambda^2}$$

$$G_0(k^2) = \frac{E(k)}{1-k^2}$$

$$G_1(k^2) = \frac{2K(k)-E(k)}{k^2} - \frac{E(k)}{k^2(1-k^2)}$$

3 Numerical program for the calculation of the frictionless thrust, torque and efficiency.

3,1 Data for the calculations
3,2 Calculation of the frictionless thrust, torque and efficiency
3,3 Calculation of the camberline of the shroud.
3,4 Calculatum of the pressure along the shroud

3,1 Data for the calculations

$\lambda, a; \eta, d, \xi$

$\bar{H}(\bar{\xi})$ for some values of $\bar{x}$ $[-a\eta \leq \bar{x} \leq (1-a)\eta]$
$\bar{G}(\bar{\xi})$ id $[-d\xi \leq x \leq (1-d)\xi]$

$X_a^{(1)}(0,\bar{r})$ for some values of r $[\lambda \leq r \leq 1]$
$X_a^{(2)}(0\,\bar{r})$ id
$X_a^{(3,m)}(0,\bar{r})$ id
$X_T^{(1)}(0,\bar{r})$ id

$X_r^{(1)}(\bar{x},1)$ for some values of $\bar{x}$ $[-a\eta \leq x \leq (1-a)\eta]$
$X_r^{(2)}(\bar{x},1)$ id
$X_r^{(3,m)}(\bar{x},1)$ id
$X_a^{(1)}(\bar{x},1)$ id
$X_a^{(2)}(\bar{x},1)$ id
$X_a^{(3,m)}(\bar{x},1)$ id

$X_a^{(1)}(\bar{x},\lambda)$ for some values of $\bar{x}$ $[-d\xi \leq x \leq (1-d)\xi]$
$X_a^{(2)}(\bar{x},\lambda)$ id
$X_a^{(3,m)}(\bar{x},\lambda)$ id

$\mu, \gamma, \gamma_1; \gamma_2, \cdots, \gamma_m$

some values of $\bar{y}$ $[-a\eta \leq \bar{y} \leq (1-a)\eta]$

3,2 Calculation of the frictionless thrust, torque and efficiency.

Calculate $K_Q^{(1)}$; $K_S^{(1)}$, $K_S^{(2)}$, $K_S^{(3)}$, K_S and η^* with the aid of the following relations.

$$K_Q^{(1)} = \frac{\pi^3(1-\lambda^2)\gamma}{8\mu^2} + \frac{\pi^3\gamma}{4\mu^2}\left[\mu\gamma I_1 + I_2 + \sum_m \gamma_m I_{3,m}\right]$$

$$K_S^{(1)} = \frac{\pi^3(1-\lambda^2)\gamma}{4\mu} + \frac{\pi^3\gamma}{2\mu^2}\left[\mu\gamma I_4\right]$$

$$K_S^{(2)} = \frac{-\pi^3\gamma}{4\mu\sqrt{a(1-a)}}\left[\mu\gamma I_5 + I_6 + \sum_m \gamma_m I_{7,m}\right] +$$

$$- \frac{\pi^3}{2\mu^2}\sum_m \gamma_m\left[\mu\gamma I_{8,m} + I_{9,m} + \sum_n \gamma_n I_{10,m,n}\right] +$$

$$+ \frac{\pi^3\gamma}{2\mu} H(0)$$

$$+ \frac{\pi^3}{\mu^2}\left[\mu\gamma I_{11} + I_{12} + \sum_m \gamma_m I_{13,m}\right]$$

$$K_S^{(3)} = + \frac{\pi^3\lambda^2\gamma}{8\mu} + \frac{\pi^3}{2\mu^2}\left[\mu\gamma I_{14} + I_{15} + \sum_m \gamma_m I_{16,m}\right] +$$

$$+ \frac{\pi^3}{4\mu^2}\left[\mu\gamma I_{17} + I_{18} + \sum_m \gamma_m I_{19,m}\right] - \frac{\pi^3 G^2\{(1-d)\xi\}\gamma}{8\mu}$$

$$K_S = K_S^{(1)} + K_S^{(2)} + K_S^{(3)}$$

$$\eta^* = \frac{1}{2\mu}\frac{K_S}{K_Q^{(1)}}$$

and

$$I_1 = \int_\lambda^1 X_a^{(1)}(0,\bar{r})\,\bar{r}\,d\bar{r}$$

$$I_2 = \int_\lambda^1 X_a^{(2)}(0,\bar{r})\,\bar{r}\,d\bar{r}$$

$$I_{3,m} = \int_\lambda^1 X_a^{(3,m)}(0,\bar{r})\,\bar{r}\,d\bar{r}$$

$$I_4 = \int_\lambda^1 X_T^{(1)}(0,\bar{r})\,d\bar{r}$$

$$I_5 = \int_{-a\eta}^{0} X_n^{(1)}(\bar{x},1)\sin\theta\,d\bar{x}$$

$$I_6 = \int_{-a\eta}^{0} X_n^{(2)}(\bar{x},1)\sin\theta\,d\bar{x}$$

$$I_{7,m} = \int_{-a\eta}^{0} X_n^{(3)}(\bar{x},1)\sin\theta\,d\bar{x}$$

$$I_{8,m} = \int_{-a\eta}^{(1-a)\eta} X_n^{(1)}(\bar{x},1)\sin m\theta\,d\bar{x}$$

$$I_{9,m} = \int_{-a\eta}^{(1-a)\eta} X_n^{(2)}(\bar{x},1)\sin m\theta\,d\bar{x}$$

$$I_{10,m,n} = \int_{-a\eta}^{(1-a)\eta} X_n^{(3,n)}(\bar{x},1)\sin m\theta\,d\bar{x}$$

$$I_{11} = \int_{-a\eta}^{(1-a)\eta} X_a^{(1)}(\bar{x},1)\,\frac{d\bar{H}(\bar{x})}{d\bar{x}}\,d\bar{x} = -\int_{-a\eta}^{(1-a)\eta} \bar{H}(\bar{x})\,\frac{dX_a^{(1)}(\bar{x},1)}{d\bar{x}}\,d\bar{x}$$

$$I_{12} = \int_{-a\eta}^{(1-a)\eta} X_a^{(2)}(\bar{x},1)\,\frac{d\bar{H}(\bar{x})}{d\bar{x}}\,d\bar{x} = -\int_{-a\eta}^{(1-a)\eta} \bar{H}(\bar{x})\,\frac{dX_a^{(2)}(\bar{x},1)}{d\bar{x}}\,d\bar{x}$$

$$I_{13,m} = \int_{-a\eta}^{(1-a)\eta} X_a^{(3,m)}(\bar{x},1)\,\frac{d\bar{H}(\bar{x})}{d\bar{x}}\,d\bar{x} = -\int_{-a\eta}^{(1-a)\eta} \bar{H}(\bar{x})\,\frac{dX_a^{(3,m)}(\bar{x},1)}{d\bar{x}}\,d\bar{x}$$

$$I_{14} = \int_{-d\zeta}^{(1-d)\zeta} \frac{d\bar{G}(\bar{x})}{d\bar{x}}\,\bar{G}(\bar{x})\,X_a^{(1)}(\bar{x},\lambda)\,d\bar{x}$$

$$I_{15} = \int_{-d\zeta}^{(1-d)\zeta} \frac{d\bar{G}(\bar{x})}{d\bar{x}}\,\bar{G}(\bar{x})\,X_a^{(2)}(\bar{x},\lambda)\,d\bar{x}$$

$$I_{16,m} = \int_{-d\zeta}^{(1-d)\zeta} \frac{d\bar{G}(\bar{x})}{d\bar{x}}\,\bar{G}(\bar{x})\,X_a^{(3,m)}(\bar{x},\lambda)\,d\bar{x}$$

$$I_{17} = \int_{-d\zeta}^{(1-d)\zeta} \frac{d\bar{q}(\bar{x})}{d\bar{x}}\, \bar{q}(\bar{x})\, x_0(\bar{x})\, d\bar{x} = \int_{-d\zeta}^{0} \frac{d\bar{q}(\bar{x})}{d\bar{x}}\, q(\bar{x})\, x_0^{(1)}(\bar{x})\, d\bar{x} + \int_{0}^{(1-d)\zeta} \frac{dq(\bar{x})}{d\bar{x}}\, q(\bar{x})\, x_0^{(2)}(\bar{x})\, d\bar{x}$$

$$I_{18} = \int_{-d\zeta}^{(1-d)\zeta} \frac{d\bar{q}(\bar{x})}{d\bar{x}}\, \bar{q}(\bar{x})\, x_d(\bar{x})\, d\bar{x}$$

$$I_{19,m} = \int_{-d\zeta}^{(1-d)\zeta} \frac{d\bar{q}(\bar{x})}{d\bar{x}}\, \bar{q}(\bar{x})\, x_m(\bar{x})\, d\bar{x}$$

3,2 Calculation of the camberline of the shroud

Calculate $\bar{s}(\bar{y})$ with the aid of the following relations

$$\bar{s}(\bar{y}) = \mu\gamma\, I_{20}(y) + I_{21}(y) + \sum_m \gamma_m\, I_{22,m}(y)$$

and

$$I_{20}(\bar{y}) = \int_0^{\bar{y}} X_n^{(1)}(\bar{x},1)\, d\bar{x}$$

$$I_{21}(\bar{y}) = \int_0^{\bar{y}} X_n^{(2)}(\bar{x},1)\, d\bar{x}$$

$$I_{22,m}(\bar{y}) = \int_0^{\bar{y}} X_n^{(3,m)}(\bar{x},1)\, d\bar{x}$$

3,3 Calculation of the pressure along the shroud

Calculate $\Delta p^+(x)$ and $\Delta p^-(x)$ with the aid of the following relations (for $x = y$)

$$\Delta p^+(\bar{x}) = -2\mu\gamma\, X_a^{(1)}(\bar{x},1) - 2X_a^{(2)}(\bar{x},1) - 2\sum_m \gamma_m X_a^{(3,m)}(\bar{x},1) +$$

$$+ \frac{\mu\gamma}{2\sqrt{a(1-a)}} \sin\theta + \sum_m \gamma_m \sin m\theta \qquad [-a\eta \leq \bar{x} \leq 0]$$

$$\Delta p^{+}(\bar{x}) = -2\mu\gamma\, X_a^{(1)}(\bar{x},1) - 2X_a^{(2)}(\bar{x},1) - 2\sum_m \gamma_m X_a^{(3,m)}(\bar{x},1) +$$

$$+ \mu\gamma + \sum_m \gamma_m \sin m\theta \qquad [\,0 < \bar{x} \leq (1-a)\eta\,]$$

$$\Delta p^{-}(\bar{x}) = -2\mu\gamma\, X_a^{(1)}(\bar{x},1) - 2X_a^{(2)}(\bar{x},1) - 2\sum_m \gamma_m X_a^{(3,m)}(\bar{x},1) +$$

$$- \frac{\mu\gamma}{2\sqrt{a(1-a)}} \sin\theta - \sum_m \gamma_m \sin m\theta \qquad [\,-a\eta \leq \bar{x} \leq 0\,]$$

$$\Delta p^{-}(\bar{x}) = -2\mu\gamma\, X_a^{(1)}(\bar{x},1) - 2X_a^{(2)}(\bar{x},1) - 2\sum_m \gamma_m X_a^{(3,m)}(\bar{x},1) +$$

$$+ \mu\gamma - \sum_m \gamma_m \sin m\theta$$

4 Numerical program for the calculation of the effect of friction on torque, thrust and efficiency

4,1 Data for the calculations

4,2 Calculation of the effect of friction on torque, thrust and efficiency

4,1 Data for the calculations

$\lambda, a, \eta, d, \zeta, U, \mu, R_1, \nu, z, s^{(2)}, \bar{\gamma}, s^{(1)}$.

$g(x)$ for some values of x . $[-d\zeta \leq \bar{x} \leq (1-d)\zeta]$.

$X_a^{(1)}(0,\bar{r})$ for some values of r $[\lambda \leq \bar{r} \leq 1]$
$X_a^{(2)}(0,\bar{r})$ id
$X_a^{(3,m)}(0,\bar{r})$ id
$X_T^{(1)}(0,\bar{r})$ id

$X_a^{(1)}(\bar{x},1)$ for some values of x . $[-a\eta \leq \bar{x} \leq (1-a)\eta]$.
$X_a^{(2)}(\bar{x},1)$ id
$X_a^{(3,m)}(\bar{x},1)$ id

$X_a^{(1)}(\bar{x},\lambda)$ for $\bar{x}=0$
$X_a^{(2)}(\bar{x},\lambda)$
$X_a^{(3,m)}(\bar{x},\lambda)$

$\bar{c}(\bar{r})$ for some values of r . $[\lambda \leq \bar{r} \leq 1]$
$\bar{s}^{(1)}(r)$

$\gamma_1, \gamma_2, \cdots, \gamma_m, K_Q^{(1)}, K_s$.

4.2 Calculation of the effect of friction on torque, thrust and efficiency

Calculate $K_{Q_w}^{(1)}$, $K_{S_w}^{(1)}$, $K_{S_w}^{(2)}$, $K_{S_w}^{(3)}$, $K_{Q_{TOT}}$, K_{STOT}, η_w with the aid of the following relations

$$K_{Q_w}^{(1)} = \frac{\pi^2 z}{16\mu}\left[\mathrm{II}_1 + \mu\gamma\,\mathrm{II}_2 + \mathrm{II}_3 + \sum_m \gamma_m\,\mathrm{II}_{4,m} + \mu\gamma\,\mathrm{II}_5\right]$$

$$K_{S_w}^{(1)} = \frac{\pi^2 z}{8\mu^2}\left[\mathrm{II}_6 + \mu\gamma\,\mathrm{II}_7 + \mathrm{II}_8 + \sum_m \gamma_m\,\mathrm{II}_{9,m} + \mu\gamma\,\mathrm{II}_{10}\right]$$

$$K_{S_w}^{(2)} = \frac{\pi^3 \eta\, C_d^{(2)}}{4\mu^2}\left[1 + \frac{2}{\eta}\left\{\mu\gamma\,\mathrm{II}_{11} + \mathrm{II}_{12} + \sum_m \gamma_m\,\mathrm{II}_{13,m}\right\}\right]$$

$$K_{S_w}^{(3)} = \frac{\pi^3 C_d^{(3)}}{4\mu^2}\left[1 + \mu\gamma\,X_a^{(1)}(0,\lambda) + X_a^{(2)}(0,\lambda) + \sum_m \gamma_m X_a^{(3,m)}(0,\lambda)\right]\mathrm{II}_{14}$$

$$K_{STOT} = K_S - K_{S_w}^{(1)} - K_{S_w}^{(2)} - K_{S_w}^{(3)}$$

$$K_{Q_{TOT}} = K_Q^{(1)} + K_{Q_w}^{(1)}$$

$$\eta_w = \frac{1}{2\mu}\,\frac{K_{STOT}}{K_{Q_{TOT}}}$$

and

$$\mathrm{II}_1 = \int_\lambda^1 \bar{c}(\bar{r})\, C_d^{(1)}(\bar{r})\,(1+\mu^2\bar{r}^2)^{1/2}\,\bar{r}^2\,d\bar{r}$$

$$\mathrm{II}_2 = \int_\lambda^1 \bar{c}(\bar{r})\, C_d^{(1)}(\bar{r})\,(1+\mu^2\bar{r}^2)^{-1/2}\,\bar{r}^2\,X_a^{(1)}(0,\bar{r})\,d\bar{r}$$

$$\mathrm{II}_3 = \int_\lambda^1 c(\bar{r})\, C_d^{(1)}(\bar{r})\,(1+\mu^2\bar{r}^2)^{-1/2}\,\bar{r}^2\,X_a^{(2)}(0,\bar{r})\,d\bar{r}$$

$$\mathrm{II}_{4,m} = \int_\lambda^1 c(\bar{r})\, C_d^{(1)}(\bar{r})\,(1+\mu^2\bar{r}^2)^{-1/2}\,\bar{r}^2\,X_a^{(3,m)}(0,\bar{r})\,d\bar{r}$$

$$\mathrm{II}_5 = \int_\lambda^1 c(\bar{r})\, C_d^{(1)}(\bar{r})\,(1+\mu^2\bar{r}^2)^{-1/2}\,(1+2\mu^2\bar{r}^2)\,\bar{r}^2\,X_T^{(1)}(0,\bar{r})\,d\bar{r}$$

$$\mathrm{II}_6 \int_\lambda^1 c(\bar{r})\, C_d^{(1)}(\bar{r})\,(1+\mu^2\bar{r}^2)^{1/2}\,d\bar{r}$$

$$\mathrm{II}_7 = \int_\lambda^1 \bar{c}(\bar{r})\, c_d^{(1)}(\bar{r})\, (1+\mu^2\bar{r}^2)^{-1/2}\, (2+\mu^2\bar{r}^2)\, X_a^{(1)}(0,\bar{r})\, d\bar{r}$$

$$\mathrm{II}_8 = \int_\lambda^1 \bar{c}(\bar{r})\, c_d^{(2)}(\bar{r})\, (1+\mu^2\bar{r}^2)^{-1/2}\, (2+\mu^2\bar{r}^2)\, X_a^{(2)}(0,\bar{r})\, d\bar{r}$$

$$\mathrm{II}_{9,m} = \int_\lambda^1 \bar{c}(\bar{r})\, c_d^{(3)}(\bar{r})\, (1+\mu^2\bar{r}^2)^{-1/2}\, (2+\mu^2\bar{r}^2)\, X_a^{(3,m)}(0,\bar{r})\, d\bar{r}$$

$$\mathrm{II}_{10} = \int_\lambda^1 \bar{c}(\bar{r})\, c_d^{(3)}(\bar{r})\, (1+\mu^2\bar{r}^2)^{-1/2}\, \mu\bar{r}\, X_T^{(1)}(0,\bar{r})\, d\bar{r}$$

$$\mathrm{II}_{11} = \int_{-a\eta}^{(1-a)\eta} X_a^{(1)}(\bar{x},1)\, d\bar{x}$$

$$\mathrm{II}_{12} = \int_{-a\eta}^{(1-a)\eta} X_a^{(2)}(\bar{x},1)\, d\bar{x}$$

$$\mathrm{II}_{13,m} = \int_{-a\eta}^{(1-a)\eta} X_a^{(3)}(\bar{x},1)\, d\bar{x}$$

$$\mathrm{II}_{14} = \int_{-d\zeta}^{(1-d)\zeta} \bar{G}_j(\bar{x}) \sqrt{1+\left[\frac{d\bar{G}_j(\bar{x})}{d\bar{x}}\right]^2}\, d\bar{x}$$

and

$$c_d^{(1)}(\bar{r}) = 2\, c_f^{(1)}(\bar{r}) \left[1 + 2\bar{s}^{(1)}(\bar{r}) + \frac{c_L^2(\bar{r})}{16}\right]$$

$$c_d^{(2)}(\bar{r}) = 2\, c_f^{(2)} \left[1 + 2\bar{s}^{(2)}\right]$$

$$c_d^{(3)}(\bar{r}) = c_f^{(3)}$$

and

$$c_L(\bar{r}) = \frac{4\pi\bar{\gamma}}{2\,c(\bar{r})\,(1+\mu^2\bar{r}^2)^{1/2}}$$

$$c_f^{(1)}(\bar{r}) = 0{,}455 \left[\log\left\{(1+\eta^2\bar{r}^2)^{1/2}\, c(\bar{r})\, \frac{UR_1}{\nu}\right\}\right]^{-2{,}58}$$

$$c_f^{(2)}(\bar{r}) = 0{,}455 \left[\log\left\{\eta\, \frac{UR_1}{\nu}\right\}\right]^{-2{,}58}$$

$$c_f^{(3)}(\bar{r}) = 0{,}455 \left[\log\left\{\zeta\, \frac{UR_1}{\nu}\right\}\right]^{-2{,}58}$$

η = 0.36
a = 0.60
Λ = 1.35
K_T = 0.10 → $f \simeq 0.8$
λ = 0.80
THE SHROUD HAS A NACA 0007 BASIS THICKNESS FORM

X	S(x) FOR f_1=0	S(x) FOR f_1=0.2	S(x) FOR f_1=0.4
-0.216	+0.53	+2.51	+4.49
-0.186	+0.10	+1.43	+2.77
-0.156	-0.20	+0.62	+1.44
-0.126	-0.38	+0.34	+0.47
-0.096	-0.45	-0.32	-0.20
-0.066	-0.40	-0.44	-0.47
-0.036	-0.27	-0.36	-0.45
-0.006	-0.05	-0.09	-0.12
+0.024	+0.21	+0.34	+0.46
+0.054	+0.49	+0.91	+1.34
+0.084	+1.08	+1.90	+2.72
+0.114	+1.99	+3.32	+4.66
+0.144	+2.95	+4.93	+6.51

THEORETICALLY DETERMINED CAMBERLINES OF SHROUDS

TABLE 4.1

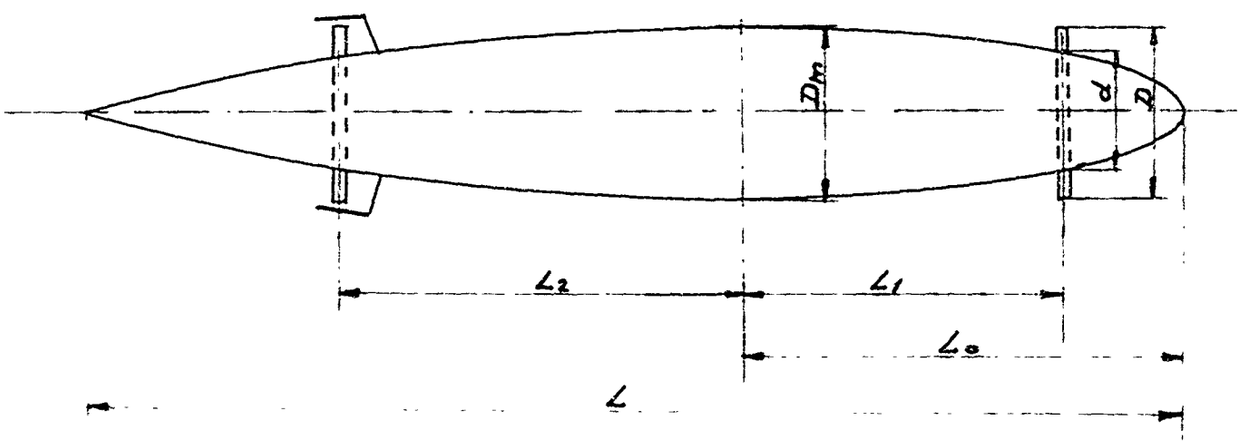

$L = 4.10$ m

$D_m = 0.60$ m

$L_o = 1.78$ m

$L_1 = 1.32$ m

$L_2 = 1.32$ m

$D = 0.49$ m

$d = 0.40$ m

MODEL OF THE TANDEM PROPELLER SUBMARINE

FIG. 3.3

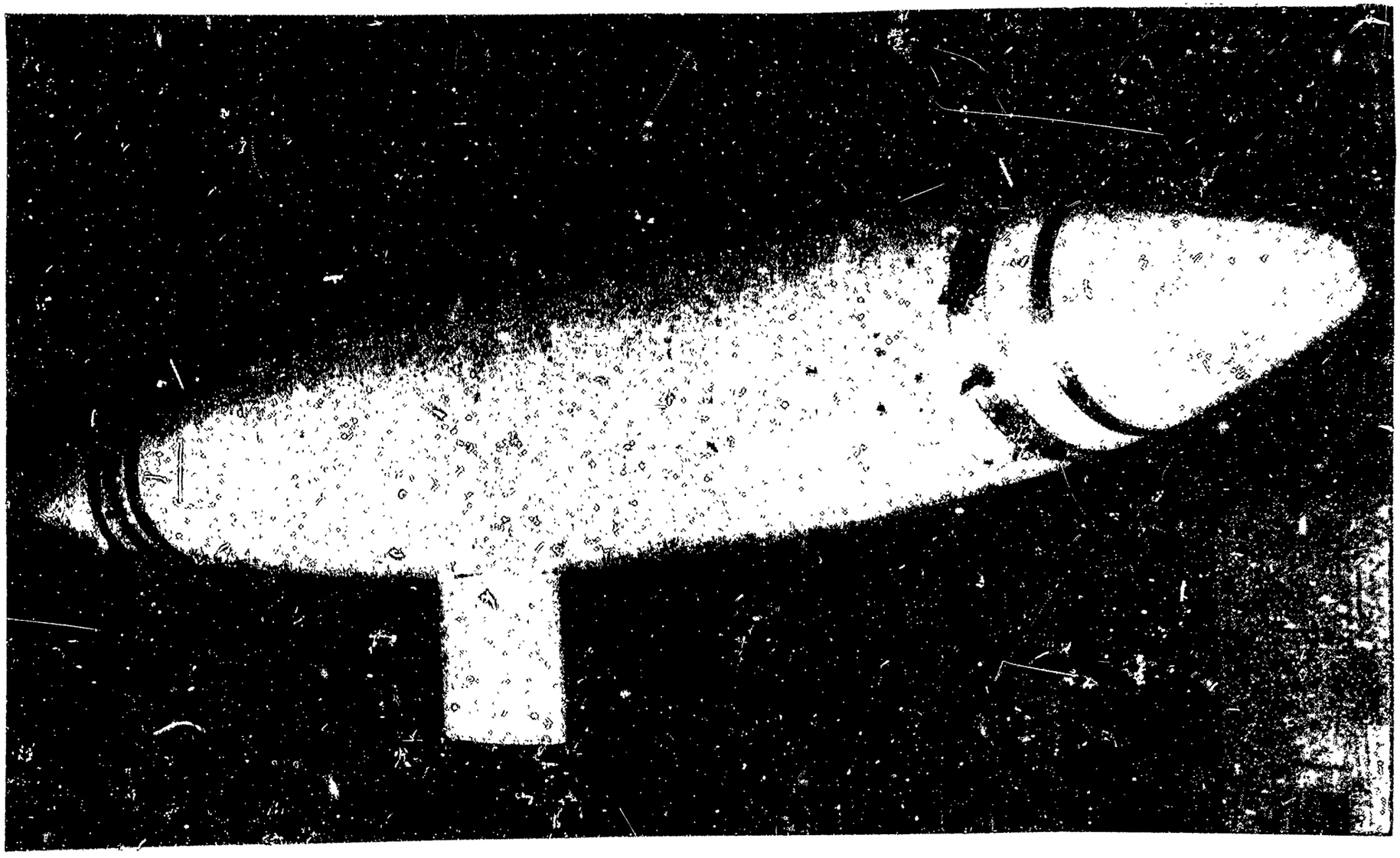

FIG. 33

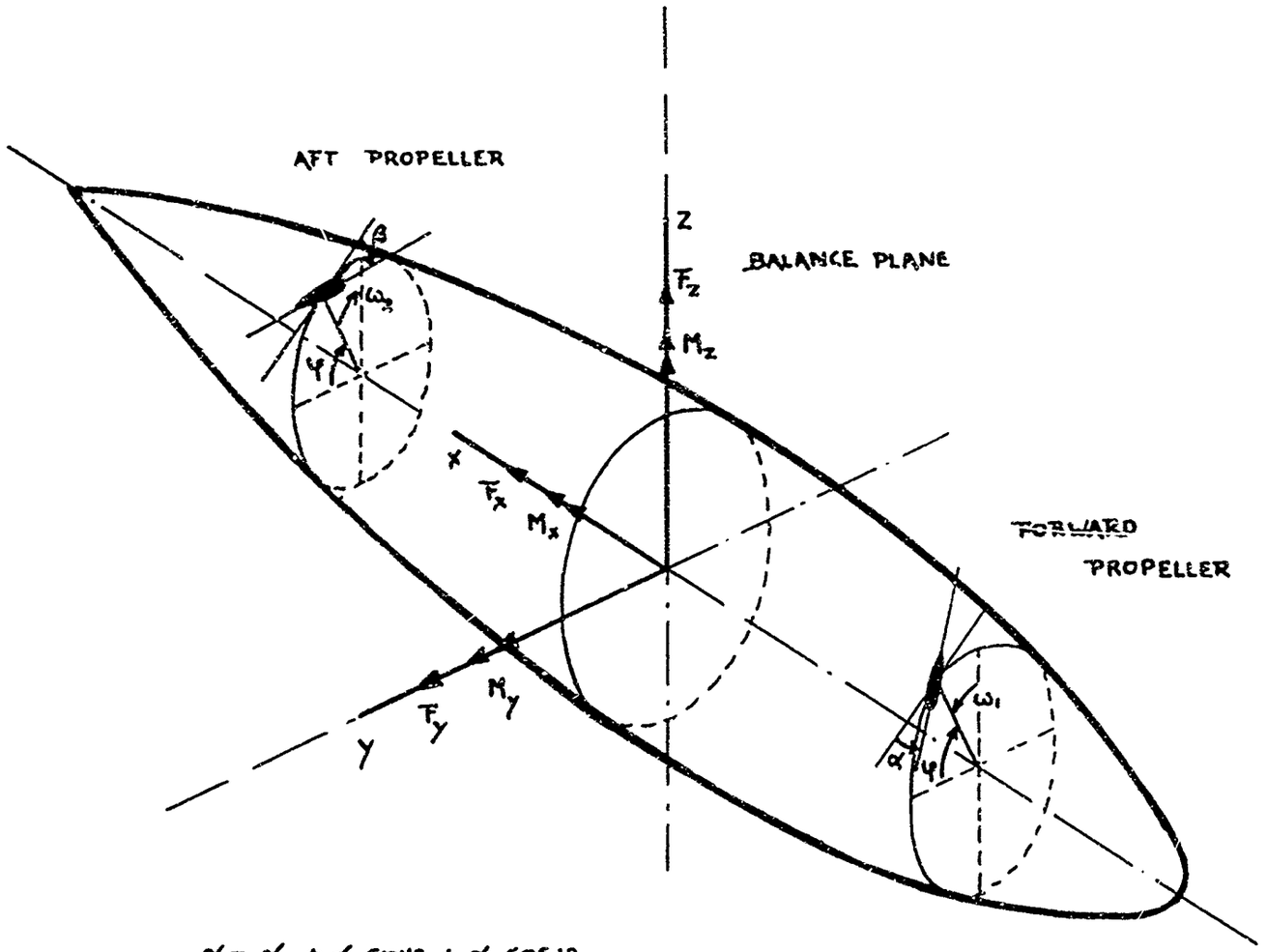

$$\alpha = \alpha_0 + \alpha_1 \sin\varphi + \alpha_2 \cos\varphi$$

$$\beta = \beta_0 + \beta_1 \sin\varphi + \beta_2 \cos\varphi$$

TANDEM PROPELLER SUBMARINE SIGN CONVENTIONS

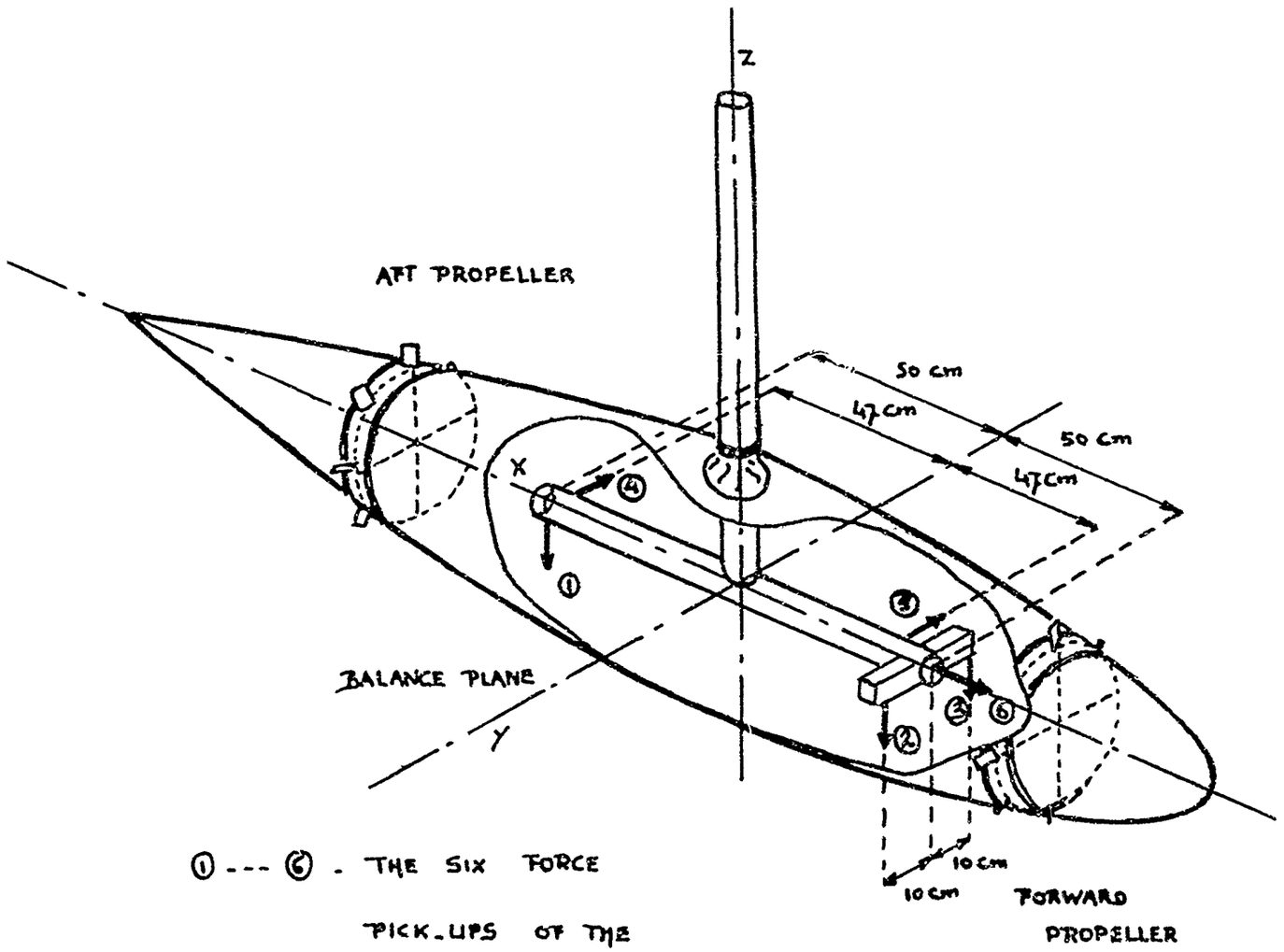

① --- ⑥ . THE SIX FORCE PICK-UPS OF THE BALANCE

CONFIGURATION OF THE BALANCE

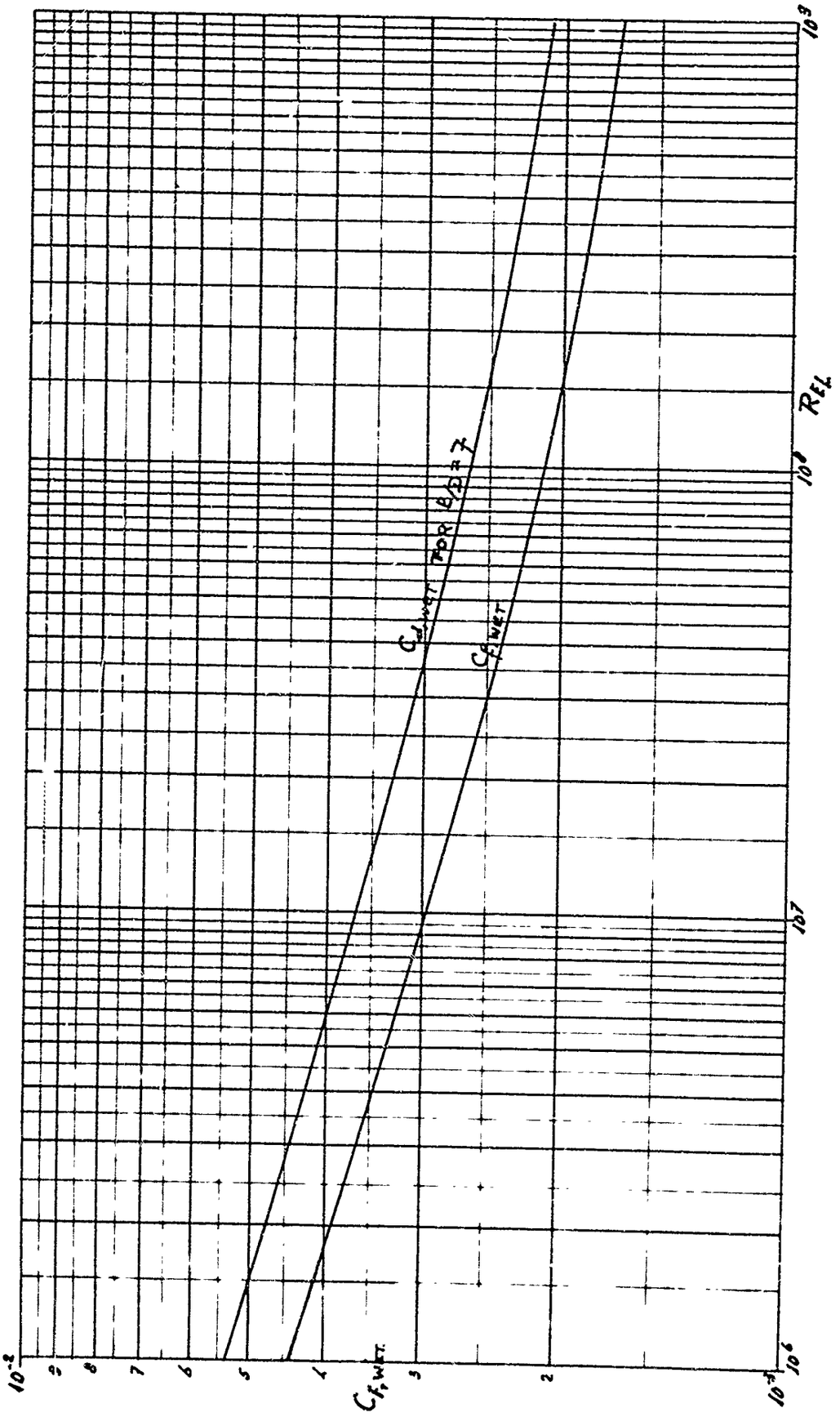

DRAG COEFFICIENTS AS A FUNCTION OF REYNOLDS NUMBERS

NEDERLANDSCH SCHEEPSBOUWKUNDIG PROEFSTATION WAGENINGEN	NR.	BLZ.

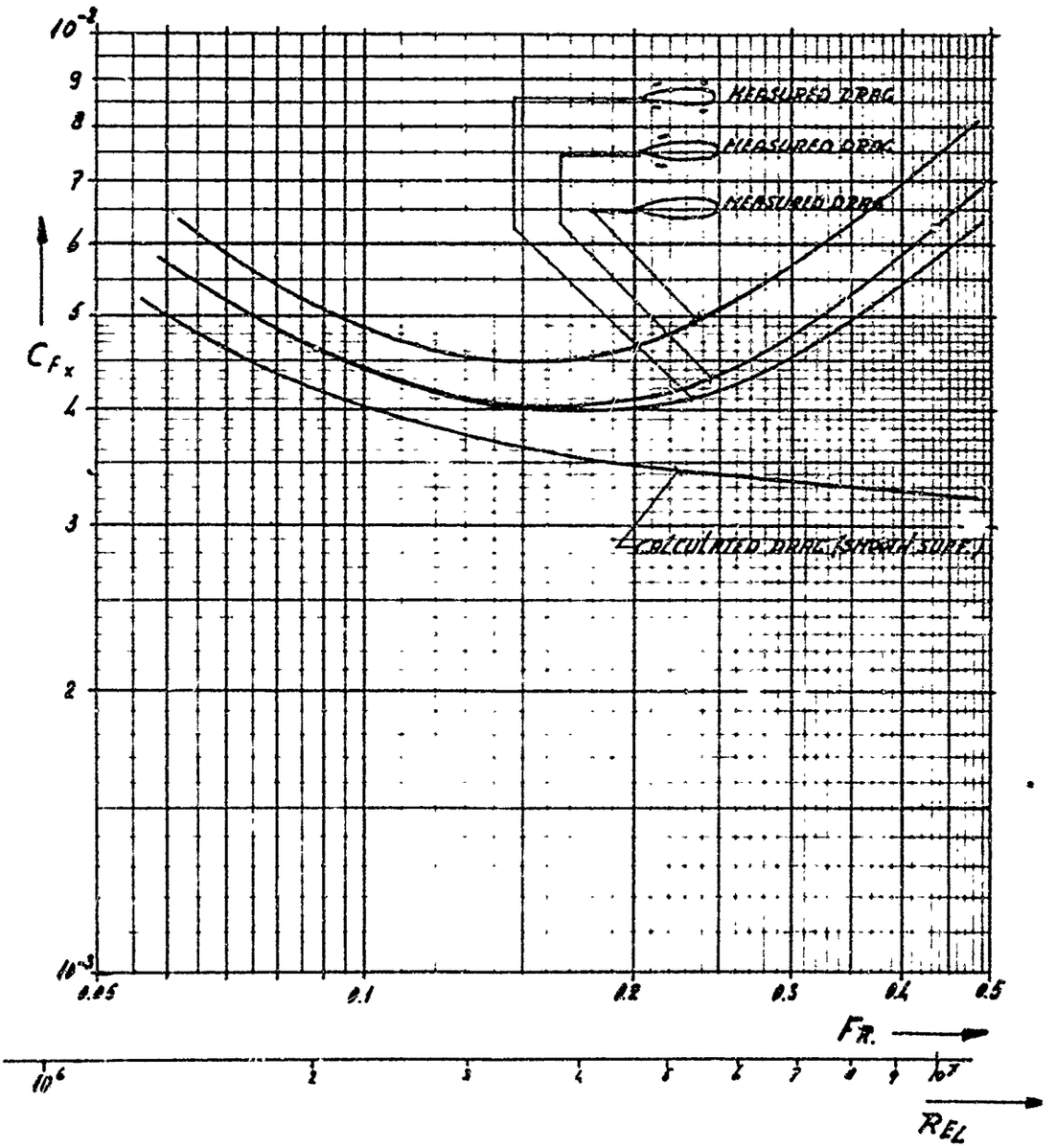

DRAG COEFFICIENTS AS FUNCTIONS OF

FROUDE AND REYNOLDS NUMBERS

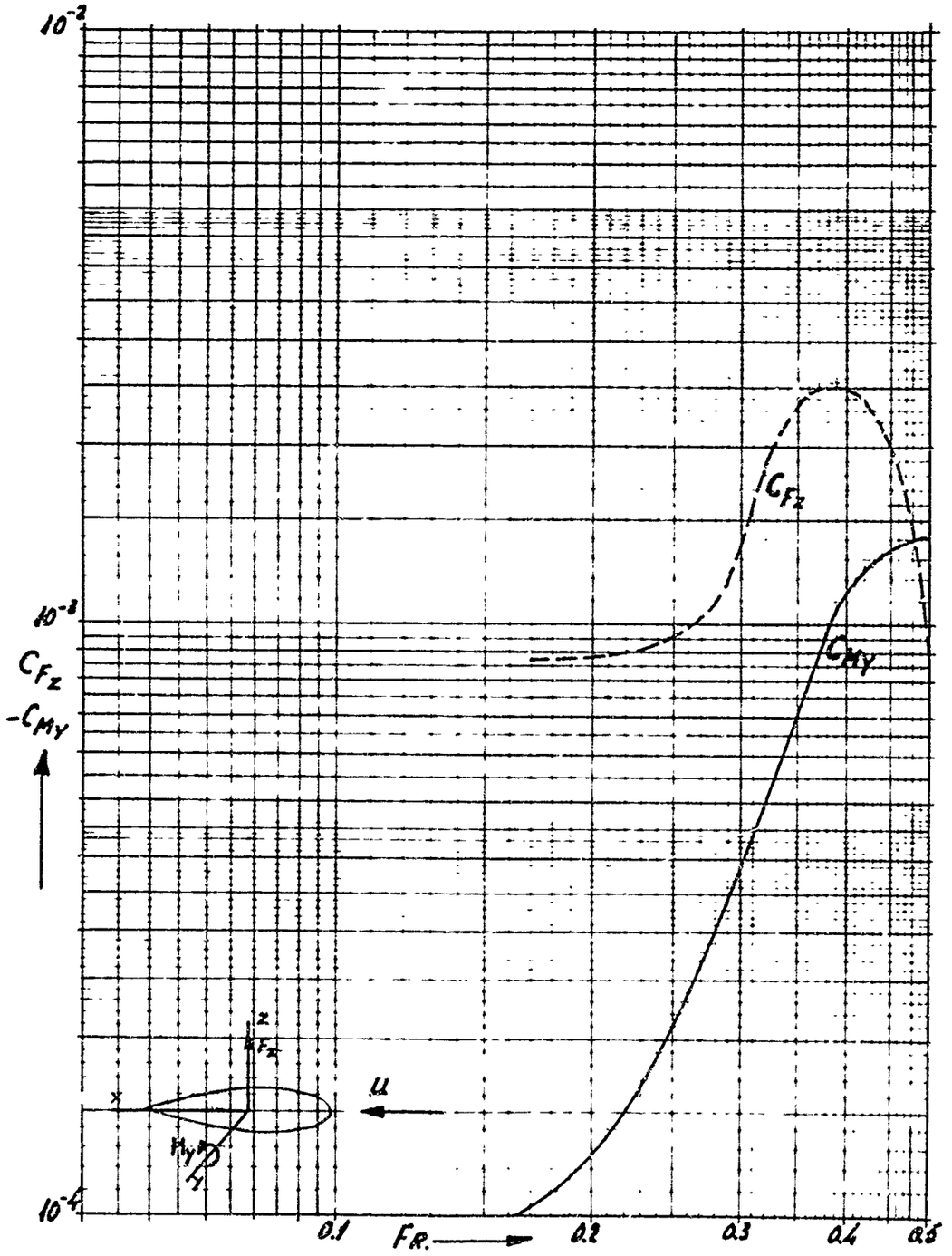

C_{F_z} AND C_{M_y} AS FUNCTIONS OF FROUDE NUMBERS

FIG. 3.8

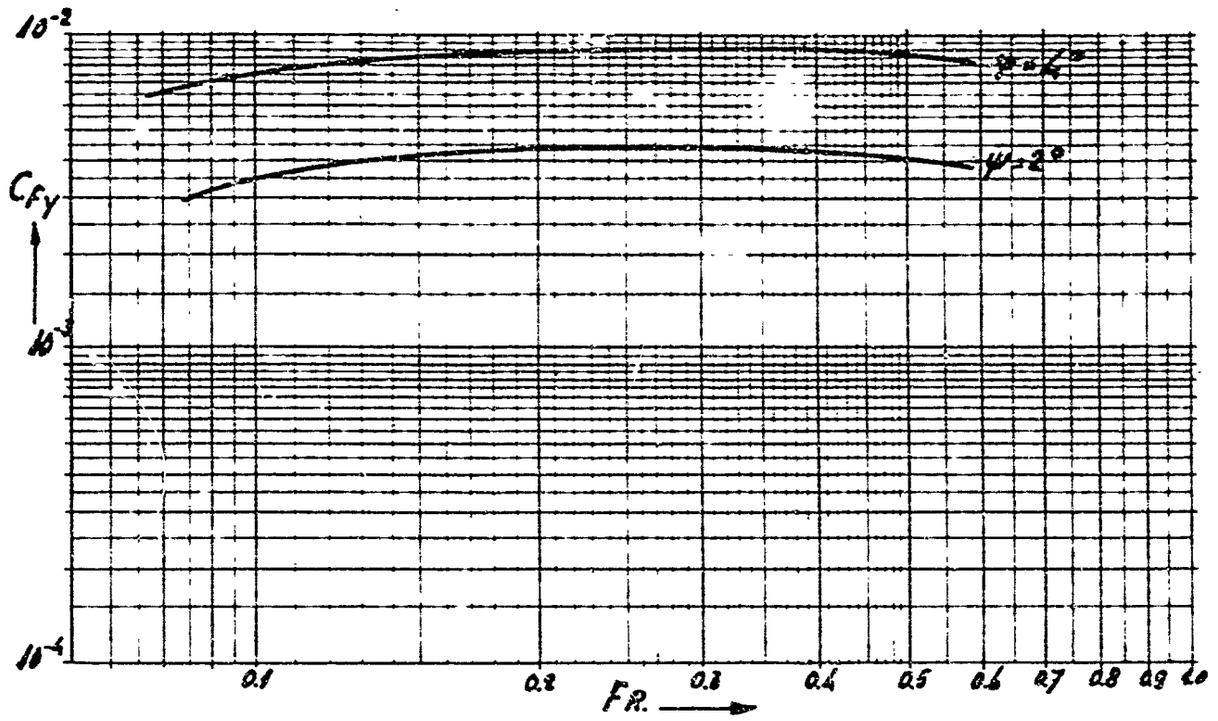
10^{-2}
C_{F_y}
10^{-3}
10^{-4}
$\psi = 4°$
$\psi = 2°$
0.1
0.2
0.3
0.4
0.5
0.6
0.7
0.8
0.9
1.0
FR.

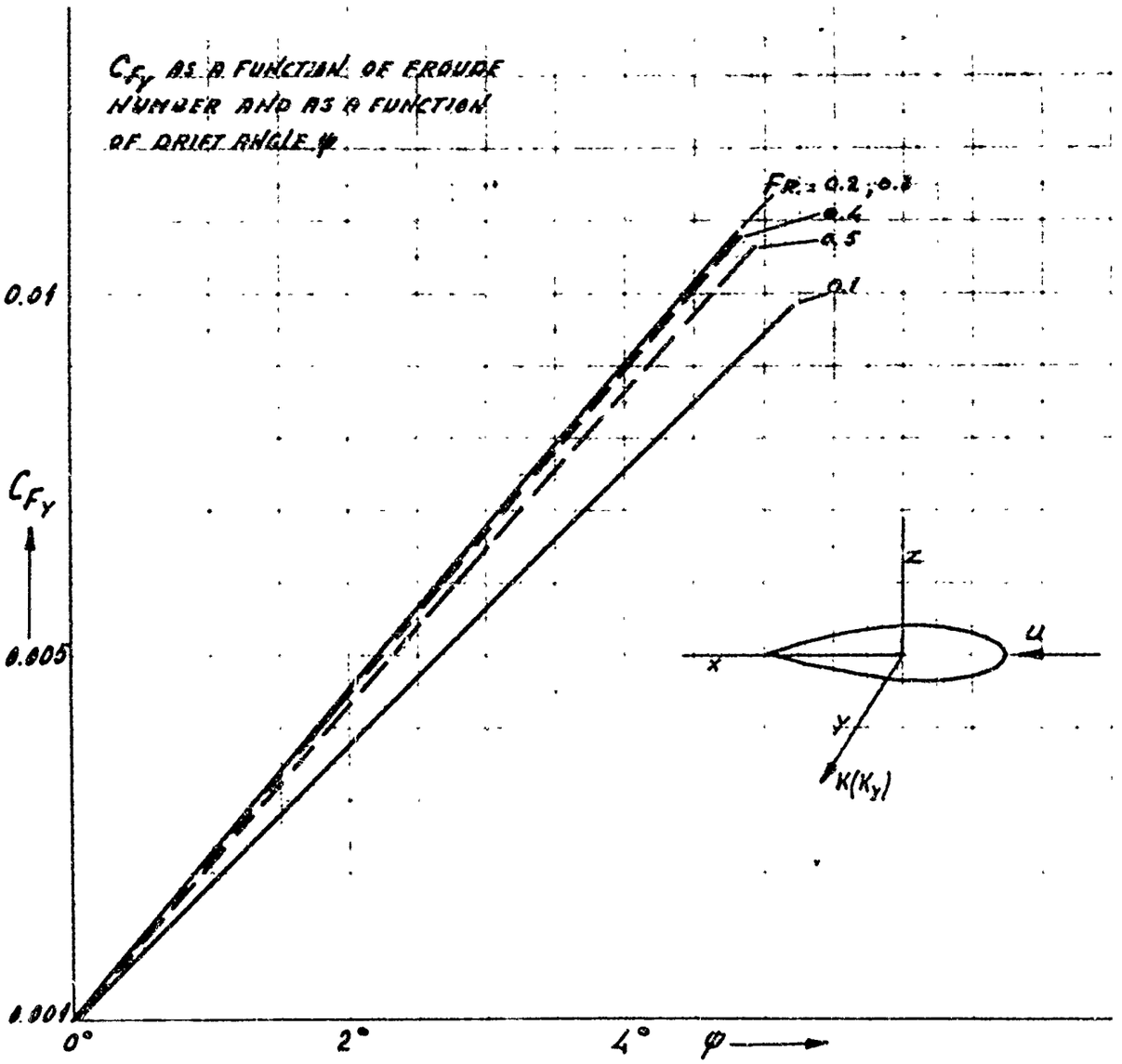
C_{F_y} AS A FUNCTION OF FROUDE NUMBER AND AS A FUNCTION OF DRIFT ANGLE ψ.
FR. = 0.2 ; 0.3
0.4
0.5
0.1
0.01
C_{F_y}
0.005
0.001
z
u
x
y
K(K_y)
0°
2°
4°
ψ

NEDERLANDSCH SCHEEPSBOUWKUNDIG PROEFSTATION WAGENINGEN	NR.	BLZ.

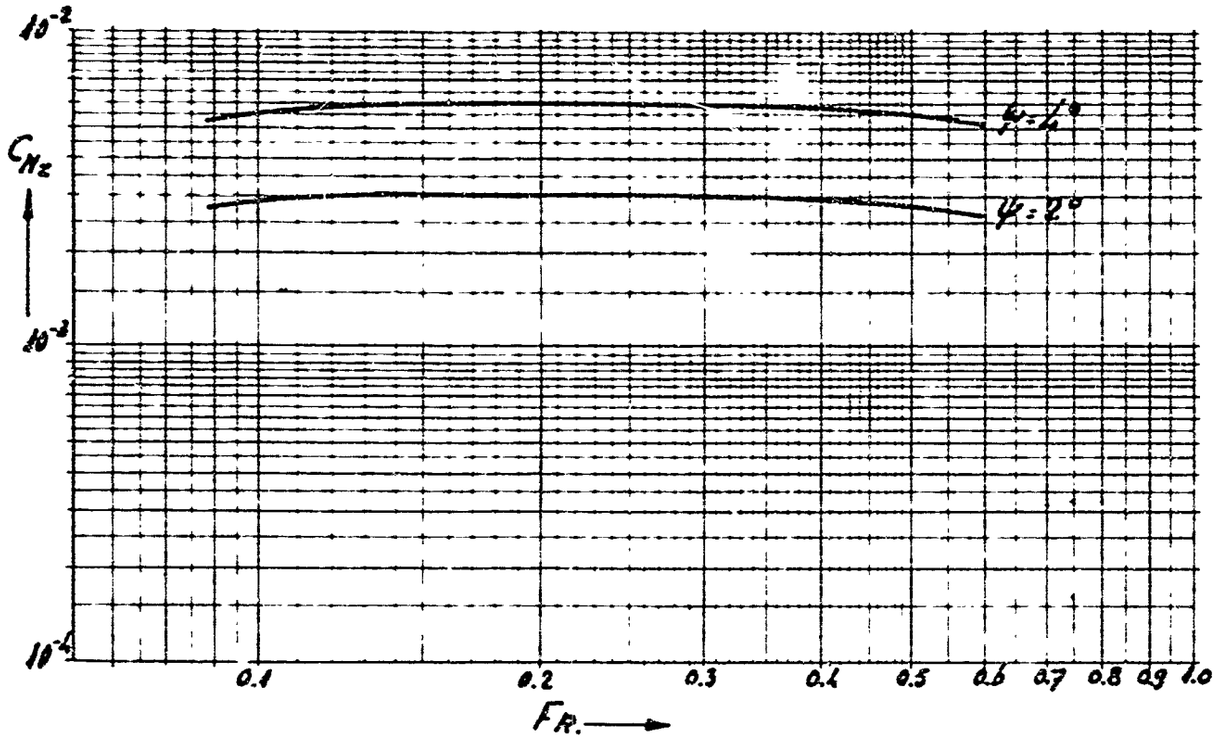

C_{Mz} AS A FUNCTION OF FROUDE NUMBER AND AS A FUNCTION OF DRIFT ANGLE ψ.

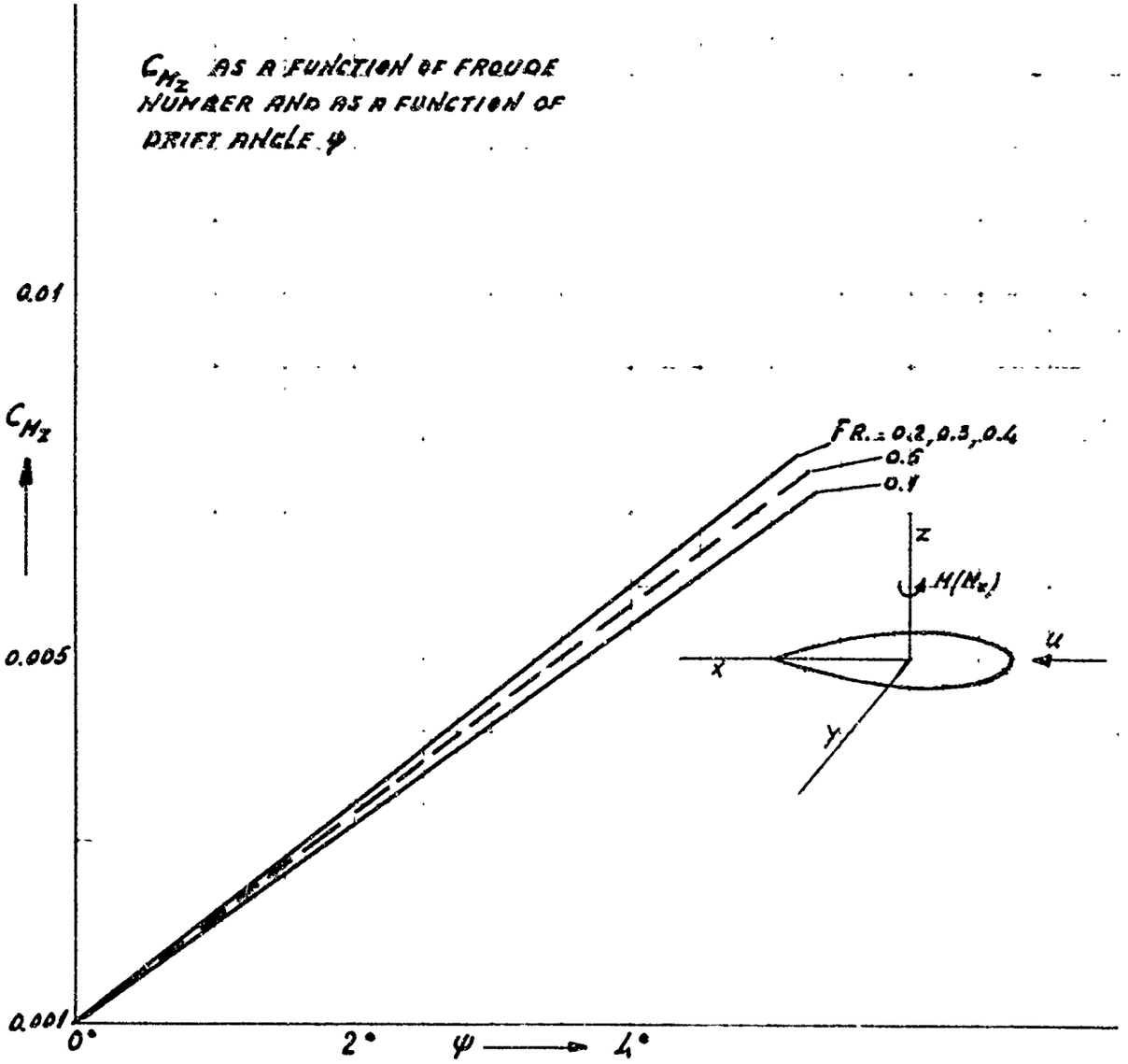

NEDERLANDSCH SCHEEPSBOUWKUNDIG PROEFSTATION WAGENINGEN	NO.	BLZ.

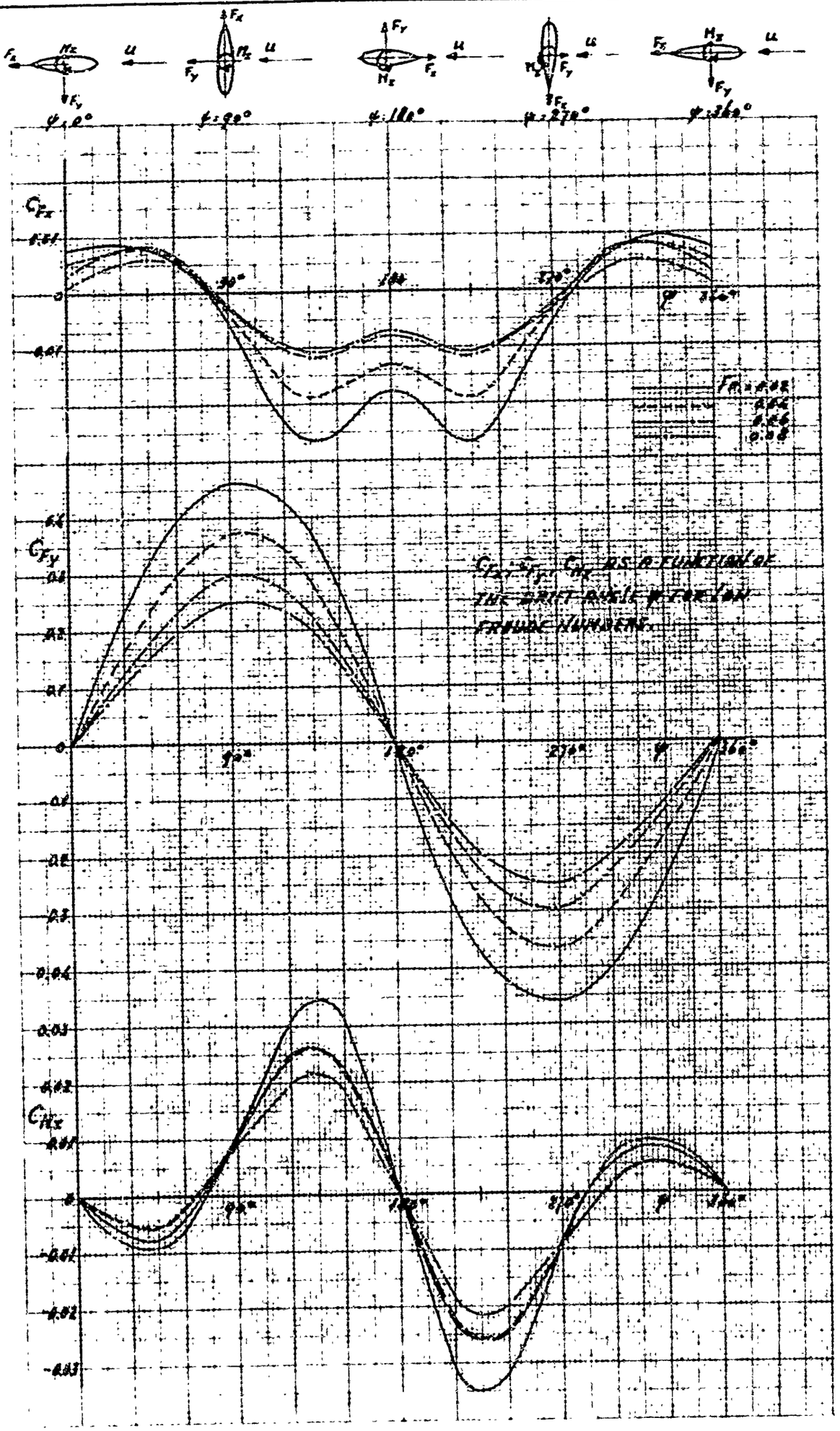

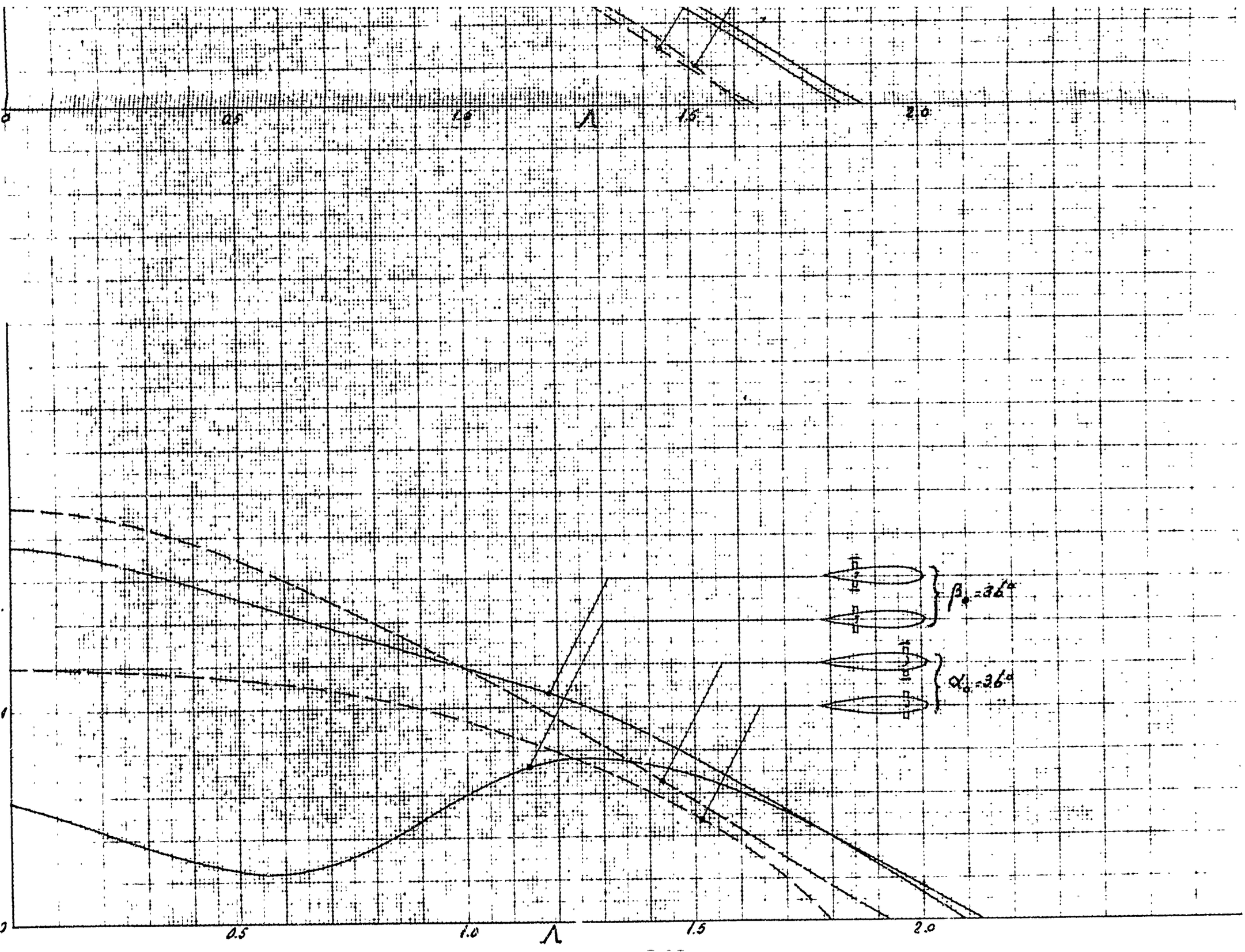
0.5
1.0
Λ
1.5
2.0
$\beta_0 = 36^\circ$
$\alpha_0 = 36^\circ$

FIG. 15 AS A FUNCTION OF A FOR SEVERAL PROPELLER CONFIGURATIONS

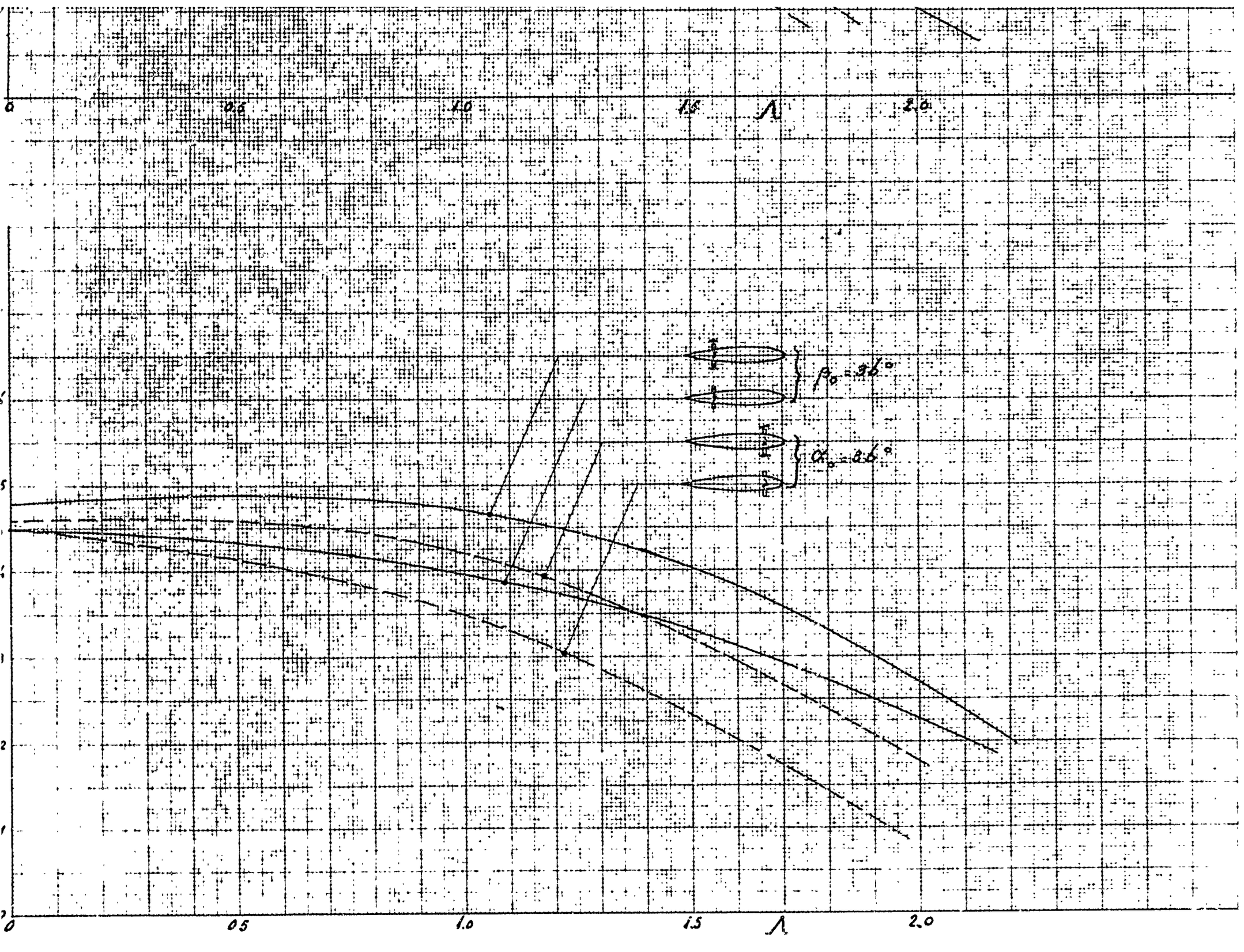
0
0.5
1.0
1.5
λ
2.0
$\beta_0 = 36°$
$\alpha_0 = 26°$
0
0.5
1.0
1.5
λ
2.0

fig 314

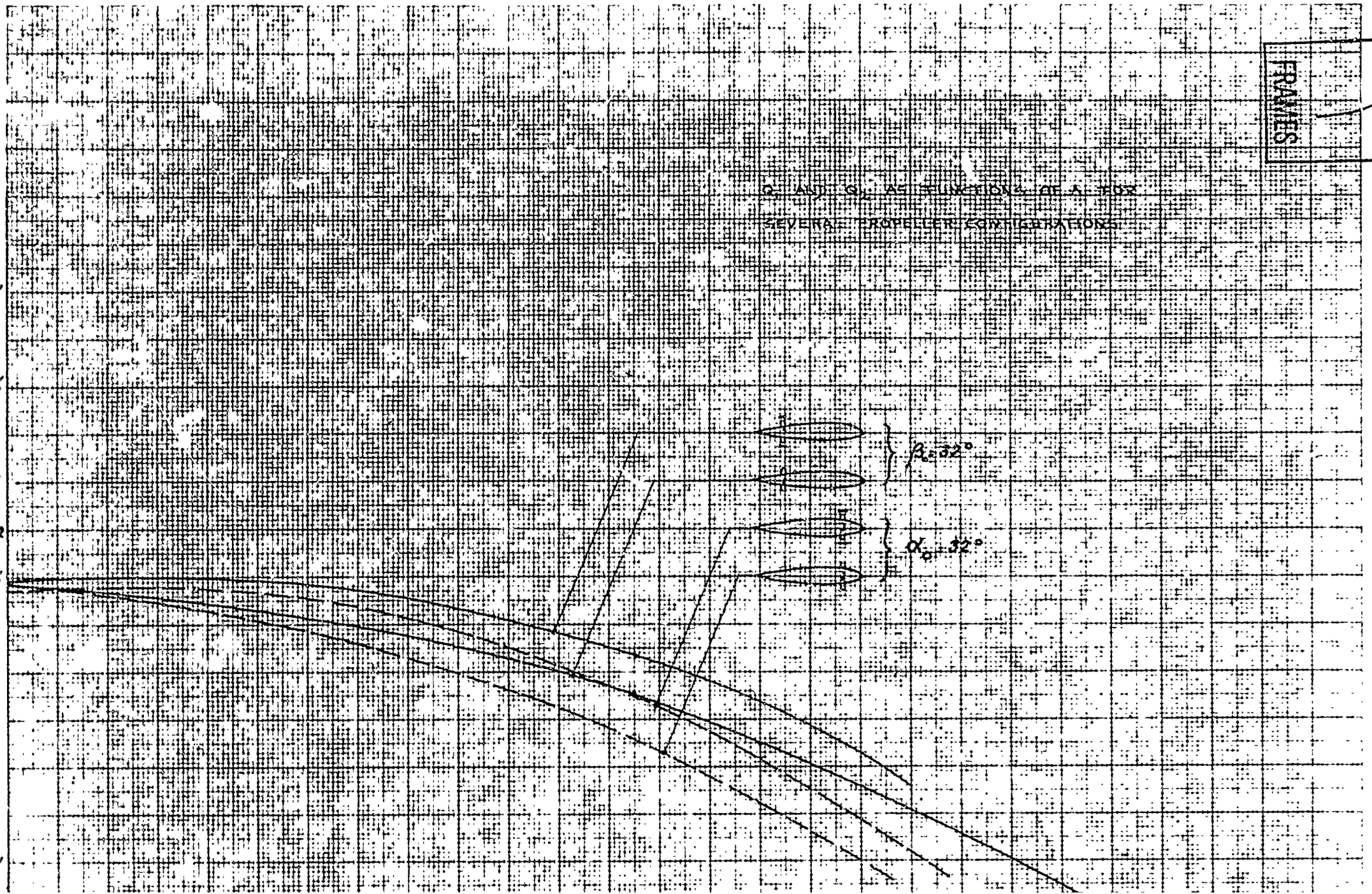
FRAMES
C_T AND C_L AS FUNCTIONS OF λ FOR
SEVERAL PROPELLER CONFIGURATIONS
$\beta_{.75} = 32°$
$\alpha_0 = 32°$

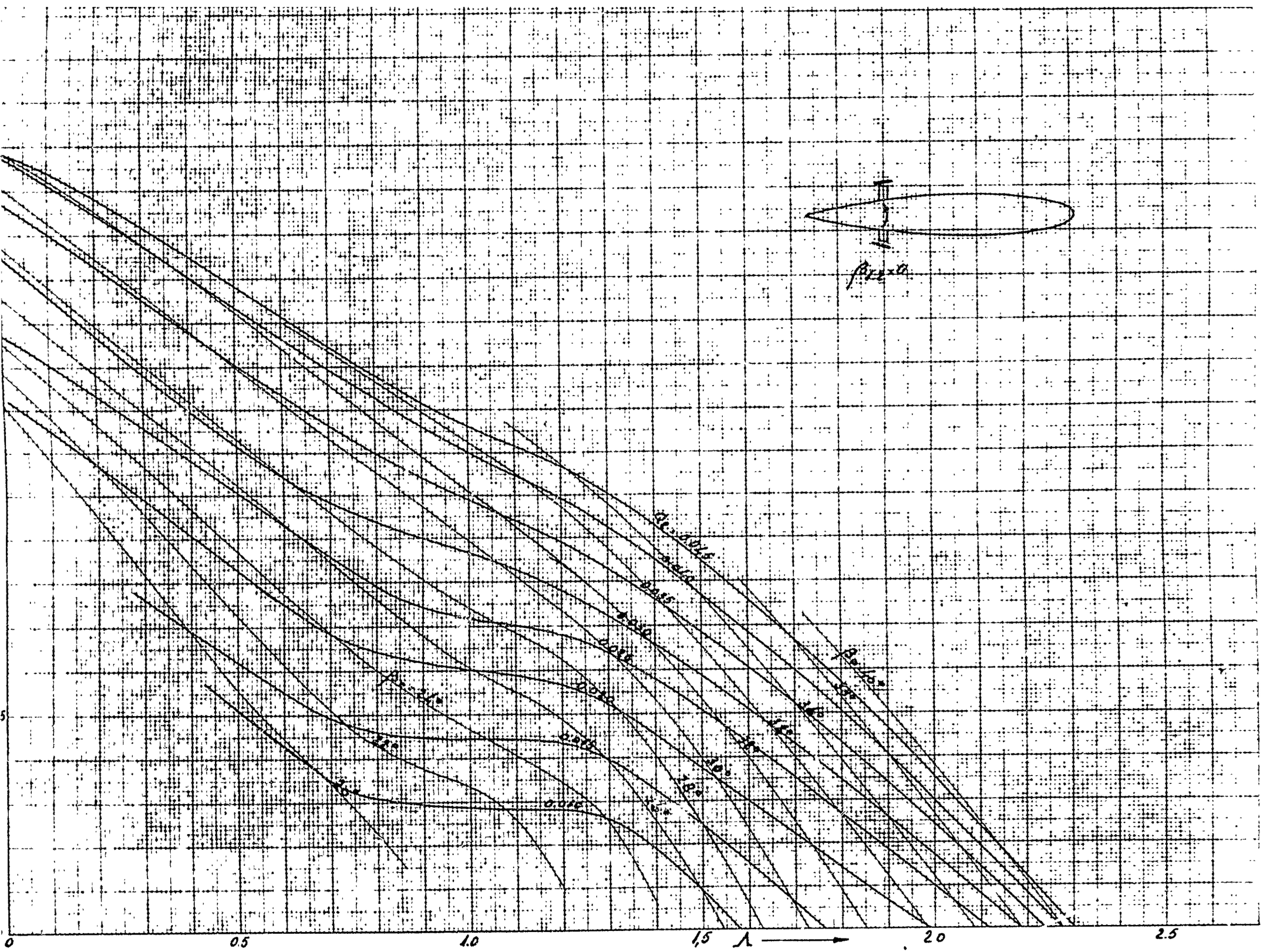
$\beta_{12}=0$
0.055
0.050
0.045
0.040
0.035
0.030
0.025
0.020
0.015
0.010
0.005
λ
0
0.5
1.0
1.5
2.0
2.5

MAXIMUM THRUST COEFFICIENT OF THE
SHROUDED AFT PROPELLER AS A FUNCTION
OF J FOR A GIVEN TORQUE COEFFICIENT

FRAMES

NEDERLANDSCH SCHEEPSBOUWKUNDIG PROEFSTATION WAGENINGEN	NO.	BLZ.

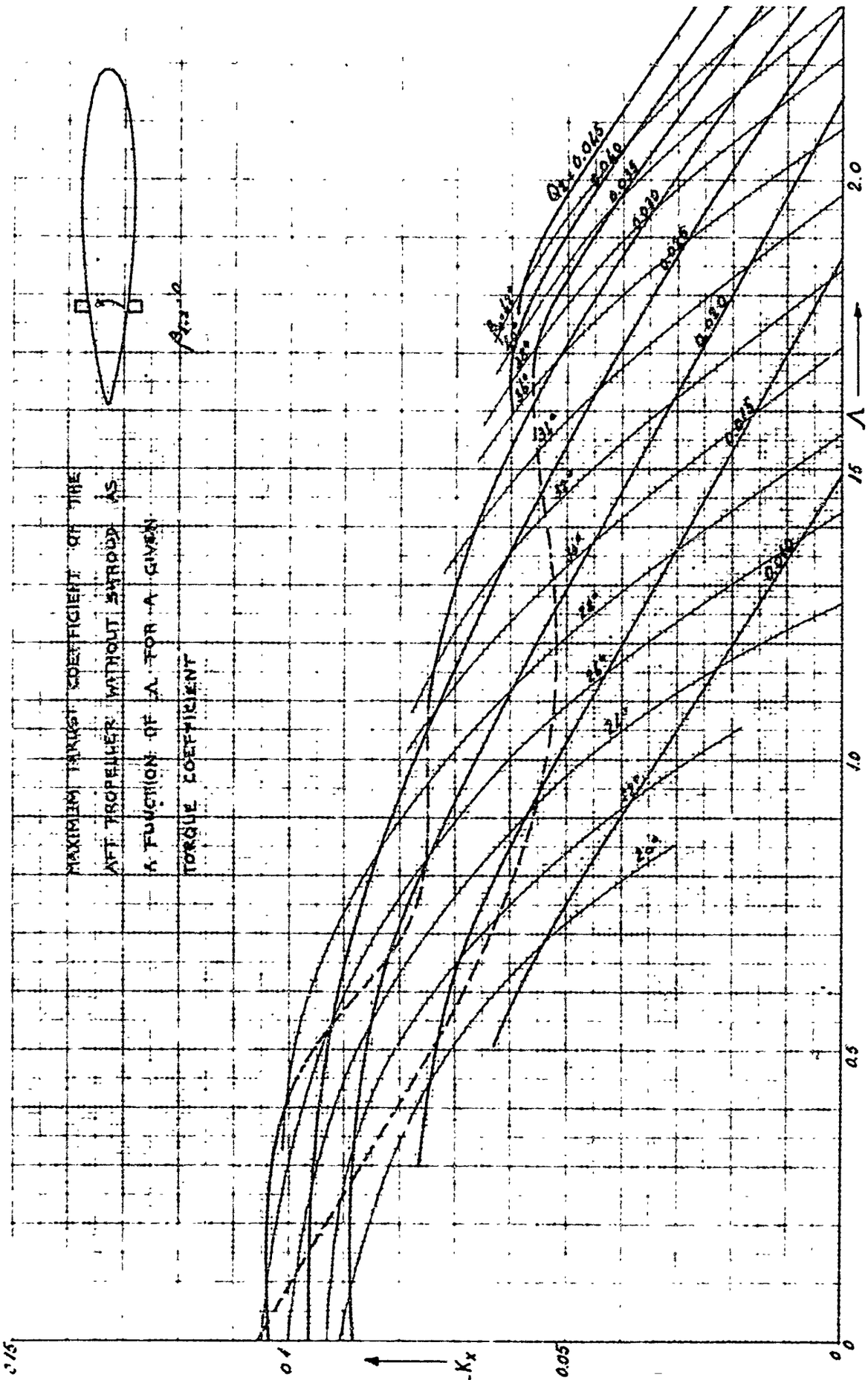

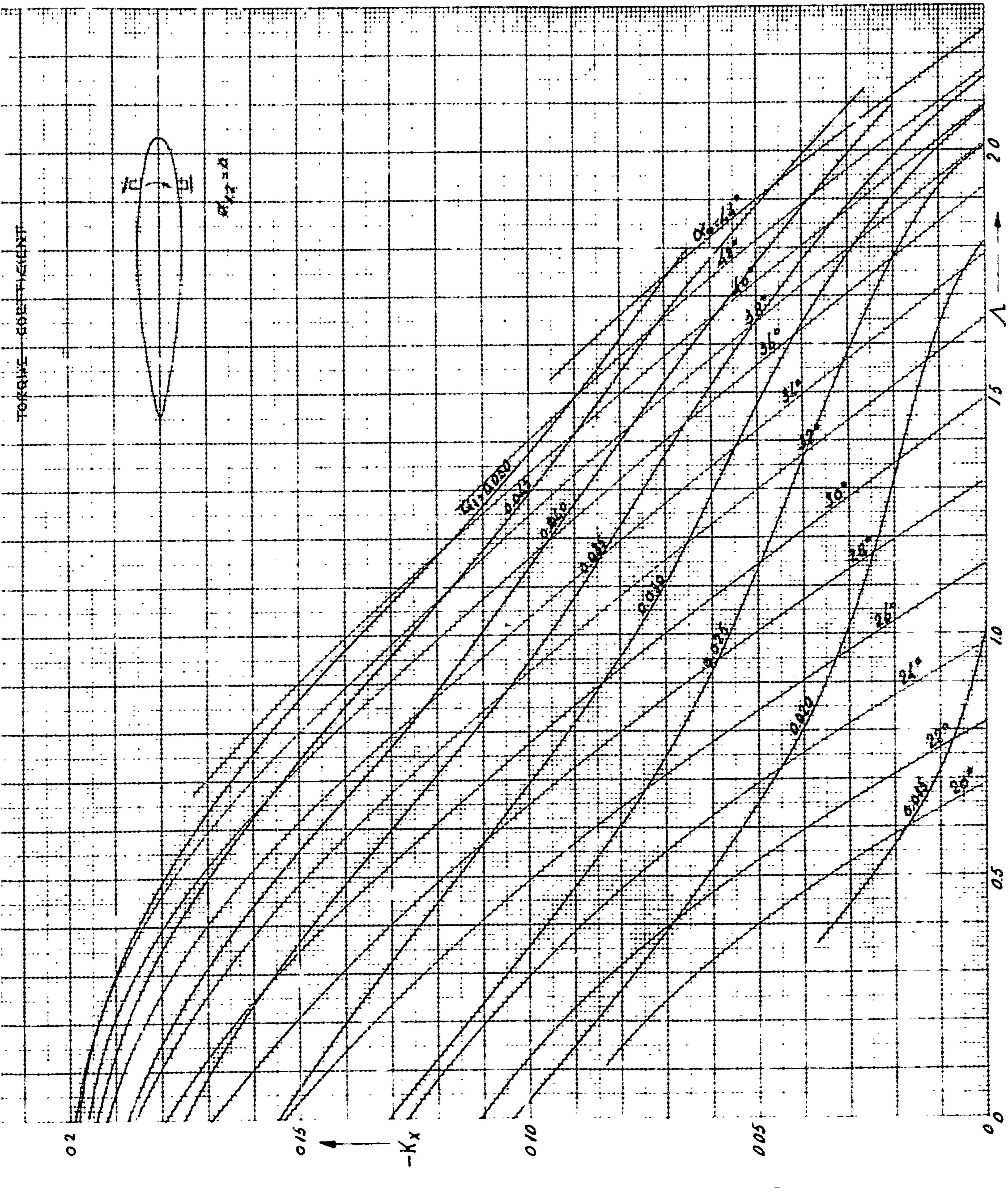
TORQUE COEFFICIENT
−Kx
Λ
0.2
0.15
0.10
0.05
0.0
0.5
1.0
1.5
2.0
αo = 43°
42°
40°
38°
36°
34°
32°
30°
28°
26°
24°
22°
20°
G1 = 0.050
0.045
0.040
0.035
0.030
0.025
0.020
0.015

FRAMES

MAXIMUM THRUST COEFFICIENT OF THE SHROUDED FORWARD PROPELLER AS A FUNCTION OF λ FOR A GIVEN TORQUE COEFFICIENT

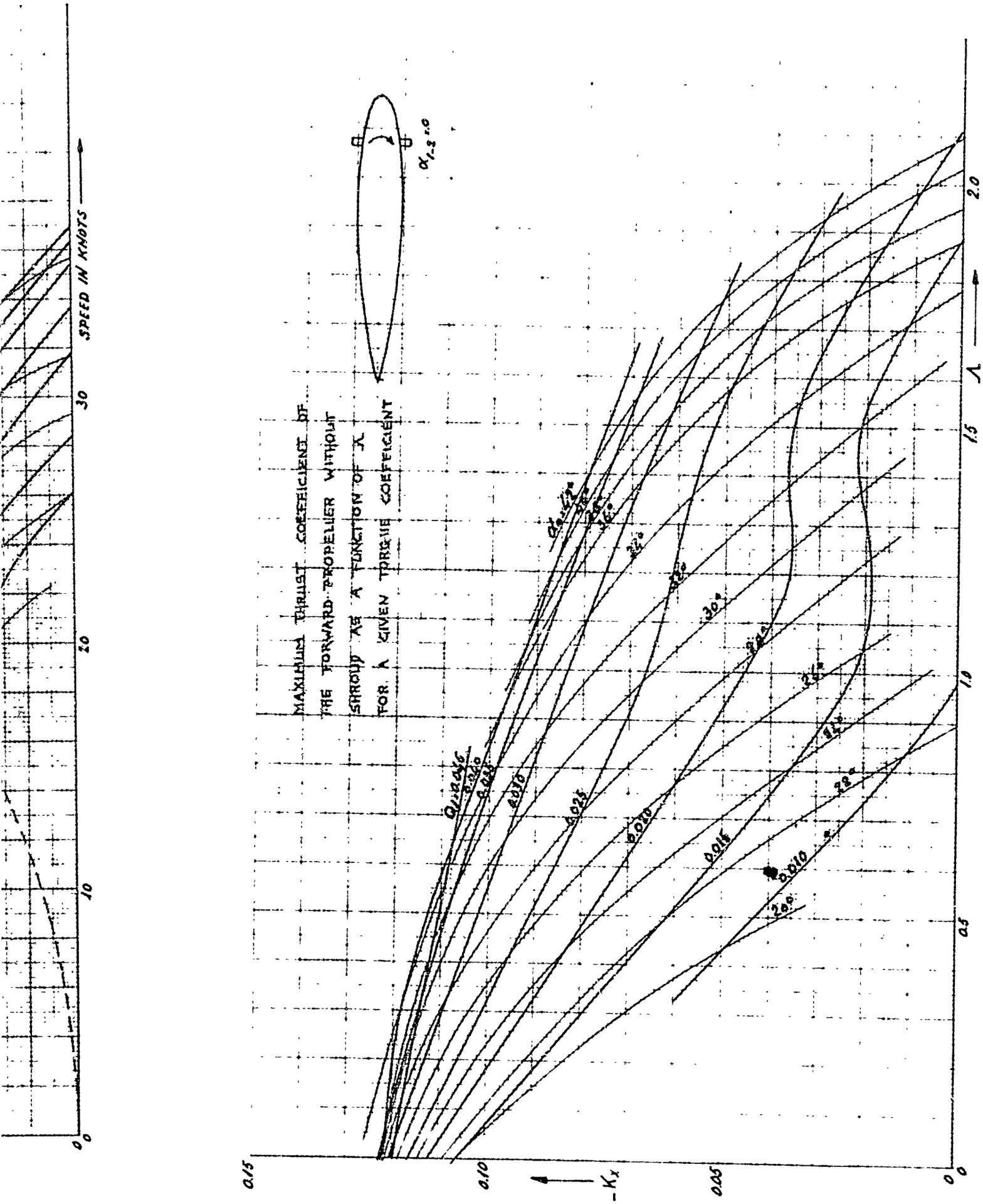
MAXIMUM THRUST COEFFICIENT OF THE FORWARD PROPELLER WITHOUT SHROUD AS A FUNCTION OF J FOR A GIVEN TORQUE COEFFICIENT
SPEED IN KNOTS
$-K_x$
λ
$\alpha_{r.s}$ 1.0
Q=0.046
0.040
0.035
0.030
0.025
0.020
0.015
0.010
32°
30°
28°
26°
24°
22°
20°
16°
12°
0.15
0.10
0.05
0
0.5
1.0
1.5
2.0
10
20
30

fig. 3.17

NEDERLANDSCH SCHEEPSBOUWKUNDIG PROEFSTATION WAGENINGEN	NO.	BLZ

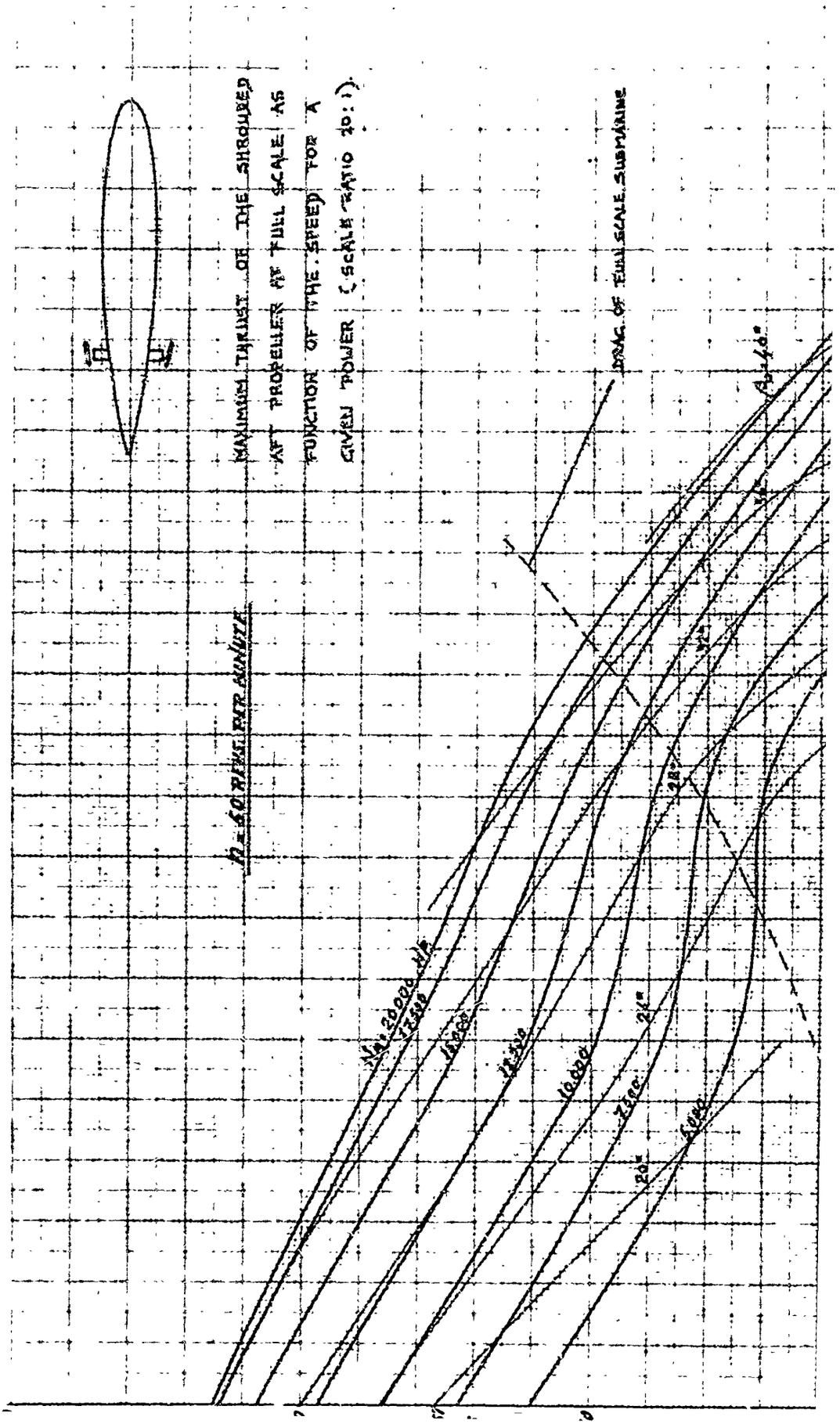

NEDERLANDSCH SCHEEPSBOUWKUNDIG PROEFSTATION WAGENINGEN	NO.	BLZ.

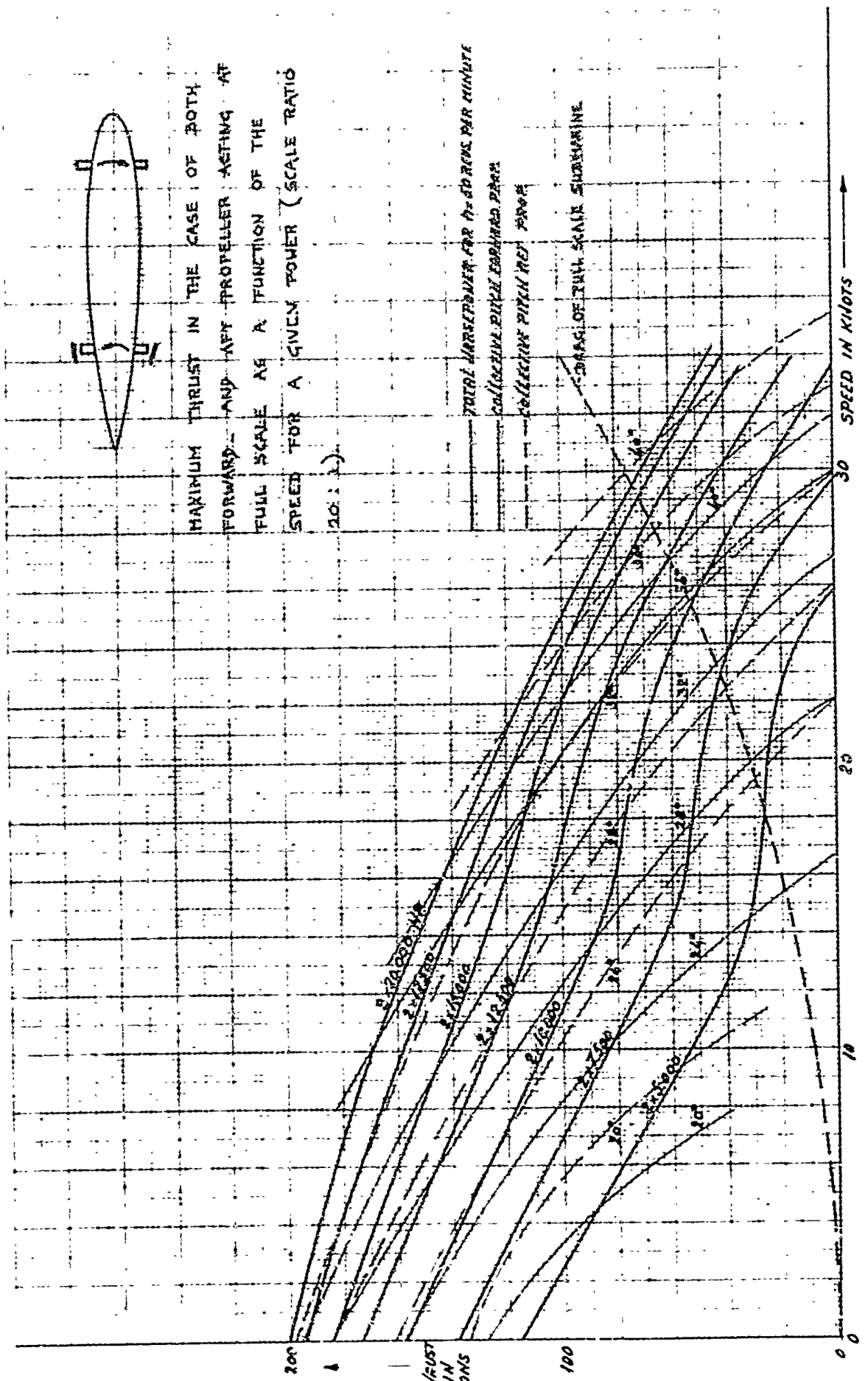

fig 3.20

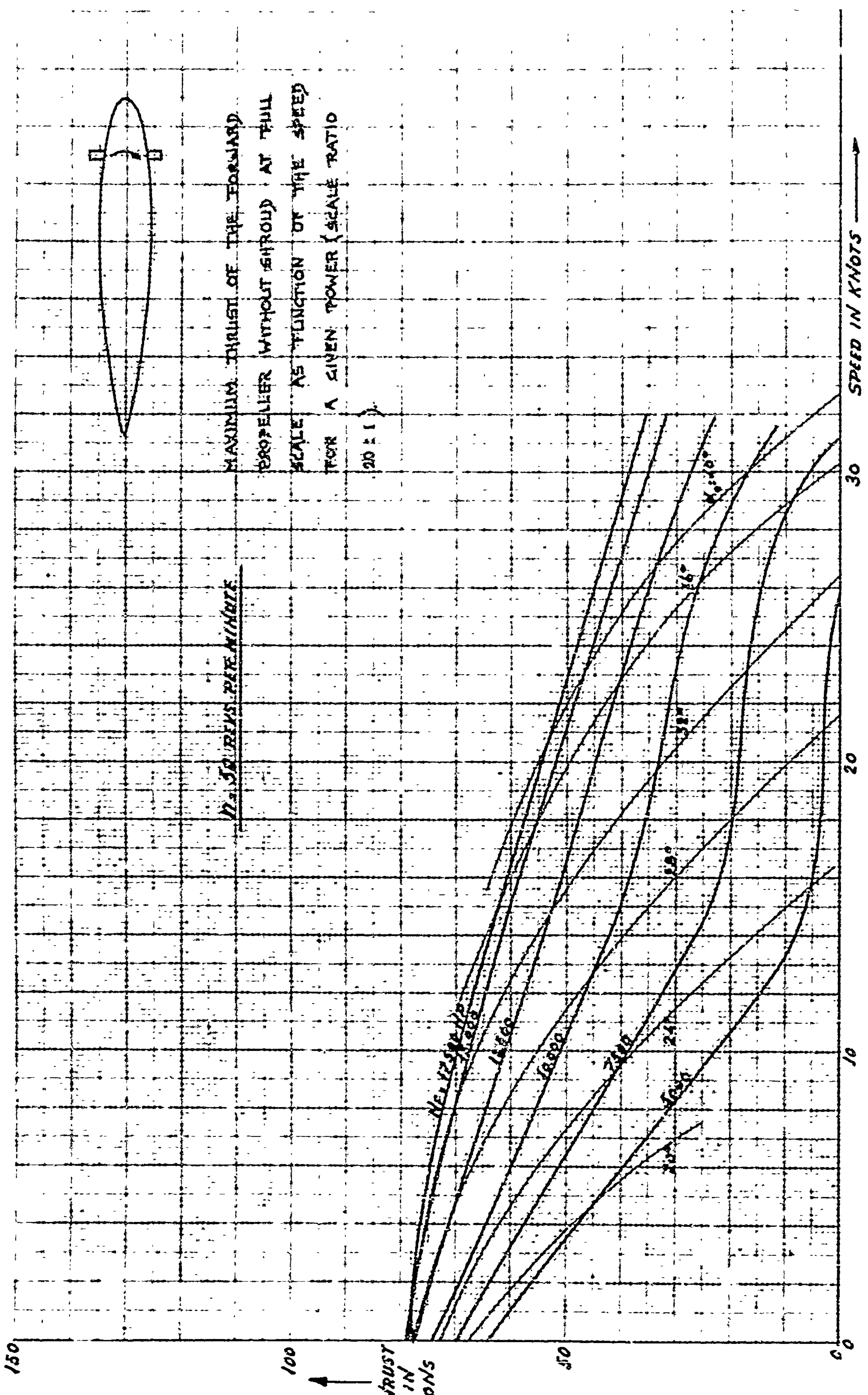

n = 52 REVS PER MINUTE
MAXIMUM THRUST OF THE FORWARD PROPELLER WITHOUT SHROUD AT FULL SCALE AS FUNCTION OF THE SPEED FOR A GIVEN POWER (SCALE RATIO 20 : 1).
Ne = 17500 HP
10000
7500
5000
20°
24°
28°
32°
36°
K = 40°
150
100
50
0
THRUST IN TONS
0
10
20
30
SPEED IN KNOTS

fig 2.19

NEDERLANDSCH SCHEEPSBOUWKUNDIG PROEFSTATION WAGENINGEN	NO.	BLZ.

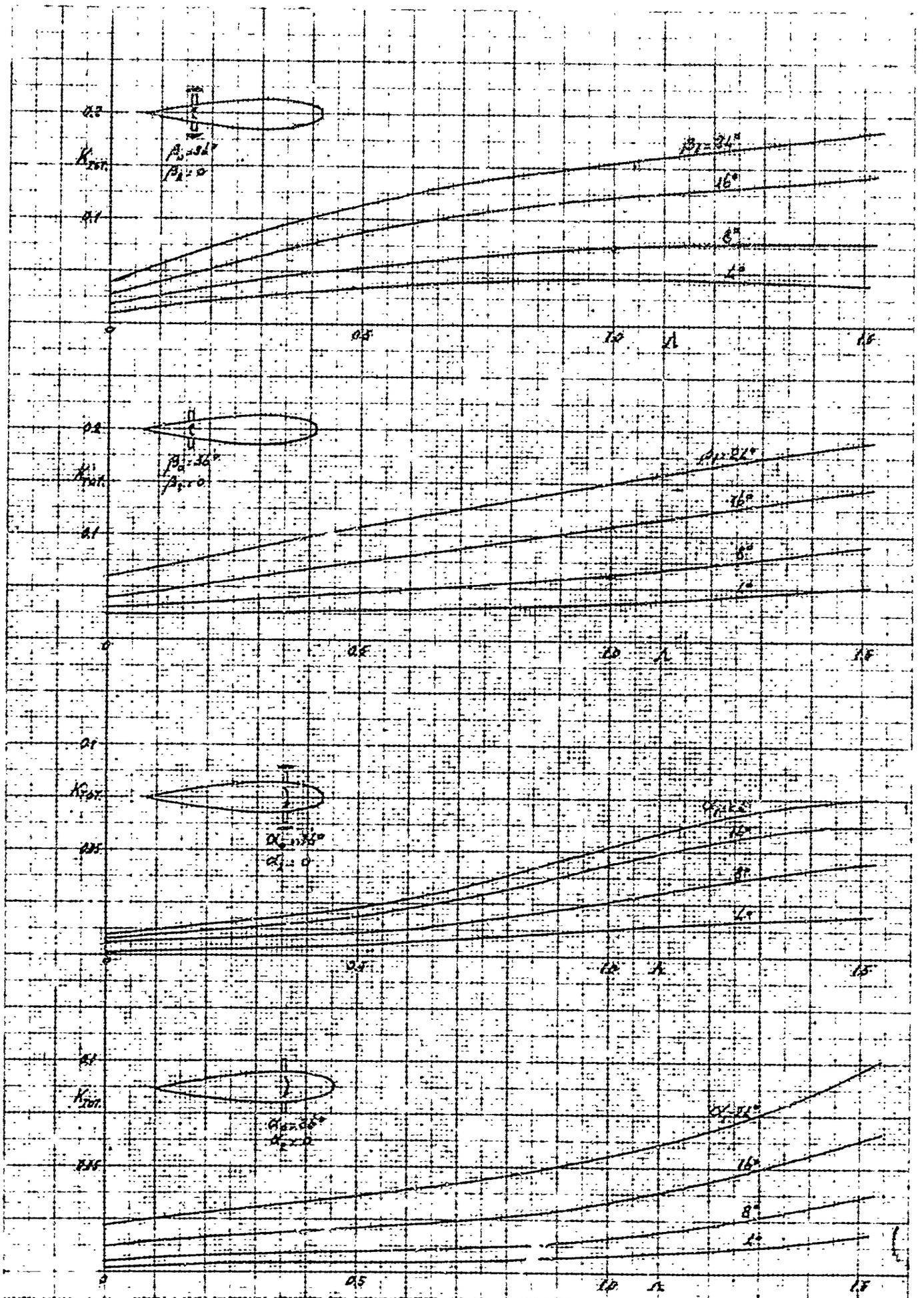

TOTAL TRANSVERSE FORCE AS A FUNCTION OF λ FOR SEVERAL PROPELLER CONFIGURATIONS

Fig. 3.21

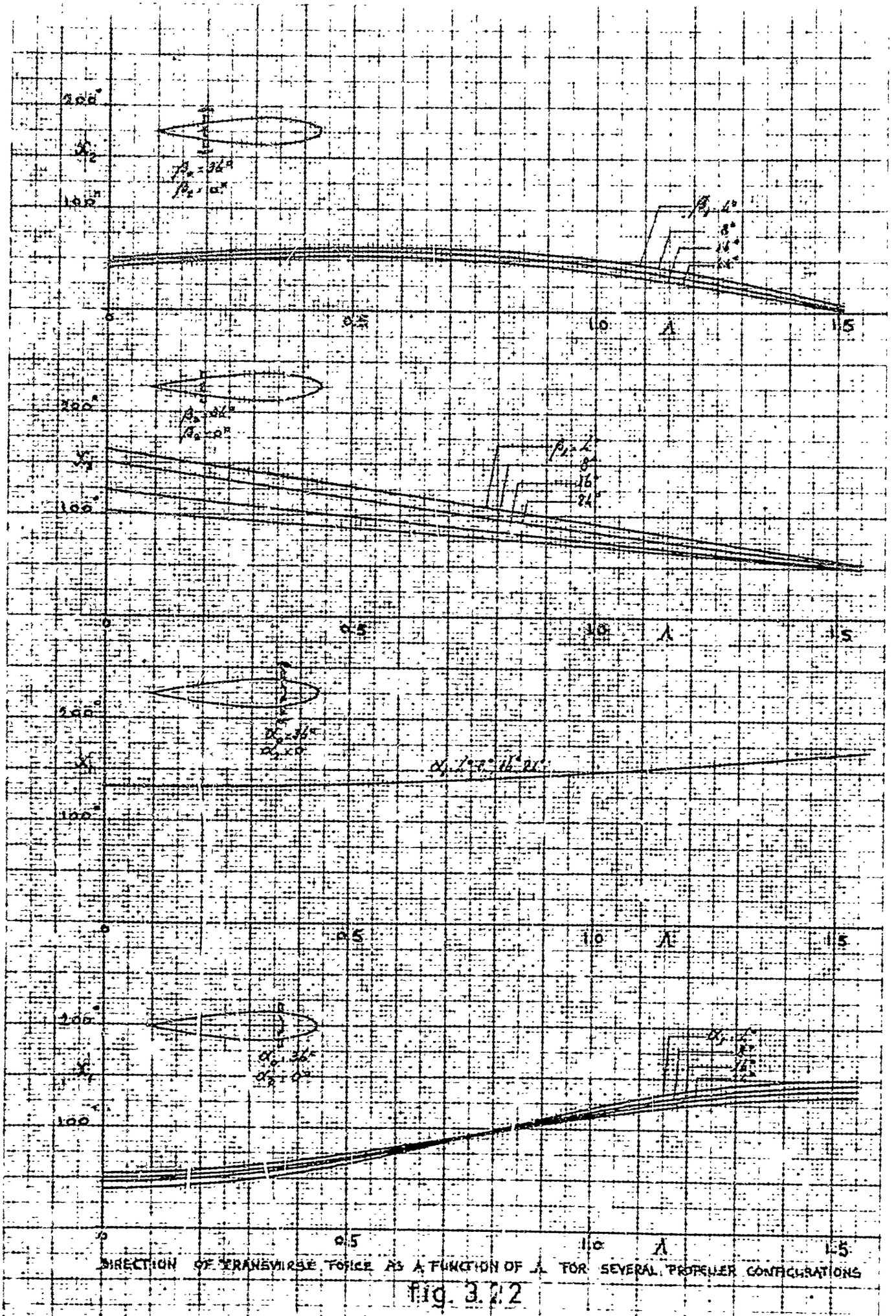

DIRECTION OF TRANSVERSE FORCE AS A FUNCTION OF λ FOR SEVERAL PROPELLER CONFIGURATIONS

Fig. 3.7.2

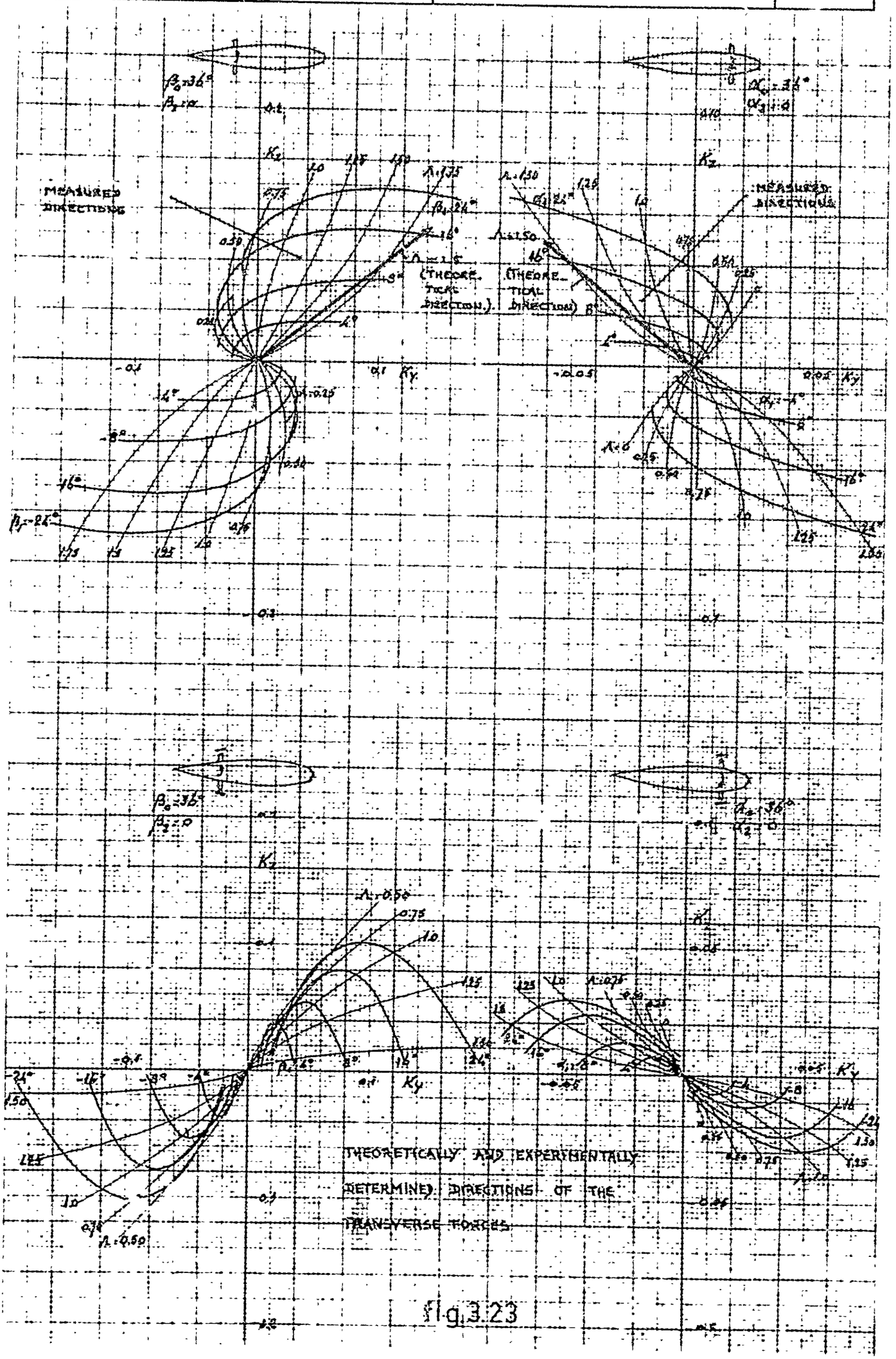

THEORETICALLY AND EXPERIMENTALLY DETERMINED DIRECTIONS OF THE TRANSVERSE FORCES.

Fig. 3.23

BLANK PAGE

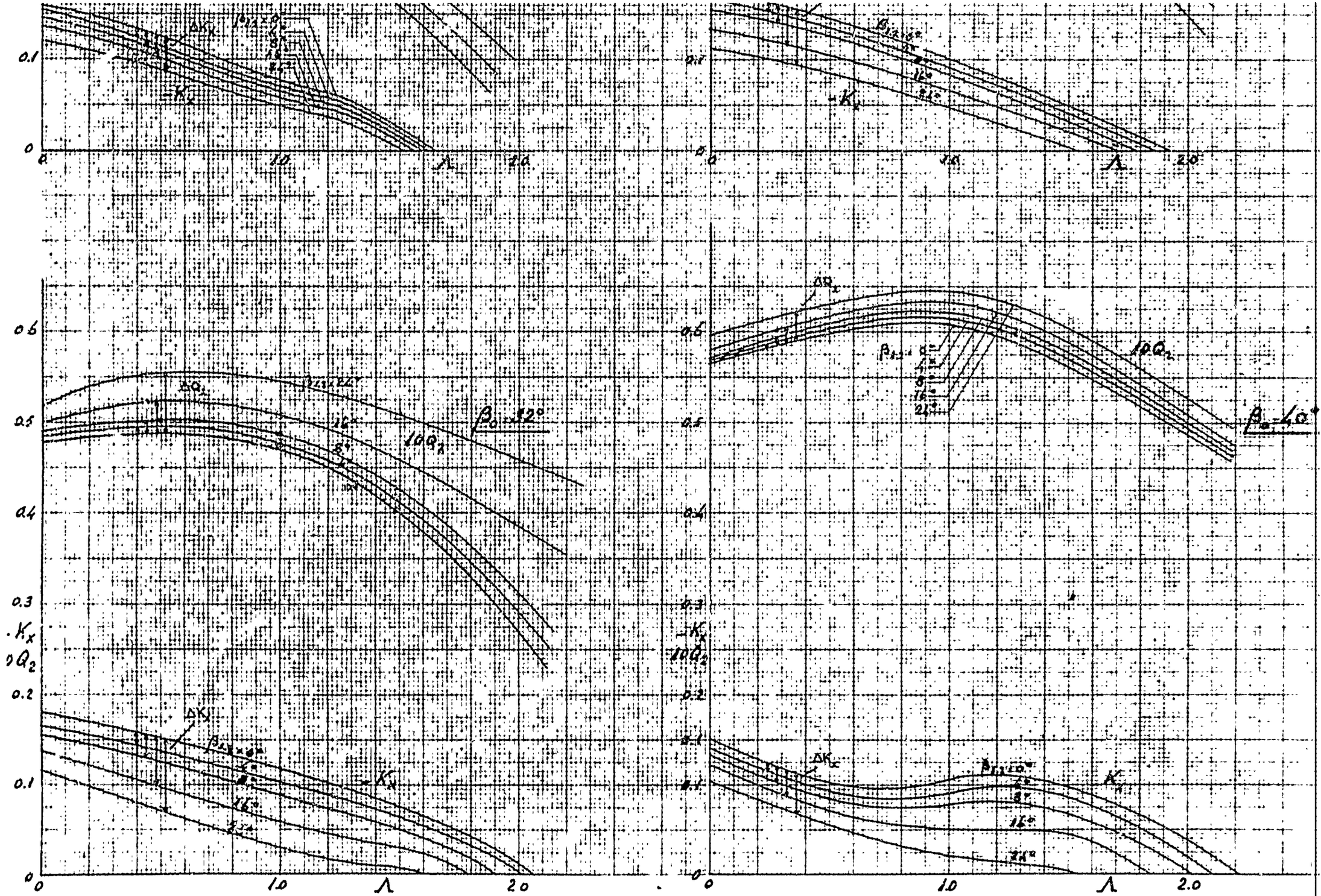

fig. 3.24

EFFECT OF CYCLIC PITCH ON THRUST AND TORQUE

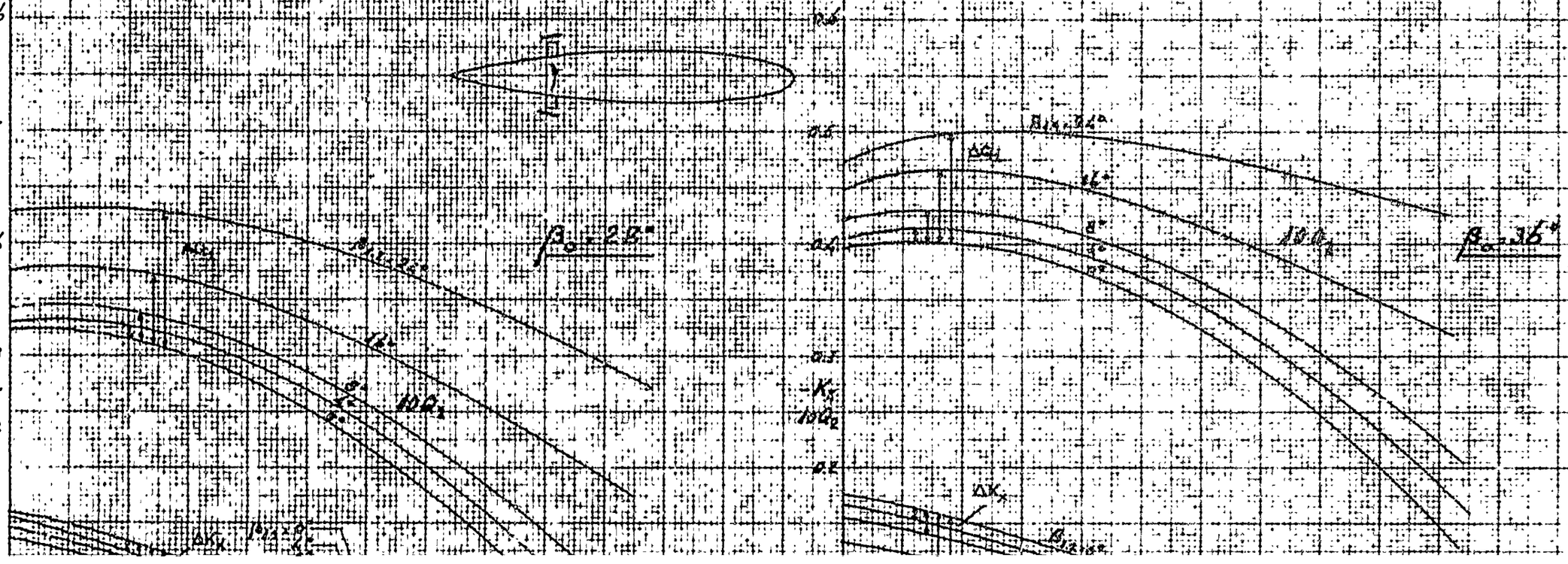

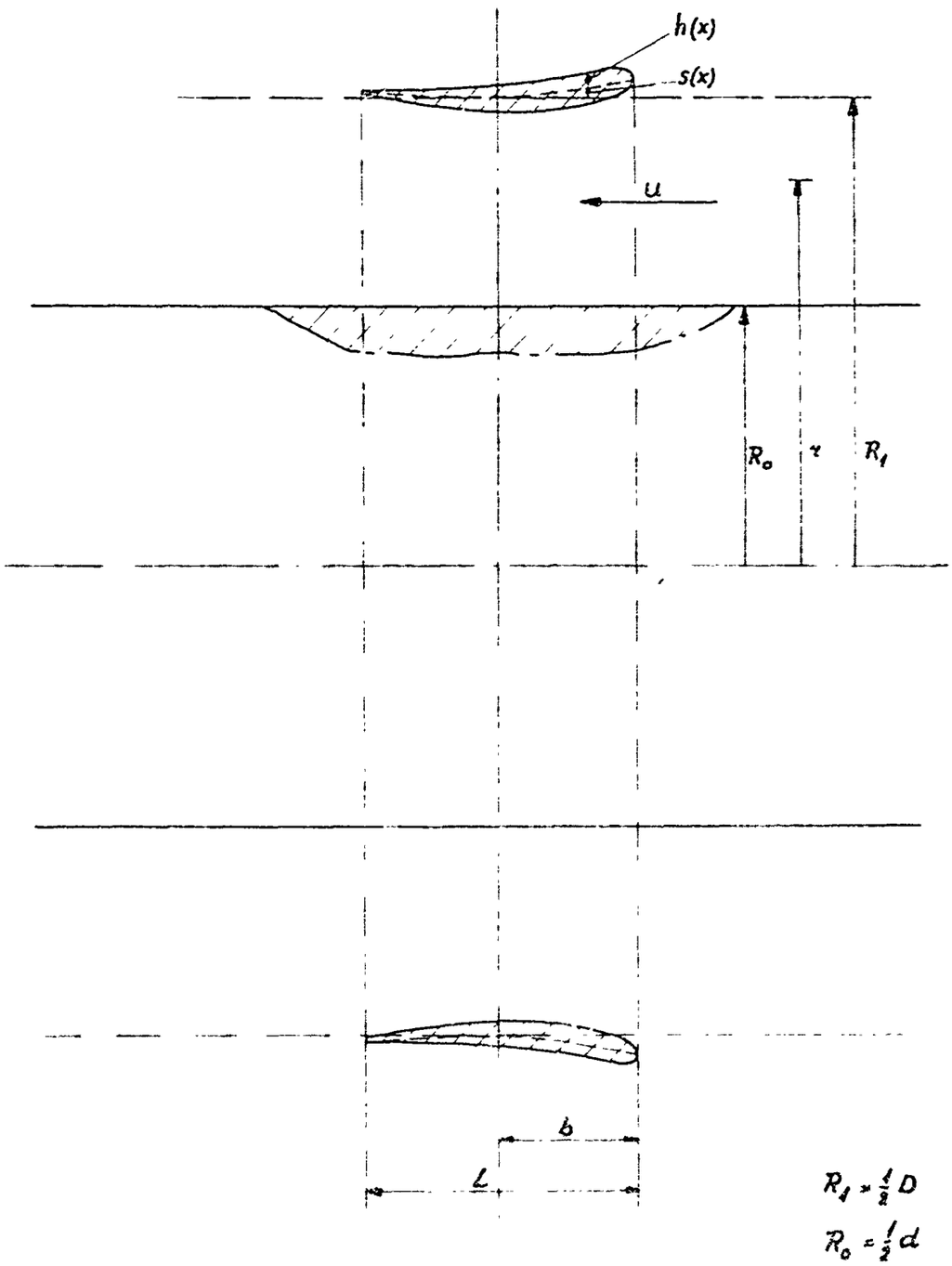

Shrouded large hub to diameter ratio propeller configuration.

Figure 4.1.

Figure 4.2.

Mathematical model of the large hub to diameter ratio propeller.

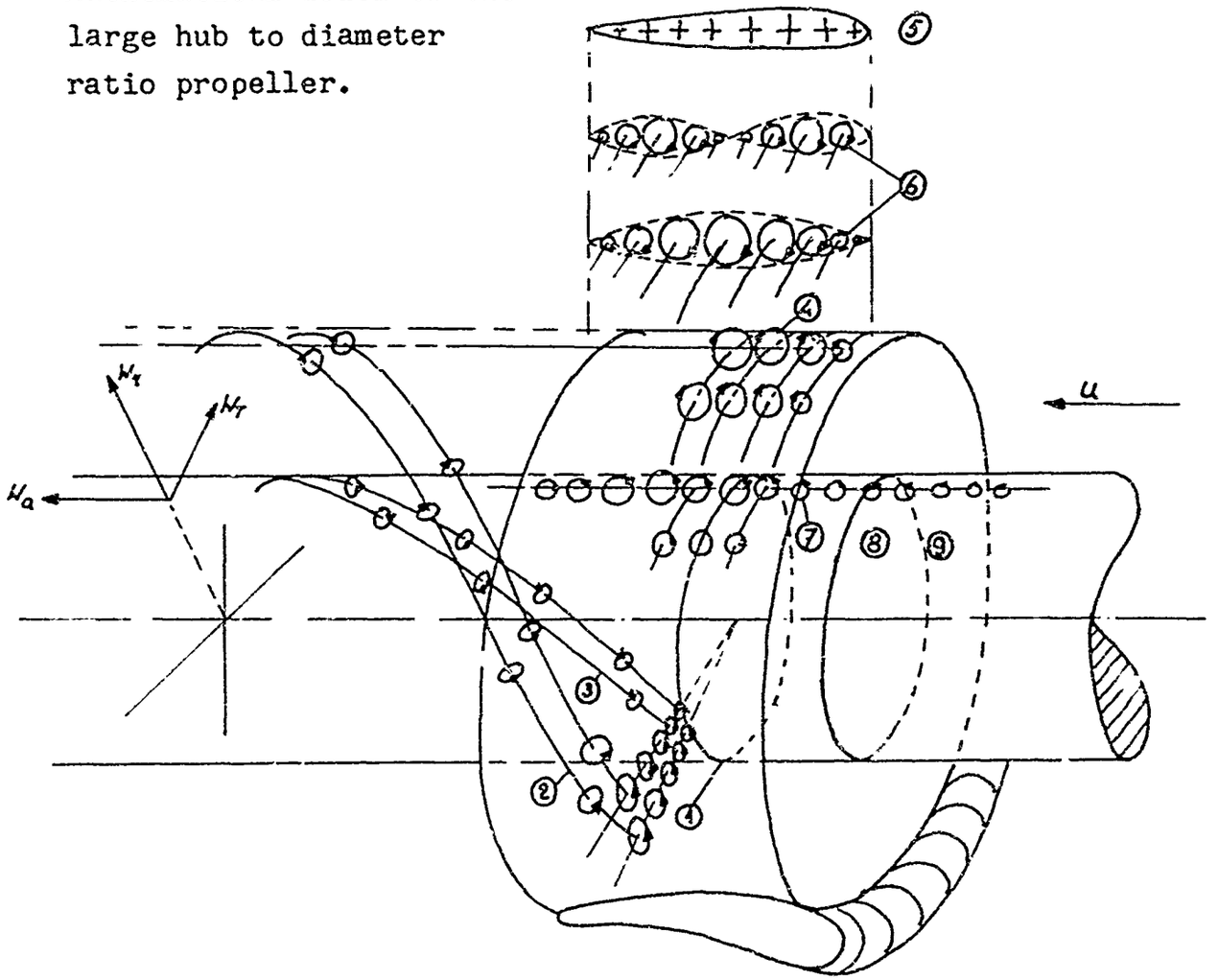

propeller flow field	①	screw disk with bound vortices (γ)
	②	helical trailing vortices starting from shroud (γ)
	③	helical trailing vortices from hub (γ)
	④	discontinuous bound ring vortex distribution along shroud ($o \rightarrow u_\gamma$)
shroud	⑤	source distribution along shroud ($q(\xi)$)
	⑥	sinusoidal ring vortex distributions (γ_m)
hub	⑦	ring vortex distribution along hub $h_o(\xi)$
	⑧	id $h_d(\xi)$
	⑨	id $h_m(\xi)$

SHROUD OF T.P.S.

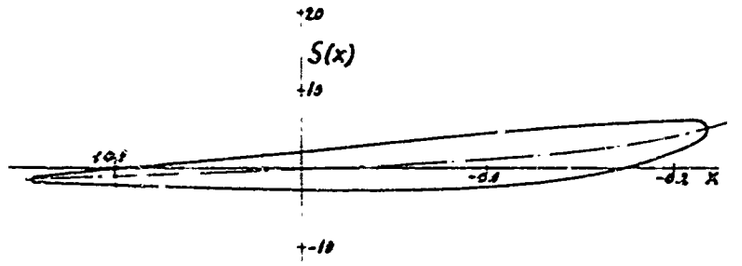

SHROUD 1
(f_1=0)

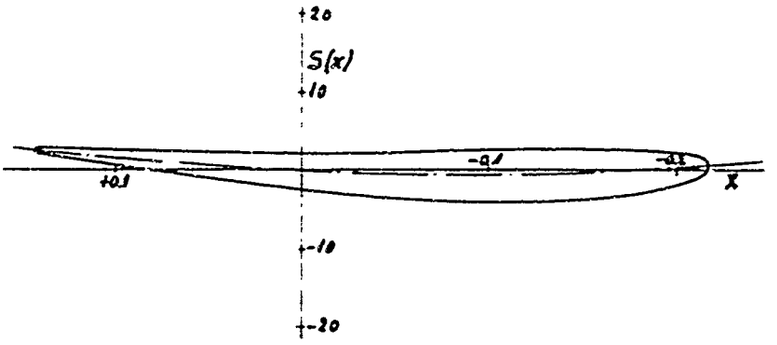

SHROUD 2
(f_1=0.2)

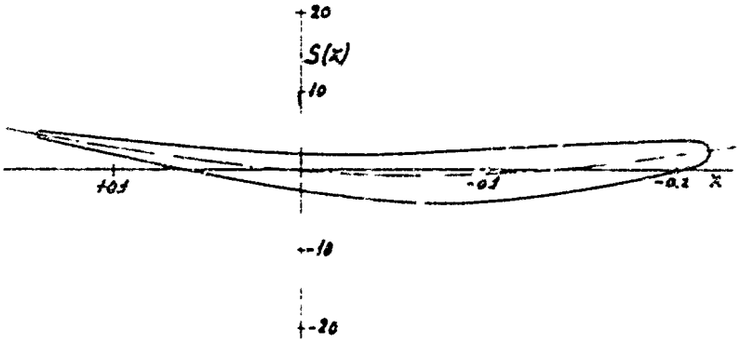

SHROUD 3
(f_1=0.4)

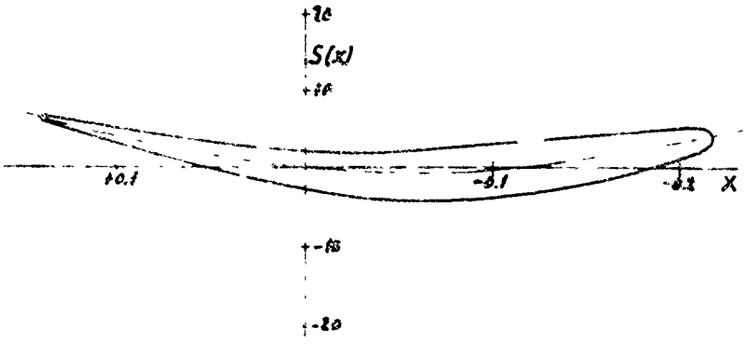

SHAPE OF CAMBER LINE AS A FUNCTION OF THE LOADING OF THE SHROUD.

FIG. 1.3

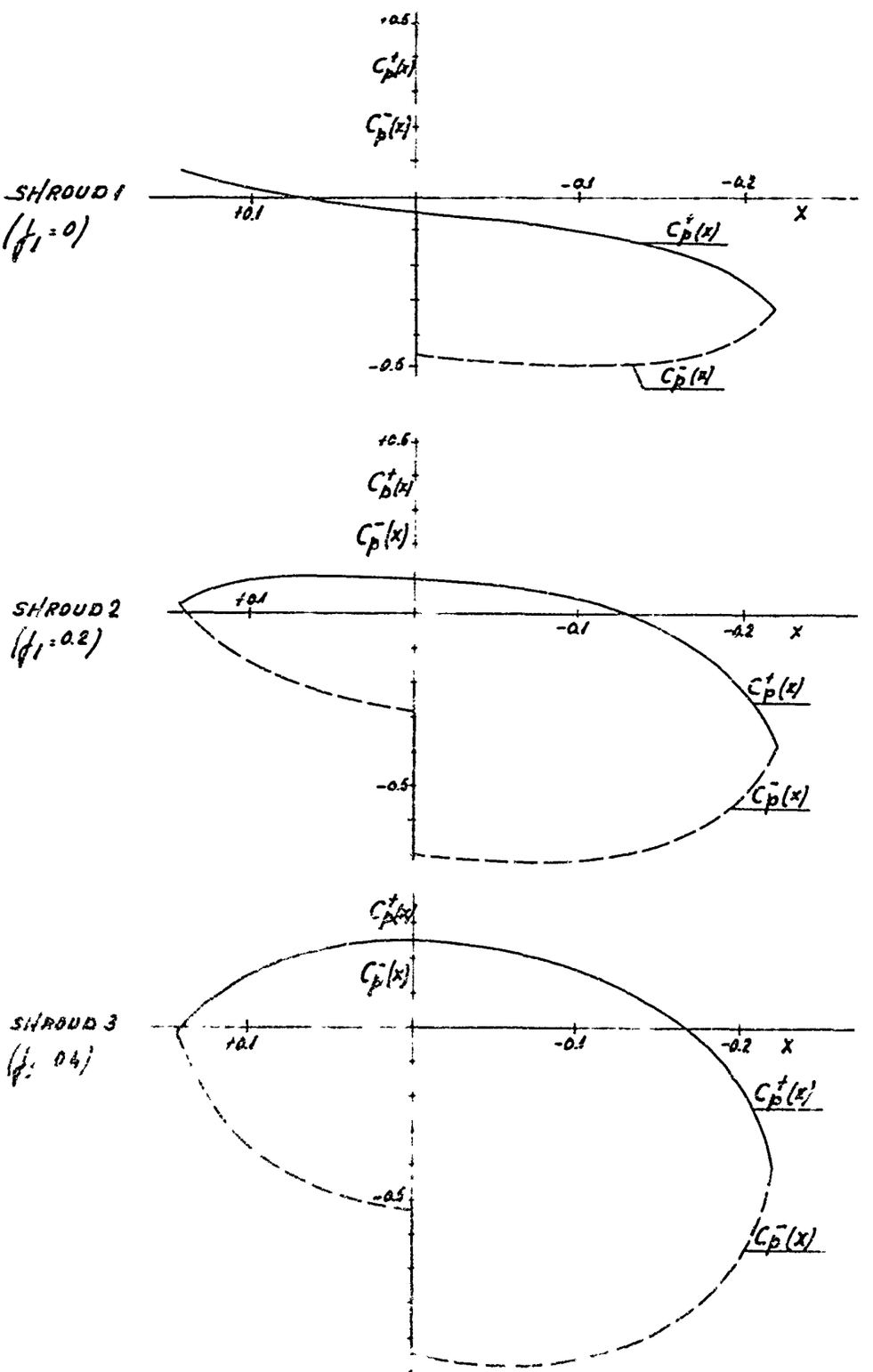

PRESSURE COEFFICIENTS ALONG THE SHROUD AS A FUNCTION OF THE LOADING OF THE SHROUD.

7

NEDERLANDSCH SCHEEPSBOUWKUNDIG PROEFSTATION WAGENINGEN	NR.	BL

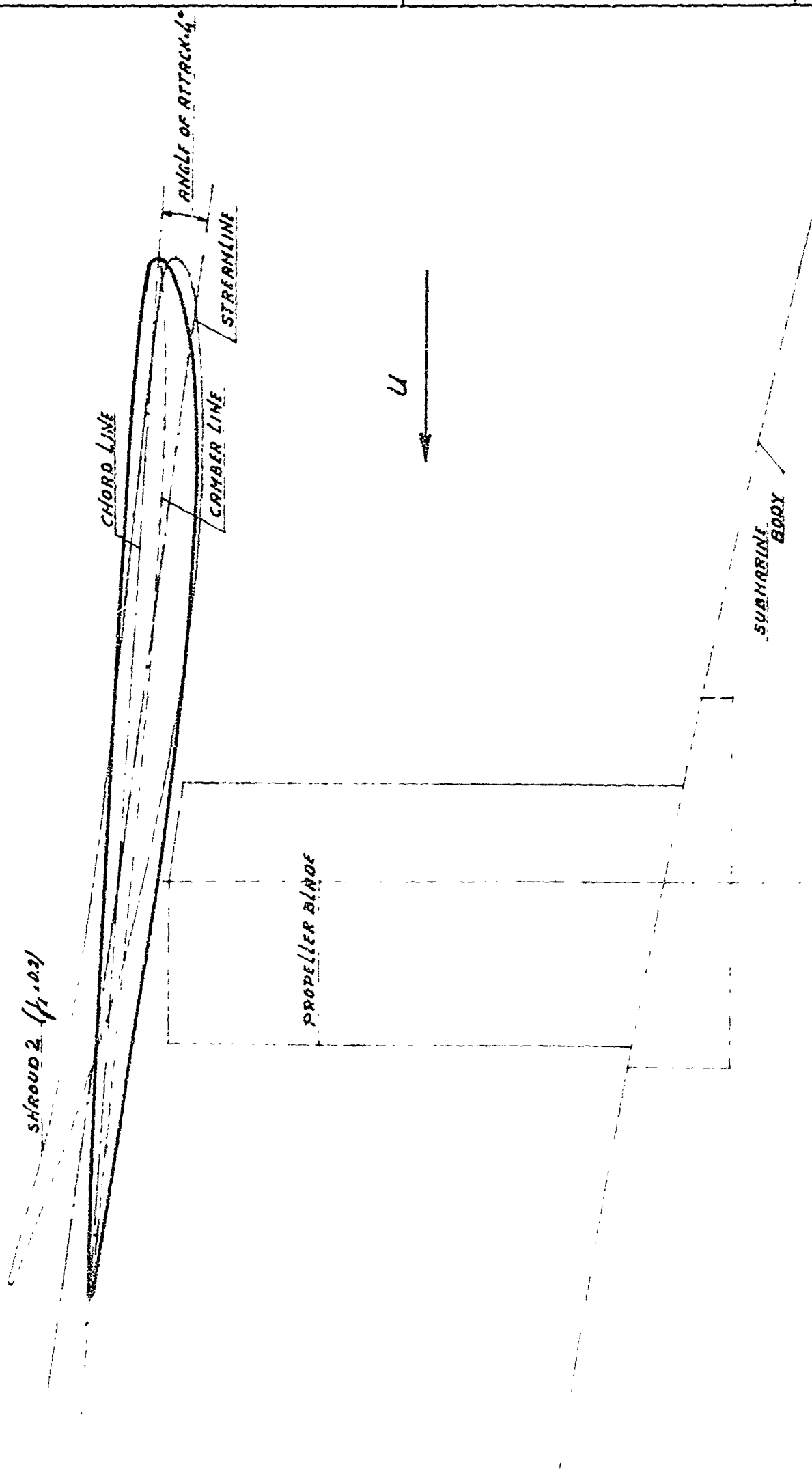

FIG 4.5 FORWARD SHROUD WITH PROPELLER BLADE

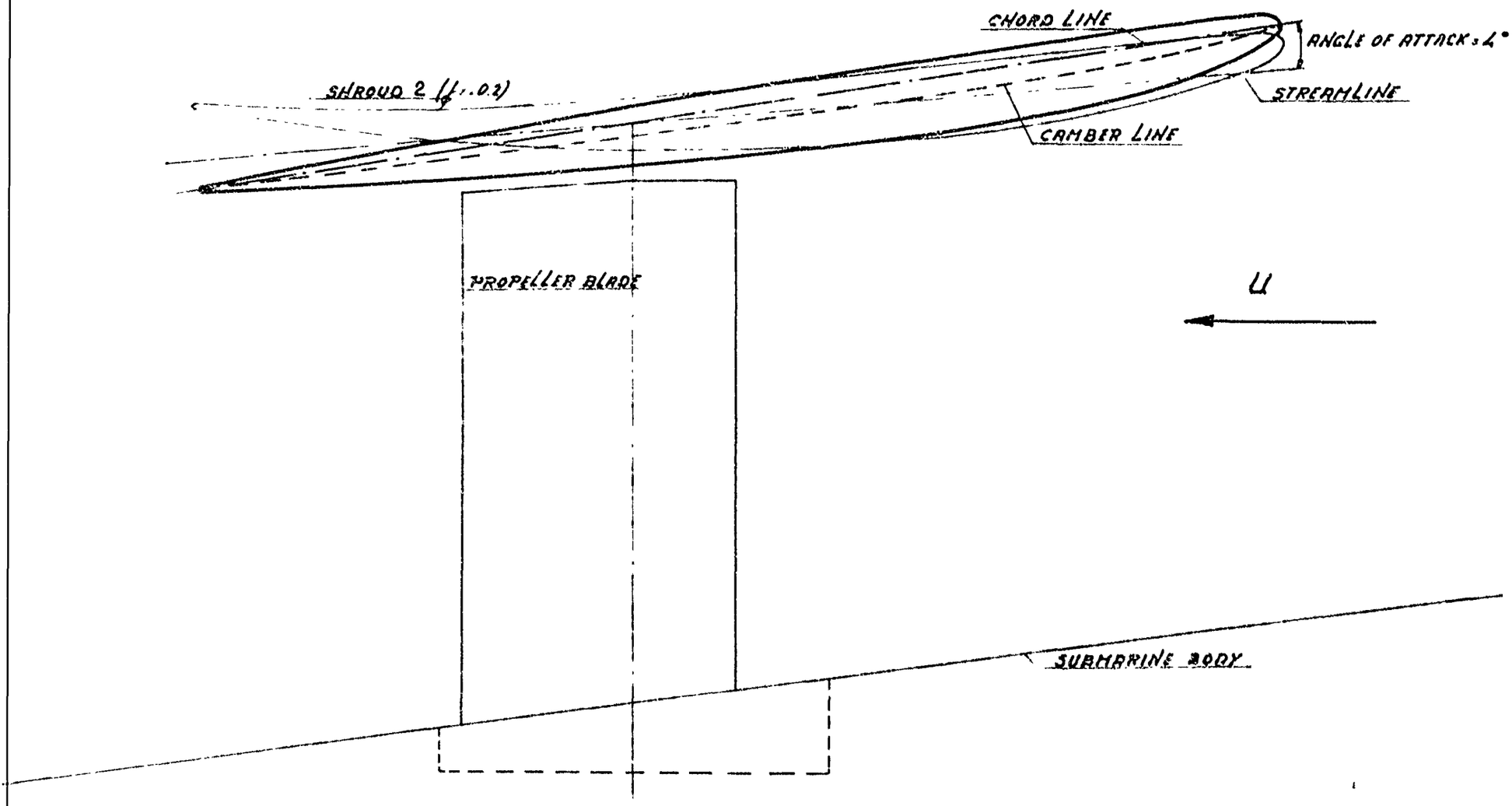

FIG. 4.6 AFT SHROUD WITH PROPELLER BLADE